TECHNICAL UNIVERSITY OF LIBEREC

FACULTY OF MECHATRONICS AND INTERDISCIPLINARY ENGINEERING STUDIES

Ph.D. THESIS

MODEL OF FLOW AND SOLUTE TRANSPORT
IN DUAL-POROSITY MEDIA

MILAN HOKR

LIBEREC, JUNE 2003

Technická univerzita v Liberci

Fakulta mechatroniky a mezioborových inženýrských studií

Obor: Přírodovědné inženýrství

Název disertační práce:

Model proudění a transportu látek v porézním prostředí se zahrnutím vlivu dvojí porozity

Ing. Milan Hokr

Školitel: Doc. Dr. Ing. Jiří Maryška, CSc.

Rozsah práce

počet stran textu: 112
počet tabulek: 4
počet obrázků: 31

Místopřísežné prohlášení:

Místopřísežně prohlašuji, že jsem disertační práci vypracoval samostatně s použitím uvedené literatury.

V Liberci dne 16. 6. 2003

Milan Hokr

PODĚKOVÁNÍ:

ANOTACE

Předkládaná disertační práce se zabývá modelem proudění a transportu látek v porézním prostředí s dvojí porozitou. Jsou popsány fyzikální mechanismy průsakového proudění, advekčně–disperzního transportu a difuzní výměny rozpuštěné látky mezi průtočnými (mobile) a slepými (immobile) póry v nerovnovážném režimu a odvozeny řídící diferenciální rovnice. Hlavní částí práce jsou metody numerického řešení a jejich implementace. Úloha proudění je řešena smíšenou-hybridní metodou konečných prvků. Úloha transportu je diskretizována v čase metodou rozkladu operátoru (operator splitting) a v prostoru metodou konečných objemů. Rozklad umožňuje nezávisle řešit úlohy advekce, disperze a výměny mezi pórovými zónami různými metodami. Úloha výměny je výhodně řešena pomocí vztahů pro analytické řešení. Pro řešení úlohy advekce je použito explicitní upwind schéma. Aplikace uvedené kombinace metod na úlohu transportu s nerovnovážnou výměnou je původní prací autora.

Implementace modelu pro úlohy praxe zahrnuje procesy advekce a výměny mezi póry jako základní aproximaci obecného prosesu transportu dostatečně vyhovující pro aplikace v praxi. Model byl testován na několika standardních 1D a 2D úlohách. Důležitým výsledkem je shoda s analytickým řešením 1D úlohy, po odečtení vlivu numerické disperze u upwind schématu advekce.

Motivací pro vytvoření modelu byla jeho aplikace při plánování sanace podzemních vod v oblasti Stráže pod Ralskem. Součástí práce je řešení reálné úlohy středního rozsahu – čerpání z vyluhovacího pole o ploše $1.2 km^2$. Porovnáváním modelu a naměřených koncentrací byly potvrzeny předpokládané vlastnosti dvojí porozity u geologických vrstev zahrnutých v úloze. Programátorská práce a příprava vstupních dat je společnou prací autora a týmu v s.p. DIAMO, výpočet a vyhodnocení výsledků jsou dílem autora.

Tato anotace je zkráceným překladem části úvodní kapitoly práce (str. 6).

This abstract is a brief Czech version of the Introduction (page 6).

Contents

List of notation

Abbreviations

Abbreviation	Meaning
1D, 2D, 3D	one-, two-, three-dimensional
ADE	Advection-dispersion equation
ADX(E)	Advection–dispersion–exchange (equation)
BC(s)	Boundary condition(s)
CFL	Courant–Friedrichs–Lévy condition
FDM	Finite difference method
FEM	Finite element method
FVM	Finite volume method
MH(-FEM)	Mixed-hybrid (finite element method)
MIE	Mobile–immobile exchange
ODE, PDE	Ordinary/partial differential equation
OS	Operator splitting
REV	Representative elementary volume

Mathematical symbols

Symbol	Meaning
$\mathbb{R}$	set of real numbers
$\mathbb{N}$	set of natural (non-negative integer) numbers
$\boldsymbol{x} = (x, y, z)$, $\boldsymbol{\xi}$	point in $\mathbb{R}^3$
$\boldsymbol{\nu}$	unit normal
∇	$\left(\frac{\partial}{\partial x_1}, \frac{\partial}{\partial x_2}, \frac{\partial}{\partial x_3} \right)$ or $\left(\frac{\partial}{\partial x}, \frac{\partial}{\partial y}, \frac{\partial}{\partial z} \right)$
Ω	problem domain $\Omega \subset \mathbb{R}^3$
$\partial\Omega \equiv \Gamma$	boundary of Ω
δ_{ij}	Kronecker delta
$\delta(x)$	Dirac δ-function
$L_2(X)$	Lebesgue space of square intergable functions on X
$\boldsymbol{L}_2(X)$	space of vector functions $\left\{ \boldsymbol{u} : X \to R^3 \ ; \ \int_X |\boldsymbol{u}|^2 \, dX \ < \ +\infty \right\}$
$(u, v)_{0, X}$	scalar product in $L_2(X)$
$\langle u, v \rangle_X$	L_2-scalar product on boundary

Physical quantities

Quantity	Dimension	Meaning
$\boldsymbol{A}$	$[\mathrm{L^{-1}\cdot T}]$	coefficient of resistance ($\boldsymbol{A} = \boldsymbol{K}^{-1}$)
c	$[\mathrm{M\cdot L^{-3}}]$	concentration (c_m mobile, c_i immobile)
c_s	$[1]$	sorbed concentration
Cr	$[1]$	Courant number
$D, \boldsymbol{D}$	$[\mathrm{L^2\cdot T}]$	diffusion/dispersion
g	$[\mathrm{L\cdot T^{-2}}]$	gravity constant
h	$[\mathrm{L}]$	discretisation parameter
$k, \boldsymbol{k}$	$[\mathrm{L^2}]$	permealibility of the porous medium
$K, \boldsymbol{K}$	$[\mathrm{L\cdot T^{-1}}]$	hydraulic conductivity
K_D	$[\mathrm{L^3\cdot M^{-1}}]$	distribution coefficient of linear sorption
l	$[\mathrm{L}]$	characteristic length of pores
L	$[\mathrm{L}]$	characteristic length in dimensionless problems
m	$[\mathrm{M}]$	solute mass
m_{vg}	$[1]$	coefficient in Van Genuchten formula
n	$[1]$	porosity (n_m mobile, n_i immobile)
p	$[\mathrm{M\cdot L^{-1}\cdot T^{-2}}]$	pressure
Pe	$[1]$	Péclet number
q_s	$[\mathrm{T^{-1}}]$	density of fluid sources (q_s^+)/ sinks (q_s^-)
q_c	$[\mathrm{M\cdot L^{-2}\cdot T^{-1}}]$	mass flux
R	$[1]$	retardation factor
S, S_e	$[1]$	saturation (effective)
t	$[\mathrm{T}]$	time
$T_{1/2}$	$[\mathrm{T}]$	characteristic time of the M-I exchange
$\boldsymbol{u}$	$[\mathrm{L\cdot T^{-1}}]$	Darcy velocity (flux)
$\boldsymbol{v}$	$[\mathrm{L\cdot T^{-1}}]$	seepage velocity
$\boldsymbol{w}$	$[\mathrm{L\cdot T^{-1}}]$	Darcy velocity (MH-FEM base functions)
x, y, z	$[\mathrm{L}]$	space coordinates
α	$[\mathrm{T^{-1}}]$	coefficient of non-equilibrium exchange
α_L, α_T	$[\mathrm{L}]$	longitudinal and transversal dispersivity
α_{vg}	$[1]$	coefficient in Van Genuchten formula
μ	$[\mathrm{M\cdot L^{-1}\cdot T^{-1}}]$	dynamical viscosity
ϕ	$[\mathrm{L}]$	piezometric (pressure) head
ψ	$[\mathrm{L}]$	piezometric head (MH-FEM base functions)
ϱ, ϱ_s	$[\mathrm{M\cdot L^{-3}}]$	fluid and solid density
θ	$[1]$	water content
ω	$[1]$	Damkohler number (Da)

Introduction

The thesis deals with the modelling of fluid flow and solute transport in porous media with immobile pore zone ("dual-porosity" media). It covers physical and mathematical aspects of the model and experiments with testing and real-world problems.

In the following paragraphs, we mention the importance of the presented work in the context of application of the model as wanted for problems of underground remediation in Stráž pod Ralskem and in the context of research in numerical methods for complex groundwater problems. Finally, the structure of the thesis and new results presented are described.

In spite of the direct motivation and realisation is related to the activities of DIAMO Stráž pod Ralskem, the most of the presented work is general and can be applied for other porous media problems with the considered properties.

Motivation – uranium mining in northern Bohemia

Mathematical modelling accompanies the chemical uranium leaching and related operations by the state enterprise DIAMO in the Stráž pod Ralskem region since its beginning in 60s in the last century. In the last decade, after closing of mining activities in 1996, a problem of remediation of contaminated underground water in place of former leaching has been solved.

An extent of contamination is very large: more than 4 million tons of H_2SO_4, 300 thousand tons of HNO_3, 120 thousand tons of NH_3 and other chemicals were injected in Cenomanian sandstones [Nov01, NSŠ98]. The problem is very complicated as the total contaminated volume is about 190 million m^3 in the area of $28km^2$ and the contamination is quite unevenly distributed, also out of the leaching area of Cenomanian aquifer due to geological structures and failures of technologies [MMSŠ00].

6

The model developed in this thesis deals with the contamination in the Turonian aquifer which lies above the Cenomanian and contains some isolated contamination in the places of communication with Cenomanian aquifer through the failures. The remediation of the Turonian aquifer is necessary for protection of drinking water sources in the neighbourhood. During extraction process in the last years, there were identified dual-porosity properties in the aquifer, and since it plays important role in the remediation, a construction of a special computational model seems to be necessary.

There were many specific requirements on the model, mainly for full compatibility with other software tools used, for reasonable computational cost, to be applied for middle and large problems in both spatial and temporal measure (forecasts for up to few decades). A use of tailored numerical method, laying stress on the most significant processes in the problems concerned, was expected.

Mathematical models of flow and transport (state of the art)

Numerical methods for solution of problems in porous media are intensively studied in the last 40 years, together with the development of computer technology allowing the use of the methods for more and more complex problems. An overview of the approaches and methods for flow and transport problems relating to the matter of this thesis is given in the section 3.1.

Even if many advanced methods exist for the standard problems, there are still many limitations of the methods and many open problems. A typical conflict arises from large size of the underground problems and uncertainty of parameters – the sophisticated methods are often difficult to use with complex 3D discretisation mesh and moreover the "exact calculation with inexact data" can appear inappropriate (except of special cases, e.g. inverse problems).

Thus there is space for tailored models for specific situations, which well represent the major processes, overriding the drawbacks in the less important aspects.

Structure of the thesis

In the first chapter, the solved physical problem is introduced: steady flow governed by the Darcy's law and solute transport governed by the advection-

dispersion equation coupled with a system of ODEs for non-equilibrium mass exchange between mobile and immobile pore water. Aspects of representation of the reality and the relation to other interaction processes are discussed.

Next, the mathematical formulation, in terms of initial–boundary problems for the governing PDEs, is defined in the second chapter.

The third chapter deals with the numerical methods for the presented flow and transport problems. The mixed-hybrid FEM approximation by lowest-order base functions for the fluid flow is derived. The transport problem is discretised in time using the operator-splitting method, separating the transport processes: advection, dispersion, and non-equilibrium mobile–immobile exchange. In the presented model realisation, the transport is discretised by cell-centred FVM and the advection is solved by explicit upwind scheme and the mobile–immobile exchange is determined analytically.

The practical model realisation concerned in the fourth chapter was quite extensive programming work, in the cooperation of the author and the team in DIAMO. Important in this context is the topology of the discretisation and relating data structures.

The sixth chapter presents results of several experiments for examination of the model function and properties. A good match in the comparison of numerical results and analytical solution (under specified conditions) was achieved for the 1D non-equilibrium transport problem.

In the last seventh chapter, we describe application of the model for solution of local underground remediation problem in the Stráž pod Ralskem region. Comparing with the measurements from the period of 19 months of extraction operations, the values of material parameters were estimated, with good correspondence of the results.

New results

Important new results are in the derivation of numerical method and in the area of experimental calculations. Beside that, the physical description of the processes contains some consideration beyond the results in the cited literature (identification of the parameters of microscopic structure in the mobile–immobile exchange, section 1.3.3). Next, the model was used in the context of groundwater practice as the first "sample" solution of dual-porosity problems in the framework of the important ecological problem faced in Stráž pod Ralskem.

The numerical solution is based on standard approaches, combined in

original way for the specific coupling of processes in the solved problem: Inspired with a common operator splitting approach for the advection-dispersion problem, we formulate the operator splitting method for the non-equilibrium transport, where the problem described by a system of two coupled equations with two unknowns is split into single processes: advection, dispersion and non-equilibrium exchange between the mobile and immobile zone.

This approach allowed to use the simple analytical solution of the split exchange process (derived by the author) and as a whole to obtain a method different from the others used in the literature (mentioned in section 3.1). On the other hand, it is related to methods for the problem of non-equilibrium adsorption developed in parallel in the recent years [KF02, Rem03] – for more general non-linear problems, but under other restrictions (e.g. one-dimensional domain and computational cost).

We also mention the programming work of the author in the framework of the team in DIAMO. The model was implemented with full user interface, compatible with other existing software tools. A solution of real-world problem was done, with results in good correspondence with field measurements. The calculation confirmed the expected dual-porosity properties of the underground media in the region, which is also an important author's contribution.

Chapter 1

Physical model

In this chapter, we present physical principles of the phenomena in porous media, we explain how to understand the term *dual porosity* and we propose possible approaches of modelling. First, we describe basic assumptions commonly posed on porous media properties and then we describe equations governing flow and transport and we derive some variations suitable for numerical solution in the following chapters.

The description is based on the classical literature [BV90] (and also [ZB95, Kaz97, Ben95]) and the parts concerning the effect of immobile (blind) pores result from e.g. [CS64, vGW76]. The main result of this chapter is the final formulation of the physical problem to solve, sections 1.3.3, 1.3.4.

A note on terminology

There are many different notations in the literature for the character of porous (or fractured) media represented by dual-porosity (or double-porosity) model. What we call here immobile pores is also referred as blind, dead-end, inactive pores, stagnant zone. The mobile pores are also denoted as active pores. In the context of fractured rock, the mobile zone are the fractures and the immobile zone is the solid matrix. The adjectives "mobile" and "immobile" primarily belong to "water" and with clear meaning are used with "pores". The mass exchange between pore zones is denoted as non-equilibrium, rate-limited, or kinetic.

1.1   Description of porous media

In our models, we consider a porous medium representing sedimentary rock, but in most aspects it does not mean any loss of generality. According to [BV90], we assume that it is possible to define *a representative elementary volume* (REV), which is large enough to contain many pores and thus it can be regarded as a continuous medium (i.e. "representative"). On the other hand, it is small enough in comparison with the domain size and is approximately homogeneous and can be associated with a state in a single point in the space (i.e. "elementary").

In the following, we always use the continuum approach for differential equations of the model, even if we sometimes must take into account the real microscopic structure for deriving some relations, especially in the case of effects caused by dual porosity, which is the main topic studied in this work (the "dual-continuum approach" or two-region model, see below) .

In all the text, we assume both the water and the solid matrix of porous medium to be incompressible and that the fluid density does not depend on the concentration (not the density-driven flow).

1.1.1   Physical quantities of the fluid flow

We remind the definitions of basic continuum quantities describing the porous media and hydraulic processes. In general, we define *porosity* as

$$n = \frac{\text{volume of pores in REV}}{\text{total volume of REV}} \ . \tag{1.1}$$

This definition in the context of this thesis should be considered rather as a general framework for further definition of mobile and immobile porosity (section 1.3.3). In the next few sections, we use this basic definition for simpler and clearer derivation of the relations, below transformed for the quantities concerning the dual-porosity media.

On the level of REV, the fluid motion can be determined by flow rate per cross-sectional area, we denote

$$u = \frac{\text{flow rate}}{\text{area}} \ , \tag{1.2}$$

where the flow rate is expressed as fluid volume per time ($L^3 \cdot T^{-1}$) and the area in square meters. The quantity u has a dimension of velocity (we will

call it *Darcy velocity* – see below), but in fact, it is not the velocity of the real movement of the fluid. Beside it, we define

$$v = \frac{u}{n} \tag{1.3}$$

the *seepage velocity*, which is the velocity of fluid averaged over the pore volume in REV and expresses the macroscopically detectable velocity of contaminant particles (without regard to their microscopic movement).

In the hydrogeological practice, the values of pressure are expressed in meters of water column, in fact, it is a quantity called *pressure head*, defined by $p/(\varrho g)$, where p is pressure, ϱ is density of the fluid and g is the gravity constant. We do not state any special notation and sometimes use the term pressure in both meanings, but it will always be clear from the context. Beside it, we define the *piezometric head*, which plays a role of potential for the fluid flow (see below (1.14)-(1.16)), as

$$\phi = z + \frac{p}{\varrho g}, \tag{1.4}$$

where z is the vertical coordinate.

1.1.2 Capillarity

Capillarity effects play important role in the case of flow in unsaturated porous media, i.e. if an interface between liquid phase and gas phase exist. Situation in unsaturated porous media is described by the ratio of liquid and air (free space) in certain place, using the quantities the water (moisture) content θ or the saturation S which are defined by

$$\theta = \frac{\text{volume of water in REV}}{\text{total volume of REV}}, \qquad 0 \leq \theta \leq n, \tag{1.5}$$

$$S = \frac{\text{volume of water in REV}}{\text{volume of pores in REV}}, \qquad 0 \leq S \leq 1, \; S = \frac{\theta}{n}. \tag{1.6}$$

For more precise description of the processes, we must take into account the structure of pores. Commonly, there is a part of pores fully isolated from others with no interaction (neither water flow nor solute diffusion). To exclude them, we denote θ_0 the residual water content (in the disconnected

pores and we introduce the effective water content and effective saturation by

$$\theta_e = \theta - \theta_0 \,, \qquad S_e = \frac{\theta - \theta_0}{n - \theta_0} \,.$$ (1.7)

The relation between the effective saturation and capillary pressure in the unsaturated zone is given by the Van Genuchten formula [vG80]. Written jointly for the saturated and the unsaturated zone, it holds

$$S_e(p) = \begin{cases} \dfrac{1}{\left(1 + \alpha_{\mathrm{vg}} |p|^{m_{\mathrm{vg}}}\right)^{\frac{m_{\mathrm{vg}}-1}{m_{\mathrm{vg}}}}} & p < 0 \\ \\ 1 & p \geq 0 \,, \end{cases}$$ (1.8)

where α_{vg} and m_{vg} are material constants of the porous medium (statistical distribution of pore/grain dimensions).

The hydraulic conductivity of the unsaturated medium depends on the effective saturation by [Irm54]

$$\boldsymbol{K}(S) = \boldsymbol{K} S_e^3 \,,$$ (1.9)

where $\boldsymbol{K}$ is the conductivity of saturated medium.

1.1.3 Structured porous media

In this section we discuss the influence of microscopic pore structure to the fluid flow and solute transport in the porous media. Concerning the model presented in the thesis, we define the conditions/principals it is based on, i.e. what we understand by the term dual porosity and how such a type of porous media is represented.

For the flow calculation, the microscopic structure is in fact not important. The flow is expressed by the Darcy velocity, which expresses the flow in a "global" sense (as a water flux per unit area of cross section, eq.(1.2)) and all the information necessary is contained in the permeability tensor.

The situation begins to be more complicated, when we try to express the seepage velocity (1.3), using some value of porosity. The values of seepage velocity obtained by the use of the porosity with basic definition does not often correspond to the field experiments with the seepage velocity observed from the results of advection-dispersion process (1.17) where the seepage
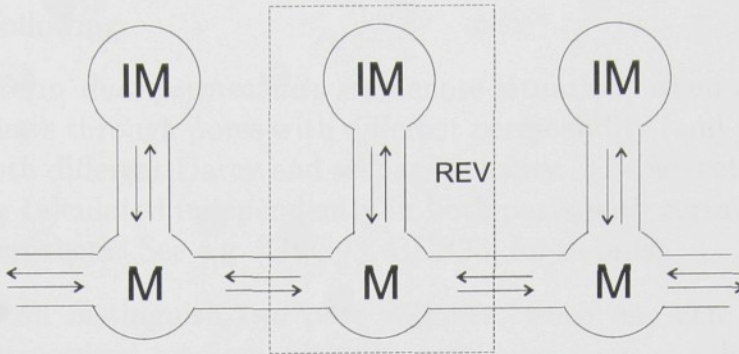
Figure 1.1: Two-region model. Communication structure of mobile and immobile pores at the level of the representative elementary volume (REV).

velocity is the major input parameter. The reason is improperly defined porosity with respect to the microscopic structure [BV90, ZB95].

In most cases, the problem can be solved by introducing the effective porosity, where we extract the part of pores which is fully isolated from others and cannot influence any process. This approach was mentioned in description of unsaturated media, section 1.1.2. This adjustment is in fact standard and we usually use the term porosity in the sense of effective porosity when dealing with Darcy velocity, seepage velocity and advection-dispersion process.

We obtain more general situation when considering the real microscopic velocities of the fluid. In the classical models, the pore structure is considered as "random" and the distribution of velocities in REV as well. As a consequence of the variations in velocity, the process of hydrodynamic dispersion is identified [BV90]; more precisely, by the homogenization in the REV we transform the microscopic advection and molecular diffusion to the macroscopic processes – advection by the (average) seepage velocity, molecular diffusion (with the coefficient modified by so called tortuosity) and hydrodynamic dispersion in addition, see (1.18). We will be now interested in a situation when the pore structure and velocity distribution is special – such a case we denote as structured porous media in contrast to the unstructured considered above in this paragraph.

There are several approaches how to describe the media with distinctly different pore structure, either distributed to the volume zone or in the sense of different properties in a different measure of observation. We refer mainly

to the two following:

- By a term *dual permeability* we denote situation, when a part of the fluid flows through pores with different permeability (and porosity) and has both different Darcy and seepage velocity. The advective transport is then calculated independently in both parts with certain interaction between them. See e.g. [GvG93, BER93] for details.

- If we can distinguish two pore volumes, when one can be described as unstructured medium with one particular seepage velocity and the second contains pores which are blind or almost blind with negligible water motion but not isolated from those with mobile water [CS64]. This model is called *dual porosity*, we identify the mobile pore zone and immobile pore zone at the level of REV, see Fig. 1.1. This is the approach we apply and study in this thesis.

The concept of dual-porosity media, namely the transport influenced by the interaction with zone of immobile water was introduced by [CS64] and further developed by e.g. [vGW76, CK77]. Quantification of the interaction process is described in section 1.3.3. We also remark (will be specified below) that this kind of dual-porosity model is mathematically equivalent to other interaction processes, as e.g. the sorption (section 1.3.2).

Dual-porosity models elsewhere

Beside the dual-porosity model for structured porous media, we can derive the dual-porosity model in the same sense for a different type of media and transport process: fractured rock, composed of highly permeable fractures and a matrix of porous blocks almost impermeable in comparison but with possible diffusion and accumulation. In this case, we have two levels of homogenization, first the porous medium of matrix regarded as continuum and then fracture structure regarded as continuum [Dou99, GvG93, BER93]. In the fracture rock modelling, this is an alternative to the structured approach when we consider statistical information about fracture orientation, sizes and crossing and the 2D flow in each fracture is calculated [Sev02].

Generalisations

We also mention further generalisation behind/over the dual-porosity (mobile-immobile) model presented here. Below we describe the mechanism of solute

exchange between the mobile and immobile pores as a non-equilibrium first order transfer process. More general models involving non-equilibrium processes of different physical character are discussed in e.g. [Bru91, NIS00]. In some cases, the variations in pore structure and microscopic velocity can be more complicated and the two zone approximation does not suffice to represent the process – a model with three zones instead of two ("triple" porosity) is introduced in [BR97].

In the text below, we will first describe the standard relations for flow and transport in unstructured (single-porosity) media and then their form in the dual-porosity media will be derived.

1.2   Equations of the fluid flow

1.2.1   General case (unsteady unsaturated)

We start with the general formulation of the fluid flow problem, where unsaturated zone is involved to the model and the problem is time dependent (see e.g.[BV90, ZB95, Kaz97]).

In fact, the problem is composed of two different processes with different quantities and governing equations: in saturated zone the situation is determined by the pressure (or piezometric head) and velocity, while in the unsaturated zone we have a description through variable saturation. The problem can be written in a compact form, if we extend a sense of the variable p (normally with positive values meaning the pressure) and express both the saturation in the unsaturated zone and the pressure in the saturated zone by p as a single variable with both positive and negative values. The negative values are connected with the saturation by the retention curve (1.8).

Using this notation we can define the motion equation (Darcy's law) jointly for the saturated and unsaturated zone, defining the hydraulic conductivity by (using (1.8) and (1.9))

$$\boldsymbol{K}(p) = \begin{cases} \boldsymbol{K} \cdot \dfrac{1}{\left(1 + \alpha_{\mathrm{vg}}|p|^{m_{\mathrm{vg}}}\right)^{3 \cdot \frac{m_{\mathrm{vg}}-1}{m_{\mathrm{vg}}}}} & p < 0 \\[4mm] \boldsymbol{K} & p \geq 0\,, \end{cases} \tag{1.10}$$

where $\boldsymbol{K}$ is the tensor of hydraulic conductivity of saturated medium. The

generalised Darcy's law has a form (Darcy–Buckingham law)

$$\boldsymbol{u} = -\boldsymbol{K} \cdot \nabla\phi = \boldsymbol{K}(p) \cdot (\nabla \frac{p}{\varrho g} + \nabla z)\,, \tag{1.11}$$

with $\boldsymbol{u}$ and p as unknown variables. The second governing equation expresses the mass balance

$$\frac{\partial \theta}{\partial t} + \nabla \cdot \boldsymbol{u} = q_s\,, \tag{1.12}$$

where q_s are fluid sources/sinks (external) and the first term (accumulating in the free pores) can be arranged using the retention curve (1.8) for θ to

$$C_w(p)\frac{\partial p}{\partial t} + \nabla \cdot \boldsymbol{u} = q_s\,, \tag{1.13}$$

where $C_w(p) = \frac{\partial \theta_e(p)}{\partial p}$ (the derivative of the retention curve) is called the water capacity. Substituting (1.11) into (1.13), we obtain so called Richards' equation.

In the equations above, we assumed both the water and the solid to be incompressible. In this case, the time-dependent term vanishes for $p > 0$, which means the second-order PDE obtained by a substitution of (1.11) into (1.13) would be elliptic for $p > 0$ while parabolic for $p < 0$ which causes many complication in the numerical treatment. A possible but only partly complication-avoiding way is to add a small constant to C_w which can be regarded e.g. as a compressibility of water or solid.

The numerical implementation of the unsteady flow problem described above has been realised, using the appropriately generalised form of the mixed-hybrid FEM described below. The formulation, application and tests of the model are presented [Fry02, MM00, HS00]. Even if the results were satisfactory in general, many problems arose concerning the relation of discretisation and values of parameters which strongly influenced the stability of iterations solving the non-linearity (in both generalised Darcy's law and mass balance equation).

Thus in this thesis we consider the fluid flow problem in the saturated domain (or, say, in the saturated part of the domain), which can be used as a good approximation in the practical problems.

We must also remark that the combination of capillary effect at the boundary of saturated and unsaturated zone and the distinction of mobile and immobile pores would be a very complicated problem.

1.2.2   Steady flow in saturated media

We reduce our interest to the problems in a fully saturated domain. In this case, we must automatically consider steady problems: the time-dependent term in (1.13) vanishes and also we easily imagine that the eventual changes in boundary conditions would take effect immediately in the whole domain.

The equations (1.11) and (1.13) then transform to the classical Darcy's law and mass balance equation, commonly presented ([BV90, Kaz97]).

The Darcy's Law in saturated porous media is

$$\boldsymbol{u} = -\boldsymbol{K} \cdot \nabla \phi = -\boldsymbol{K} \cdot (\nabla \frac{p}{\varrho g} + \nabla z) \,, \tag{1.14}$$

where $\boldsymbol{K}$ is hydraulic conductivity – it comprises the properties of both fluid and porous media, through

$$\boldsymbol{K} = \frac{\boldsymbol{k} \varrho g}{\mu} \,, \tag{1.15}$$

where μ is the dynamical viscosity of the fluid and $\boldsymbol{k}$ is the porous media permeability which is in general tensor for anisotropic media and a function of space coordinates for inhomogeneous media.

The mass balance equation for steady flow is

$$\nabla \cdot \boldsymbol{u} = q_s \,, \tag{1.16}$$

where q_s are sources/sinks of the fluid (volumetric flow rate), defined as injected/drawn fluid volume per unit time and unit volume of medium.

Substituting the first equation into the second, we would obtain a linear second order elliptic differential equation with one unknown function $\phi(\boldsymbol{x})$. For numerical transport calculation, this expression is not convenient, because the dual variable (velocity $\boldsymbol{u}$) is our interest and is to be calculated as accurate as possible, while by the numerical differentiation (from ϕ to $\boldsymbol{u}$) we lose accuracy. We use the numerical method based on a coupled system of two first order equations (1.14) and (1.16), which calculates the velocity directly (mixed and mixed-hybrid methods, see [KH90], [RT77] and the chapter 3 in this thesis).

1.3 Equations of the solute transport

1.3.1 Advection and dispersion

The basic solute transport mechanisms in porous media are advection and dispersion; see [BV90, Ben95, Kaz97, ZB95] for details. The unknown solute concentration $c(\boldsymbol{x}, t)$, function of space and time, is given by the advection-dispersion equation (ADE)

$$\frac{\partial c}{\partial t} + \nabla \cdot (c\boldsymbol{v}) - \nabla \cdot (\boldsymbol{D}\nabla c) = \frac{1}{n}(c^* q_s^+ + c q_s^-) \,, \qquad (1.17)$$

where $\nabla \cdot (c\boldsymbol{v})$ expresses the advection and $\nabla \cdot (\boldsymbol{D}\nabla c)$ expresses the hydrodynamic dispersion, which is in general anisotropic (transversal and longitudinal with respect to the direction of the fluid flow). The source term differs for drawing ($q_s > 0$), when the value of drawn concentration is the quantity calculated and injecting ($q_s < 0$), when the injected concentration c^* must be given.

The seepage velocity $\boldsymbol{v}(\boldsymbol{x})$ is a result of the fluid flow problem (1.14)-(1.16), for the given source/sink distribution q_s, adjusted as $\boldsymbol{v} = \frac{\boldsymbol{u}}{n}$, where n is appropriate value of porosity (standardly defined by (1.1) for unstructured media or the mobile porosity for dual-porosity media, see section 1.3.3).

The hydrodynamic dispersion coefficient $\boldsymbol{D}$ comprises both the molecular diffusion and the (mechanical) dispersion caused by microscopical inhomogeneity of the velocity field [BV90, ZB95]. It is expressed by

$$[\boldsymbol{D}]_{ij} = D_m T_{ij} + \alpha_T |\boldsymbol{v}| \, \delta_{ij} + (\alpha_L - \alpha_T) \frac{v_i \, v_j}{|\boldsymbol{v}|} \,, \qquad (1.18)$$

where D_m is the coefficient of molecular diffusion (scalar), $\boldsymbol{T}$ is the tortuosity (tensor), α_L and α_T are the longitudinal and transversal dispersivities (properties of the porous medium), δ_{ij} is the Kronecker delta and v_i, v_j are the respective components of the velocity vector $\boldsymbol{v}$.

The tortuosity $\boldsymbol{T} \equiv T_{ij}$ is a property of porous medium and expresses the effect of its structure to the molecular diffusion. For isotropic media, the tensor $\boldsymbol{T}$ is diagonal and we express $T_{ij} = \tau \delta_{ij}$ (while the mechanical dispersion is always anisotropic).

The complete description of the solute transport is much more complicated than stated above. Usually more chemical species is present in the

solution; than the concentration of each one is governed by the advection-dispersion equation and there are chemical reactions of various character among the single species. Furthermore, physical and chemical interactions with the solid phase of the porous medium must be taken into account. The processed connected with immobile pores are among them.

In the dual-porosity media, the transport in the mobile zone is governed by the equation (1.17). The velocity is determined by means of mobile porosity, see section 1.3.4.

1.3.2 Sorption

In the two-region model of the dual-porosity media, the mechanism and the mathematical description of the interaction process is similar to the sorption of the solute on the solid surface. In the context of numerical solution, we will refer to equivalent structure of the equations of transport with non-equilibrium sorption and transport with non-equilibrium mobile–immobile exchange. The significant difference is in the physical meaning of the constants in the equation, their identification, and also in the fact, that the sorption is often considered as non-linear, which bring more complications.

The sorption is determined by the sorbed concentration (e.g. solute mass par unit mass of the solid) and by the relation between the solute and sorbed concentration. The relation is given either by the function $c_s = f(c)$ for equilibrium (instant) sorption or by the dependence of sorbing rate (mass per unit time) on the concentration difference for the non-equilibrium sorption (rate-limited).

Typically, the sorption is quick process and can be approximated by the equilibrium model, while the mobile–immobile exchange is slow and the use of two unknown functions of concentration c_m and c_i and of the non-equilibrium interaction in the model is necessary.

The equilibrium sorption can be expressed by various functions, so called isotherms; the simplest example is the linear isotherm

$$c_s = K_D c, \qquad (1.19)$$

where K_D is called distribution coefficient. The non-linear isotherms are e.g. Freundlich and Langmuir, see [BV90, ZB95].

Considering the mass balance jointly in the solution and in the solid

phase, the advection-dispersion equation transforms to [ZB95, BV90, Ben95]

$$R\frac{\partial c}{\partial t} + \nabla \cdot (c\boldsymbol{v}) - \nabla \cdot (\boldsymbol{D}\nabla c) = \frac{1}{n}(q_s^+ c^* + q_s^- c)\,, \qquad (1.20)$$

where we introduced the retardation factor

$$R = 1 + \varrho_s K_D \frac{1-n}{n}\,, \qquad (1.21)$$

where ϱ_s is the density of the solid. From global point of view, the transport behaves like in the velocity field reduced by the factor R (slower), assuming $\boldsymbol{D}$ linearly dependent on $\boldsymbol{v}$, as in (1.18).

A relation of the same type holds for in our model of dual porosity between concentration in mobile and immobile pores for a limit case of immediate diffusion exchange. We will refer to this situation as the limit case of the non-equilibrium model (1.34) and when testing the model on example problems for full range of the rate coefficient (chapter 5, section 5.3.1).

1.3.3   Mobile–immobile diffusion transfer

Above, in the section 1.1.3, we defined the term dual porosity as the situation when a part of the pores contain immobile water. We will deal now with the solute transport in the dual-porosity media, more precisely in **two-region representation** of structured porous media.

The basic description of porous media solute transport (single porosity) is by one value of concentration per REV. Considering the blind pores, the concentration can be complex inhomogeneous on the microscopic level, see section 1.1.3. A possible representation is the two-region model (see also [CS64, CK77]): we define two zones, one including the mobile pores and one including the immobile ones and we work with one representative concentration in each (Fig. 1.1).

We denote the porosities

n_m ...   mobile (or active) porosity

$$n_m = \frac{\text{volume of mobile pores in REV}}{\text{volume of REV}}\,, \qquad (1.22)$$

n_i ...   immobile (or blind, inactive) porosity

$$n_i = \frac{\text{volume of immobile pores in REV}}{\text{volume of REV}} \qquad (1.23)$$

and by analogy the concentrations

$$c_m \dots \text{concentration in the mobile pore zone}, \\ c_i \dots \text{concentration in the immobile pore zone}. \tag{1.24}$$

The mechanism of mass transport at the microscopic level is the molecular diffusion. The model of two disjoint zones with strictly "discrete" values of concentration can appear slightly inconsistent with this mechanism, because the diffusion correspond to a gradient of concentration (continuously varying in the immobile zone). But considering the two-region model as a simplification, we represent the diffusion as a mass exchange between both the zones. Further, we will refer the process as the **mobile–immobile exchange**, rather then using the term diffusion.

It is quite complicated to exactly quantify the process, because of complicated distribution of concentration at the microscopic level and the geometry of pores which is difficult to identify. From global point of view (the two-region model) it is natural to assume the exchange intensity (or rate) to be proportional to the difference of the concentrations in both the pore zones. This way is consistent with the nature of the diffusion and commonly used in the literature [vGW76, CK77, VMVF97]. We express the transferred mass in unit volume of porous medium per unit time as

$$q_c^{\text{exch}} = \alpha(c_i - c_m), \tag{1.25}$$

where α [T^{-1}] is a coefficient dependent on both the solid structure and the solute properties. The sign of q_c is considered to be positive for transfer from the immobile to the mobile pores (i.e. positive source term in the advection-dispersion equation (1.17) describing the transport in the mobile pores, see (1.30)).

The value of the coefficient can be expressed by solution of diffusion problems at the microscopic scale with chosen porous media geometry, e.g. spheric solid grains or 1D blind channels. If it is not possible (in case of insufficient microscopic information), the value of the coefficient must be a subject of model calibration, together with the values n_m and n_i.

A simple formula for α can be constructed by the following consideration: We represent the structure of mobile and immobile pores as two volumes connected by a linear channel of length l and cross-section S. The diffusion flux in the channel is $q_c^{\text{diff}} = D_m \nabla c$ and the total transfer relative to the

volume of media V_{REV} can is

$$q_c^{\mathrm{exch}} = \frac{S q_c^{\mathrm{diff}}}{V_{\mathrm{REV}}} = \frac{S D_m \frac{c_m - c_i}{l}}{S l} = \frac{D_m}{l^2}(c_i - c_m) , \qquad (1.26)$$

where we identify

$$\alpha \sim \frac{D_m}{l^2} \qquad (1.27)$$

the "dimensional structure" of the coefficient: coefficient of molecular diffusion divided by a square of certain characteristic length. Several relations of this structure are presented in the literature, for various geometries, with additional dimensionless shape-factors [Bru91, VMVF97].

1.3.4 Equations of two-region non-equilibrium transport (complete model)

Now we derive the equations governing the mass transport in the two-region representation of dual-porosity media, coupling the advection-dispersion equation governing the transport in the mobile zone and the relation (1.25) for the mobile–immobile exchange.

The equations of water motion (Darcy's law (1.14) and mass balance equation (1.16)) have the same form for standard porous medium and for mobile zone of dual-porosity medium, as they are expressed by means of Darcy velocity and thus they do not explicitly contain the porosity. In case of ADE (1.17) we must consider that the only the mobile zone is concerned and use the mobile porosity n_m in place of n, i.e.

$$\frac{\partial c}{\partial t} + \nabla \cdot (c\boldsymbol{v}) - \nabla \cdot (\boldsymbol{D}\nabla c) = \frac{1}{n_m}(c^* q_s^+ + c q_s^-) , \qquad (1.28)$$

where the velocity is

$$\boldsymbol{v}(\boldsymbol{x}) = \frac{\boldsymbol{u}(\boldsymbol{x})}{n_m} . \qquad (1.29)$$

The mass exchange with the immobile zone in fact corresponds to an additional source/sink term in the ADE for the mobile zone. It is necessary to note, that the exchange flux is expressed relative to the total volume of porous media while the form (1.17) of ADE is expressed as a mass balance in the volume of mobile water. Therefore the exchange term (1.25) must

be divided by the mobile porosity, to fit as a source term in the transport equation. We obtain

$$\frac{\partial c_m}{\partial t} + \nabla \cdot (c_m \boldsymbol{v}) - \nabla \cdot (\boldsymbol{D} \nabla c_m) = \frac{1}{n_m}(c^* q_s^+ + c_m q_s^-) + \frac{1}{n_m}\alpha(c_i - c_m). \quad (1.30)$$

In the immobile zone, we simply express the mass balance, considering the mobile-immobile exchange as the only transfer process. Similarly as for the mobile zone, we use the form relative to the immobile water volume

$$\frac{\partial c_i}{\partial t} = -\frac{1}{n_i}\alpha(c_i - c_m). \quad (1.31)$$

The two coupled equations (1.30) and (1.31) form a system of two differential equations for two functions $c_m(\boldsymbol{x}, t)$ and $c_i(\boldsymbol{x}, t)$. The governing equations are often written in a different structure, when the first one expresses the mass balance jointly for both the mobile and immobile zone and the second one expresses the mass balance in the immobile zone (the same as above)

$$n_m \frac{\partial c_m}{\partial t} + n_i \frac{\partial c_i}{\partial t} = -\nabla \cdot (c_m \boldsymbol{u}) + n_m \nabla \cdot (\boldsymbol{D} \nabla c_m) + c^* q_s^+ + c_m q_s^- \quad (1.32)$$

$$n_i \frac{\partial c_i}{\partial t} = -\alpha(c_i - c_m), \quad (1.33)$$

see e.g. [vGW76].

There are special situations for limit values of the exchange coefficient α (see also section 1.3.5, eqn. (1.38)):

- For almost immediate mobile-immobile exchange[1] ($\alpha \to +\infty$), the system of equations can be transformed to a form mathematically equivalent with the common equation of transport with linear equilibrium sorption (1.20). Using the form (1.32)-(1.33) the first equation transforms to

$$(1 + \frac{n_i}{n_m})\frac{\partial c_m}{\partial t} + \nabla \cdot (c_m \boldsymbol{v}) - \nabla \cdot (\boldsymbol{D} \nabla c_m) = c^{k*} q_s^+ + c_m q_s^- \quad (1.34)$$

and the second one with the undefined term becomes redundant. We introduce the retardation factor $R_{\mathrm{MI}} = 1 + \frac{n_i}{n_m}$ relating to MIE having the same meaning as for the sorption, see (1.21).

---

[1]If we put $\alpha = +\infty$ and $c_i = c_m$, the term of inter-pore flux is therefore undefined, but has of course a real physical sense and a certain value (given by $\frac{\partial c_i}{\partial t}$).

- For very slow exchange ($\alpha \to 0$) the equations are "loosely" coupled and the first one is close to the plain advection-dispersion equation in the mobile zone. But in general we cannot simplify the model in this way, because the immobile zone will always take its effect, even if weak, but permanent in long time horizon.

Remark: transport of more chemical components. In practical problems, transport of more independent solutes is usually solved. If there are also chemical reactions among the solutes, the problem is very complicated. The model described in this thesis is implemented for more chemicals without interaction (but is open to add a module of chemical reactions in the future). We consider a transport of N_ℓ solutes indexed by ℓ (superscript) governed by N_ℓ independent systems of equations

$$\frac{\partial c_m^\ell}{\partial t} + \nabla \cdot (c_m^\ell \boldsymbol{v}) - \nabla \cdot (\boldsymbol{D}^\ell \nabla c_m^\ell) = c^{\ell*} q_s^+ + c_m^\ell q_s^- + \frac{1}{n_m} \alpha^\ell (c_i - c_m) \quad (1.35)$$

$$\frac{\partial c_i^\ell}{\partial t} = -\frac{1}{n_i} \alpha^\ell (c_i - c_m). \quad (1.36)$$

In the following chapters, we will omit the superscript and everything will be formulated for one solute because of readability (without loss of generality).

1.3.5 Identification of equilibrium/non-equilibrium by dimensionless number

When more physical processes act together, the ratio of significance of the single processes is usually expressed by dimensionless numbers. For advection-dispersion process, the Péclet number (Pe) is introduced [Hir91, ZB95]

$$\mathrm{Pe} = \frac{vl}{D}, \quad (1.37)$$

where v is characteristic velocity, l characteristic length and D the diffusion/dispersion coefficient. If Pe is close to zero, the process is dispersion-dominated, when $\mathrm{Pe} \gg 1$, the process is advection-dominated. For porous media, there two levels for comparison (see [BV90, ZB95] for details): On the microscopic level the molecular diffusion D_m and the characteristic dimension of pores is considered (as a consequence, this comparison gives an information about relative significance of molecular diffusion and mechanical

dispersion). On the macroscopic level, the average velocity, characteristic dimension of domain and hydrodynamic dispersion coefficient is considered; this comparison is useful for numerical calculation, because the approaches are different for advection-dominated and dispersion-dominated processes. For completeness' sake, we also refer to the *grid Péclet number* strictly relating to a numerical discretisation, see [ZB95, Hir91].

In the non-equilibrium model, the ratio of "strength" of advection and exchange is compared and we express how far from an equilibrium the system is. The appropriate dimensionless number is Damkohler number, denoted ω or Da, see e.g. [VMVF97, Bru91, TLvG93]. A common form is

$$\mathrm{Da} = \frac{\alpha L}{u}, \tag{1.38}$$

where α is the rate of mobile–immobile exchange, L a characteristic dimension in the domain and u the Darcy velocity $u = n_m v$. For large Da, the difference between c_m and c_i is small, the system is close to equilibrium and can be approximated by single equation with retardation factor. For small Da, the non-equilibrium is significant for the transport process from global point of view.

The approximation of the non-equilibrium by equilibrium in the case of fast exchange process is often referred as local equilibrium assumption (LEA), see e.g. [PV86], also introducing other criteria besides the Damkohler number.

1.4   Initial and boundary conditions

We discuss here the boundary conditions (BC) with respect to their physical meaning. The correct mathematical formulation of the initial and boundary-value problems for PDEs are given in the next chapter 2. For expressing the conditions, we use the notation Ω for the problem domain; the exact definition will be given also there.

Stating the boundary conditions so that they correctly represented the physical process at the boundary is very complicated in general. In fact, the domain of solution is rarely bounded in a real physical sense, the natural processes continue also behind the boundary we chose for determining our problem and its solution.

We often deal with two cases while choosing the boundary: The simplest case is a "singularity" in the space, e.g. existence of impermeable layer or

technical equipment having an exactly known effect. If we cannot identify such an object in some directions, we choose the boundary in a "safe" distance from the area of interest (e.g. a cloud of contamination), where the effect of the boundary to the process is negligible. We will refer this case as a "distant boundary".

1.4.1 Steady fluid flow problem

We construct the boundary conditions for the steady problem of the fluid flow in a saturated domain (1.14)-(1.16). In general, all three types typical for the 2nd-order PDEs are necessary to cover the possible cases of interaction of the domain with the surroundings.

We consider the problem domain denoted by Ω with a boundary $\Gamma \equiv \partial\Omega$ composed of three parts Γ_1, Γ_2, and Γ_3 (such that $\overline{\Gamma}_1 \cup \overline{\Gamma}_2 \cup \overline{\Gamma}_3 = \Gamma$), with respective types of BCs prescribed.

Dirichlet boundary condition

We obtain the Dirichlet BC when the pressure or piezometric head is prescribed at the boundary, i.e.

$$\phi(\boldsymbol{x}) = \phi_D(\boldsymbol{x}) \qquad \forall \boldsymbol{x} \in \Gamma_1 \tag{1.39}$$

for a given function $\phi_D(\boldsymbol{x})$ [L]. This condition is used when the studied domain adjoins to a water volume with free surface (i.e. that given piezometric head), like ponds or rivers. A second typical case is the "distant boundary", where we put the year-averaged value of water level and we assume that the artificial water operations are far enough from the boundary (or rather, we define the model boundary far from the place of interest).

Neumann boundary condition

In this case, we prescribe the flux though the boundary

$$\boldsymbol{u} \cdot \boldsymbol{\nu} = u_N(\boldsymbol{x}) \qquad \forall \boldsymbol{x} \in \Gamma_2, \tag{1.40}$$

where u_N is given flux $[\mathrm{L\,T^{-1}}]$ (Darcy velocity). We distinguish two physically different cases: homogeneous Neumann BC ($u_N = 0$) representing an impermeable boundary (usually a clay or rock bottom) and inhomogeneous Neumann BC representing e.g. the average precipitation dotations (from the top) or the operation of some special technical equipments.

Cauchy boundary condition

The Cauchy boundary condition is the general one, it fact comprising those two previous as a special case. We can understand it as representing a semi-permeable layer at the boundary. If the flux through the layer can be assumed proportional to the piezometric difference on the both sides, we derive

$$\boldsymbol{u} \cdot \boldsymbol{\nu} = \sigma \left(\phi - \phi_{\text{out}} \right) \qquad \text{in } \Gamma_3 , \tag{1.41}$$

where σ is the proportionality factor (in fact a conductivity of the layer, $\sigma = \frac{K}{\text{thickness}}$) and ϕ_{out} is a reference piezometric head, the state outside of the "boundary layer".

   This boundary condition is used either for representation of real semi-permeable boundary layers or for more precise representation of the "distant boundary" (mentioned above).

1.4.2   Two-region solute transport

Since the transport problem is time-dependent, we need both initial and boundary conditions. In addition, the structure of the conditions is also given by a non-standard character of the physical problem considered and of its mathematical representation – there will be a special care concerning the mobile and immobile zone separately necessary.

   In particular: we prescribe the initial condition for both unknowns c_m and c_i, while the boundary conditions are prescribed for the mobile concentration only. Physically, there is no macroscopical space interaction of the immobile zone (e.g. between the area inside and outside the boundary). Mathematically, we deal with a system of one partial and one ordinary differential equation.

   The boundary conditions are constructed the same as for the standard advection–dispersion problem (e.g. [BV90, Ben95, Kaz97]). Formulation of physically realistic BC is quite complicated; we consider here simplified forms, which in fact correspond to the advection-dominated problems.

Initial condition

We must prescribe the initial distribution of the concentration in the whole domain Ω. Theoretically, we can use two independent initial distributions for mobile and immobile zone, but technically it is impossible to obtain this

information by measurements. Moreover, the problems solved typically describe the process starting in naturally steady (equilibrium) conditions and some artificial operations (drawing wells etc.) change the equilibrium and start an developing-in-time process.

Since it does not bring any problems to the model formulation and implementation, we consider the more general conditions with two independent initial functions

$$c_m(\boldsymbol{x}, 0) = c_m^0(\boldsymbol{x}) \qquad \boldsymbol{x} \in \Omega, \tag{1.42}$$

$$c_i(\boldsymbol{x}, 0) = c_i^0(\boldsymbol{x}) \qquad \boldsymbol{x} \in \Omega, \tag{1.43}$$

where $c_m^0(\boldsymbol{x})$ and $c_i^0(\boldsymbol{x})$ are given functions, for the mobile and immobile zone respectively.

Dirichlet condition

Dirichlet BC corresponds to the concentration prescribed at the boundary. We define for a certain part of the boundary (we do not specify yet the coverage of the whole boundary Γ)

$$c_m(\boldsymbol{x}, t) = c_D(\boldsymbol{x}, t) \quad \forall x \in \Gamma_D, t \in \mathbb{R}^+, \tag{1.44}$$

where $c_D(\boldsymbol{x}, t)$ is a given function. The concentration is typically known (and must be known) in the water flowing from the outside to the domain of interest. In fact, there is a hidden assumption of advection-dominated transport – that the eventual dispersion flux in the upstream direction is zero. In other words, the concentration inside does not influence the concentration outside (which is required to be given and prescribed by c_D).

Neumann condition

In contrast to the flow problem, we do not have a correspondence of Neumann BC and prescribed-flux boundary for the advection-dispersion transport: the flux depends on both the concentration (advection part) and the derivatives of concentration (dispersion), which implies the Cauchy BC for the prescribed flux (see below).

We obtain the Neumann BC in a special case of separated information about the dispersion flux. This happens in two cases: First, the impermeable boundary when the total flux is zero and also both the advection flux

and dispersion flux are of course zero. Second, when the dispersion negligibly contributes to the total flux – we can apply this assumption in all the boundary where the fluid flows out from the domain. It means that the situation outside does not influence the process inside the domain for the advection-dominated transport. We can also approximately apply the assumption of zero dispersion flux at the "distant boundary" (see above) if the natural equilibrium state exist there.

The above description implies the homogeneous Neumann BC

$$(\boldsymbol{D}\nabla c) \cdot \boldsymbol{\nu} = 0 \quad \text{at } \Gamma_N , \ t \in \mathbb{R}^+ . \tag{1.45}$$

Cauchy boundary condition (remark)

In the basic form, the Cauchy BC represent the prescribed flux

$$(c\boldsymbol{v} + \boldsymbol{D}\nabla c) \cdot \boldsymbol{\nu} = q_c^{\text{bnd}} , \tag{1.46}$$

a sum of advection and dispersion flux. Typically, this type of BC is applied for the boundary expressed as a finite thickness layer and the flux q_c^{bnd} is expressed by a particular relation, e.g. (see [Kaz97]) by

$$q_c^{\text{bnd}} = \frac{D_m}{\text{thickness}} \left(c - c_{\text{external}} \right) - c_{\text{external}} \, u_{\boldsymbol{\nu}} , \tag{1.47}$$

where $u_{\boldsymbol{\nu}}$ is the normal projection of velocity through the boundary and we assume a well-mixed zone in the outside (constant concentration c_{external}).

Definition of the boundary division

As was said in the introduction above, we will use the boundary conditions in the simplified structure, corresponding to advection-dominated problems. We prescribe the inhomogeneous Dirichlet BC and homogeneous Neumann BC and the respective parts of the boundary will be defined by the orientation of flux (velocity) with respect to the boundary. To distinguish from the boundary division of the fluid flow problem, we introduce the notation $\Gamma = \overline{\Gamma}_{\text{in}} \cup \overline{\Gamma}_{\text{out}}$ with clear meaning, rather than the subscripts used above in this section (see also Fig. 2.1). We pose

$$\boldsymbol{v} \cdot \boldsymbol{\nu} < 0 \qquad \boldsymbol{x} \in \Gamma_{\text{in}} , \tag{1.48}$$

$$\boldsymbol{v} \cdot \boldsymbol{\nu} \geq 0 \qquad \boldsymbol{x} \in \Gamma_{\text{out}} , \tag{1.49}$$

where the impermeable boundary (homogeneous Neumann condition for both the fluid flow and solute transport problems) was included to the second inequality, as described above. In this context, we will use the notation c^{in} for the input concentration, instead of c_D corresponding to the Dirichlet condition.

This division is recalled in the section 2.2 concerning the proper mathematical formulation of the problem.

Chapter 2

Mathematical formulation

In this chapter we derive the mathematically complete formulation of the physical problems comprised in the model. The equations supplemented by boundary and initial conditions and the properties of the coefficients are specified. The model is derived separately for the fluid flow and for the multiprocess solute transport, both coupled by the function of velocity field $v(x)$.

The steady potential fluid flow problem is a boundary value problem of elliptic type. The solute transport with non-equilibrium exchange is a initial–boundary value problem with terms of various nature: hyperbolic, parabolic and ordinary-derivatives. Both the problems are solved in an identical space domain $\Omega \subset \mathbb{R}^3$ with a Lipschitz continuous boundary $\partial\Omega \equiv \Gamma$. Both the flow and transport problem contains mixed Dirichlet and Neumann boundary conditions, but the division of the boundary is different for the respective problems (Fig. 2.1).

2.1 Fluid flow problem

We consider the steady saturated porous media fluid flow problem, physically described by the Darcy's Law (1.14) and mass balance equation (1.16).

2.1.1 Classical formulation

We formulate the problem in a coupled form for both the (primal and dual) unknowns: piezometric head $\phi(x)$ and Darcy velocity $u(x)$. The problem is
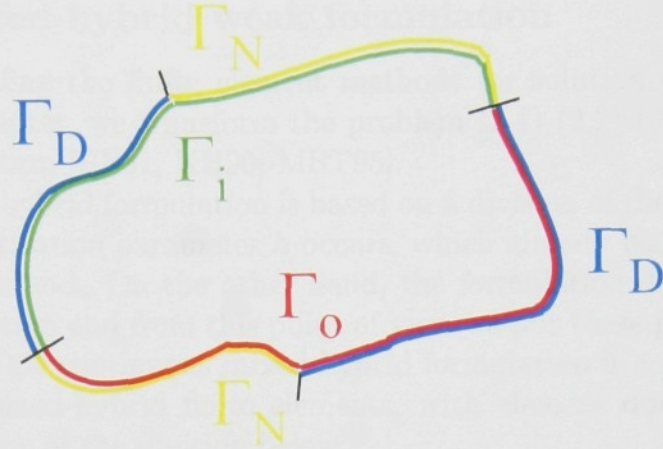
Figure 2.1: Demonstration of general non-matching division of the boundary into the Dirichlet and Neumann part for the flow problem (Γ_D and Γ_N) and for the transport problem (Γ_{in} and Γ_{out}).

given by a system of Darcy law and mass balance equation for $\boldsymbol{x} \in \Omega$

$$\boldsymbol{u} = -\boldsymbol{A}^{-1}\nabla\phi, \tag{2.1}$$
$$\nabla \cdot \boldsymbol{u} = q, \tag{2.2}$$

where q represents the density of fluid sources in the medium and $\boldsymbol{A}^{-1} \equiv \boldsymbol{K}$ is symmetric and uniformly positive definite second rank tensor of hydraulic permeability of the porous medium, i.e. there exists a positive constant a_0 such that

$$a_0\|\boldsymbol{\xi}\|_2^2 \leq (\boldsymbol{A}^{-1}(\boldsymbol{x})\boldsymbol{\xi}, \boldsymbol{\xi}) \tag{2.3}$$

holds for all $\boldsymbol{\xi} \in \mathbb{R}^3$ and almost all $\boldsymbol{x} \in \Omega$. Further we assume $[\boldsymbol{A}^{-1}(\boldsymbol{x})]_{ij} \in L_\infty(\Omega)$ for all $i,j \in \{1,2,3\}$. The tensor $\boldsymbol{A}$ (the inverse of permeability $\boldsymbol{K}$) means resistance and we prefer its use (instead of permeability) because of further mixed-hybrid formulation.

The boundary condition are given in a mixed form, we divide the boundary into two parts $\Gamma = \overline{\Gamma}_D \cup \overline{\Gamma}_N$ such that $\Gamma_D \cap \Gamma_N = \emptyset$. The respective Dirichlet and Neumann boundary conditions are given by

$$\phi = \phi_D \quad \text{on} \quad \Gamma_D, \tag{2.4}$$

$$\boldsymbol{u} \cdot \boldsymbol{\nu} = -\boldsymbol{A}^{-1}\nabla p \cdot \boldsymbol{\nu} = u_N \quad \text{on} \quad \Gamma_N, \tag{2.5}$$

where $\boldsymbol{\nu}$ is the outward normal vector defined (almost everywhere) on the boundary $\partial\Omega \equiv \Gamma$.

2.1.2   Mixed-hybrid weak formulation

In order to define the finite element methods for solution of the problem in the next chapter, we transform the problem (2.1)-(2.2)-(2.4)-(2.5) to the mixed-hybrid form [BF91, KH90, MRT95].

The mixed-hybrid formulation is based on a division of the domain Ω and "latent" discretisation parameter h occurs, which already resembles a use of a numerical method. On the other hand, the formulation does not contain any approximation and from this point of view we put these paragraphs into this chapter. This continuous mixed-hybrid formulation is a preparation for defining the mixed-hybrid finite elements, with element domains identical with subdomains of the division below.

We denote by $\mathcal{E}_h$ the set of subdomains of the domain Ω, such that for all e holds

(i) $\qquad\qquad\qquad\qquad\quad \overline{\Omega} \;=\; \cup_{e \in \mathcal{E}_h} \overline{e}\;,$

(ii) $\qquad\qquad\qquad\quad e_i \cap e_j \;=\; \emptyset\;,\;\; \text{if}\;\; i \neq j\;,$

(iii) $\quad e \in \mathcal{E}_h$ is open subset of Ω with a piecewise smooth boundary ∂e

and by Γ_h the set of faces of subdomains $e \in \mathcal{E}_h$ which are not adjacent to the boundary $\partial\Omega_D$,

$$\Gamma_h = \cup_{e \in \mathcal{E}_h} \partial e - \partial\Omega_D\;. \tag{2.6}$$

The discretisation parameter h is defined by (see e.g. [Cia78])

$$h = \max_{e \in \mathcal{E}_h}\{\text{diam } e\}. \tag{2.7}$$

Next, we denote the restriction of any function on subdomain $e \in \mathcal{E}_h$ by the superscript e, i.e. $\phi^e = \phi|_e$.

The weak formulation is based on Lebesgue and Sobolev spaces [Rek99]. We introduce the special spaces used for the mixed-hybrid formulation, defined on the subdivisions $\mathcal{E}_h$ and Γ_h.

Let $\boldsymbol{H}(div, \mathcal{E}_h)$ be the space of square integrable vector functions $\boldsymbol{v} \in \boldsymbol{L}_2(\Omega)$, whose divergences are square integrable on every subdomain $e \in \mathcal{E}_h$, i.e.

$$\boldsymbol{H}(div, \mathcal{E}_h) = \{\boldsymbol{w} \in \boldsymbol{L}_2(\Omega); \; \nabla \cdot \boldsymbol{w}^e \in L_2(e), \; \forall e \in \mathcal{E}_h\} \tag{2.8}$$

with the norm given as

$$\| \boldsymbol{w} \|_{div, \mathcal{E}_h} = \left(\| \boldsymbol{w} \|_{0,\Omega}^2 + \sum_{e \in \mathcal{E}_h} \| \nabla \cdot \boldsymbol{w}^e \|_{0,e}^2 \right)^{\frac{1}{2}}. \tag{2.9}$$

We consider also the space of traces

$$H_D^{\frac{1}{2}}(\Gamma_h) = \{\mu : \Gamma_h \to R;\ \exists \varphi \in H_D^1(\Omega),\ \mu = \gamma_h \varphi\}, \qquad (2.10)$$

where the space $H_D^1(\Omega)$ is defined as $H_D^1(\Omega) = \{\varphi \in H^1(\Omega);\ \gamma \varphi = 0 \text{ on } \partial\Omega_D\}$ and $\gamma\varphi = \varphi|_{\partial\Omega}$ is the trace of the function $\varphi \in H^1(\Omega)$ on the boundary $\partial\Omega$; $\gamma_h \varphi = \varphi|_{\Gamma_h}$ is the trace of the function $\varphi \in H^1(\Omega)$ on the structure of faces Γ_h. The space $H_D^{\frac{1}{2}}(\Gamma_h)$ is equipped with the norm

$$\| \mu \|_{\frac{1}{2},\Gamma_h} = \inf_{\varphi \in H_D^1(\Omega)} \{|\varphi|_{1,\Omega};\ \gamma_h \varphi = \mu \text{ on } \Gamma_h\}, \qquad (2.11)$$

where $|\varphi|_{1,\Omega}$ denotes the seminorm $|\varphi|_{1,\Omega} = (\nabla\varphi, \nabla\varphi)_{0,\Omega}^{\frac{1}{2}}$.

We finally note that there is no need to define a special "$\mathcal{E}_h$-type" of the Lebesgue space $L_2(\Omega)$, by the construction above we would obtain the same space $L_2(\Omega)$.

To obtain the mixed-hybrid formulation, we integrate the equations (2.1) and (2.2) over each subdomain e, apply the Green's formula in a standard manner and express the flux continuity on coinciding faces of subdomain with Lagrange multipliers into a third equation. The spaces introduced above are the appropriate domains for the unknown velocities, piezometric heads and face piezometric heads (a physical meaning of the Lagrange multipliers λ, μ) such that all the integrals exist (see also [OL77], [KH90]).

Thus, the mixed-hybrid formulation of the problem (2.1), (2.2) with boundary conditions (2.4), (2.5) and the discretisation $\mathcal{E}_h$ of the domain Ω can be stated as follows:

Find $(\boldsymbol{u}, \phi, \lambda) \in \boldsymbol{H}(div, \mathcal{E}_h) \times L_2(\Omega) \times H_D^{\frac{1}{2}}(\Gamma_h)$ such that:

$$\sum_{e \in \mathcal{E}_h} \{ (\boldsymbol{A}\boldsymbol{u}^e, \boldsymbol{w}^e)_{0,e} - (\phi^e, \nabla \cdot \boldsymbol{w}^e)_{0,e} + \langle \lambda^e, \boldsymbol{\nu}^e \cdot \boldsymbol{w}^e \rangle_{\partial e \cap \Gamma_h} \} \qquad (2.12)$$

$$= \sum_{e \in \mathcal{E}_h} \langle \phi_D^e, \boldsymbol{\nu}^e \cdot \boldsymbol{w}^e \rangle_{\partial e \cap \partial\Omega_D}, \quad \forall \boldsymbol{w} \in \boldsymbol{H}(div, \mathcal{E}_h),$$

$$- \sum_{e \in \mathcal{E}_h} (\nabla \cdot \boldsymbol{u}^e, \psi^e)_{0,e} = - \sum_{e \in \mathcal{E}_h} (q^e, \psi^e)_{0,e}, \quad \forall \psi \in L_2(\Omega), \qquad (2.13)$$

$$\sum_{e \in \mathcal{E}_h} \langle \boldsymbol{\nu}^e \cdot \boldsymbol{u}^e, \mu^e \rangle_{\partial e} = \sum_{e \in \mathcal{E}_h} \langle u_N^e, \mu^e \rangle_{\partial e \cap \partial\Omega_N}, \quad \forall \mu \in H_D^{\frac{1}{2}}(\Gamma_h). \qquad (2.14)$$

In the next chapter, we define the finite-element approximation of the equations above.

2.2 Non-equilibrium solute transport problem

We consider a classical formulation of the problem. In the space domain $\Omega \subset \mathbb{R}^3$ with appropriate regularity and time domain $\mathbb{R}_0^+ \equiv [0, +\infty)$, we solve the system of equations

$$\frac{\partial c_m}{\partial t} + \nabla \cdot (c_m \boldsymbol{v}) - \nabla \cdot (\boldsymbol{D}\nabla c_m) = c^* q_s^+ + c_m q_s^- + \frac{1}{n_m}\alpha(c_i - c_m) \quad (2.15)$$

$$\frac{\partial c_i}{\partial t} = -\frac{1}{n_i}\alpha(c_i - c_m), \quad (2.16)$$

for the unknowns

$$c_m(\boldsymbol{x}, t), \; c_i(\boldsymbol{x}, t) \qquad \boldsymbol{x} \in \Omega, \; t \in \mathbb{R}_0^+ . \quad (2.17)$$

Depending on the direction of velocity with respect to the boundary, we define two parts of boundary $\partial\Omega \equiv \Gamma$, one corresponding to the inflow boundary and one corresponding to the outflow boundary, where the Dirichlet and Neumann conditions respectively will be prescribed – see the section 1.4.2 for physical argumentation. We define $\Gamma = \overline{\Gamma}_{\text{in}} \cup \overline{\Gamma}_{\text{out}}$ such that $\Gamma_{\text{in}} \cap \Gamma_{\text{out}} = \emptyset$ and

$$\boldsymbol{v} \cdot \boldsymbol{\nu} < 0 \qquad \boldsymbol{x} \in \Gamma_{\text{in}}, \quad (2.18)$$

$$\boldsymbol{v} \cdot \boldsymbol{\nu} \geq 0 \qquad \boldsymbol{x} \in \Gamma_{\text{out}}, \quad (2.19)$$

where $\boldsymbol{\nu}$ is the outward normal to the boundary and in the second case also the impermeable boundary (isolated) was involved. We assume that the function $\boldsymbol{v}(\boldsymbol{x})$ has enough regularity so that the partitioning is possible to be done.

The boundary conditions are

$$c_m(\boldsymbol{x}, t) = c_m^{\text{in}}(\boldsymbol{x}, t) \qquad \boldsymbol{x} \in \Gamma_{\text{in}}, \quad (2.20)$$

$$\boldsymbol{D}\nabla c_m(\boldsymbol{x}, t) \cdot \boldsymbol{\nu} = 0 \qquad \boldsymbol{x} \in \Gamma_{\text{out}}, \quad (2.21)$$

while no boundary condition is prescribed for $c_i(\boldsymbol{x}, t)$ because it is bound to an in fact ordinary differential equation (2.16). The conditions used represent the simplified model for the advection-dominated process: both express the state when no dispersion mass flux through the boundary occurs.

The initial conditions are prescribed for both the unknown in the whole domain

$$c_m(\boldsymbol{x}, 0) = c_m^0(\boldsymbol{x}) \qquad \boldsymbol{x} \in \Omega, \tag{2.22}$$
$$c_i(\boldsymbol{x}, 0) = c_i^0(\boldsymbol{x}) \qquad \boldsymbol{x} \in \Omega, \tag{2.23}$$

where $c_m^0(\boldsymbol{x})$ and $c_i^0(\boldsymbol{x})$ are given functions (initial distribution of the contaminant). In most problems, both the functions are identical as we consider an equilibrium state at the beginning.

The problem requires the following parameters to be given:

$$\alpha(\boldsymbol{x}), \ n_m(\boldsymbol{x}), \ n_i(\boldsymbol{x}), \ \boldsymbol{D}(\boldsymbol{x}, \boldsymbol{v}), \tag{2.24}$$
$$c^*(\boldsymbol{x}) \text{ in places, where } q_s > 0, \tag{2.25}$$

all considered as inhomogeneous but uniformly bounded by positive bounds, whereas we are not interested if the requirement is necessary or not (it is automatically fulfilled for discrete values of real problems).

Remark on existence and uniqueness of solution

Analysis of existence and uniqueness of solution (well-posedness) for the problems above (fluid flow and mass transport) is not a subject of this thesis. Concerning the fluid flow, the question is in fact solved: the existence and uniqueness of the classical formulation (section 2.1.1) is a classical result in PDEs, see e.g. [Rek95]; for the mixed-hybrid formulation (section 2.1.2), the well-posedness is proven in [Mar94a]. The analysis of the problem of transport with mobile–immobile exchange (section 2.2) is a subject of recent work, e.g. the uniqueness is presented in [KO00] (for more general problem with also non-linear equilibrium sorption involved).

Chapter 3

Numerical solution

We derive now numerical methods for solution of the physical problems of flow and transport (or their precise mathematical forms in the chapter 2). Since we deal with composed problem (water flow and various mechanisms of solute transport including the non-equilibrium interaction), there are two requirements on the numerical methods used: to efficiently solve each of the process and to be compatible in the sense that the methods can be used together without additional interface. Also, we consider the requirement on the implementation and computational cost in order to be applicable for large problems with complex geometry.

We applied the mixed-hybrid FEM approximation of the fluid flow problem, the method presented in [MRT95], which came right for the solution of underground hydraulic problems. For the solute transport, we used an original approach to combination of the processes of mobile–immobile exchange and advection (below), turning to account the analytical solution of the split MIE problem. At the moment, we narrowed our interest to this reduced problem (advection and MIE), although the possibility of inclusion of the dispersion is clear. The reason is to better show the functionality of the numerical approach and moreover, this approximation confirmed to be sufficient for real-world problems with strong uncertainty in parameters (chapter 6).

3.1   Model structure – Choice of methods

We will discuss the present approaches for solution of potential fluid flow problem, advection–dispersion problem and the ADE coupled with kinetic (non-equilibrium) interaction. There is extensive literature dealing with the numerical methods for fluid dynamics and solute transport, from both the mathematical and applicational point of view (e.g. [ZB95, Hir91] and references below). Variants of two basic methods for PDEs are discussed: the finite element method (FEM) [Cia78] and the finite volume method (FVM) [EGH00], both able to be implemented on general unstructured mesh geometry.

Fluid Flow

Taking into account the steady case and saturated domain, i.e. linear elliptic problem, the solution methods are in fact differently sophisticated and accurate variants of FEM and FVM (with in fact similar background [CR91, Hir91]), always finally leading to a solution of a system of linear algebraic equations.

In general, the FVM is algorithmically simpler but needs the special care for inhomogeneous anisotropic coefficients, e.g. [ABBM98]. In contrast, FEM can better handle the inhomogeneity for the cost of higher complexity [Mar94b]. We must also reduce our interest to methods complying the mass balance in calculation of velocities, which is necessary for connection with the numerical solution of advection problem.

Mixed and hybrid methods in FEM were introduced to comply that requirements [BF91, KH90, RT77, OL77, MRT95]. Moreover, a large experience in implementing the method for other problems by the cooperating team (in the past) was a great advantage [Mar94b, MMSŠ00, Fry02] and mainly the possibility to use tailored matrix solvers developed at the Institute of Computer Science (ICS) of the Academy of Sciences of the Czech Republic [MRT00, BKT01].

In the "continuous" form, the used method stands on three functions, representing the pressure, velocity and side pressures, with a regularity L_2, H^1 and L_2 respectively. In the discrete (approximating) form, the unknowns are approximated by element-wise constant, element-wise linear and side-wise constant base functions (in the order above). The solved variables relating to velocities have a meaning of fluxes through the element sides; these values

are the desired output as they can be directly used by the FVM upwind advection scheme (below), if the geometrically identical mesh is used.

Advection-dispersion transport

Searching for a suitable method for solving the ADE has been one of the main interests of numerical mathematics in the last decades, with the results brought together e.g. in the monographs [Mor96, Kaz97, Hir91, PL01]. The principal difficulty in the solution comes from the coupling of the hyperbolic character of the advection and parabolic character of the dispersion, each requiring a different numerical approach. Next, since we deal with the time-dependent (initial value) problem, it automatically means further necessary care for stability.

In the terms of FDM (FVM and FEM often adopt the approaches and behaviour known at FDM [Hir91, ZB95]), the classical approach is the use of either upwind or central flux approximation scheme, each having the well-known troubles: numerical dispersion or artificial oscillations respectively. The existence of one of the undesired behaviour mentioned is typical for most of the more sophisticated schemes of higher order or with some ways of compensation [CGMZ76, Mor96]. The next thing of discussion is time discretisation and related stability conditions and choice of implicit/explicit method. Implicit methods provide better stability, but in practical problems only for separate dispersion are applicable [Hir91, MMS96]: the presence of advection leads to a non-symmetric matrix, which solution can be very difficult for large systems.

A natural way how to handle the "antagonism" of advection and dispersion is the method of operator splitting [CM80, KL98, KLN+01, DR82, Fro02]. The ADE is split into two equations, leading to a possible use of independent numerical methods of advection and dispersion with better optimization for each process, namely lagrangian methods for the advection.

Extensive study was performed on the lagrangian methods (particle-tracking; in contrast to the eulerian considered above) for the advection, in connection with the operator splitting [DR82, KvK01]. The methods in general can work well if the mesh and velocity field are in good correspondence [CFH99], in particular if we always move exactly to the mesh points with the time steps. Otherwise, due to the necessary interpolation, the same problems of numerical dispersion or oscillation appear (depending on the order of interpolation) [Fro02], but with substantial advantage of absence of

the time-step-restricting stability condition.

In the submitted thesis, we do not intend to improve the methods for calculation of advection and dispersion. For the implementation we use a basic approximation of advection, we regard it as a background for showing the use of operator splitting and the analytical method for MIE (below), whose combination is the original result of the author.

The advection is solved by explicit upwind scheme in FVM, which provides mass balance even in the simplest cell-centred approximation. This kind of discretisation is appropriate for transport in complex groundwater velocity field resulted from numerical computations and thanks to the low computational cost, it is applicable for large systems (even if limited by the stability condition and time step constraint).

Mobile–immobile exchange

Various new methods and improvements have been done for the transport with additional interactions in the ADE. The effort is aimed to both the non-linear equilibrium ([KvK01]) or non-equilibrium (mostly linear yet) models. The problems based on kinetic/non-equilibrium two-region or two-site model have been numerically solved quite recently. The common way of using Laplace transform FEM [XB95] is compared with other approaches in [GPG96]. The methods proposed are quite complicated as they consider the equations with all the terms of ADE, (with expected consequence in troubles for uncommon combinations of coefficients). An idea of separation of the advection-dispersion and kinetic exchange was presented by [vK96]: to the result on non-interacting transport calculation (by any method for ADE) is applied and analytically expressed integral transform reflecting the non-equilibrium interaction during the time-interval calculated.

In contrast with the method of [vK96], we apply the standard method of operator-splitting for ADE, considering the non-equilibrium exchange as one of the split processes, turning to account a possibility of simple analytical solution of the problem of exchange. The transport problem is solved in time steps and in each time step the processes of advection, dispersion and MIE are successively calculated. In this sense, the presented approach admits a use of any numerical method for advection and dispersion working with a fixed mesh.

The operator splitting is applied for separation of adsorption processes in the recent work of other authors, in [KF02] the problem of non-linear equi-
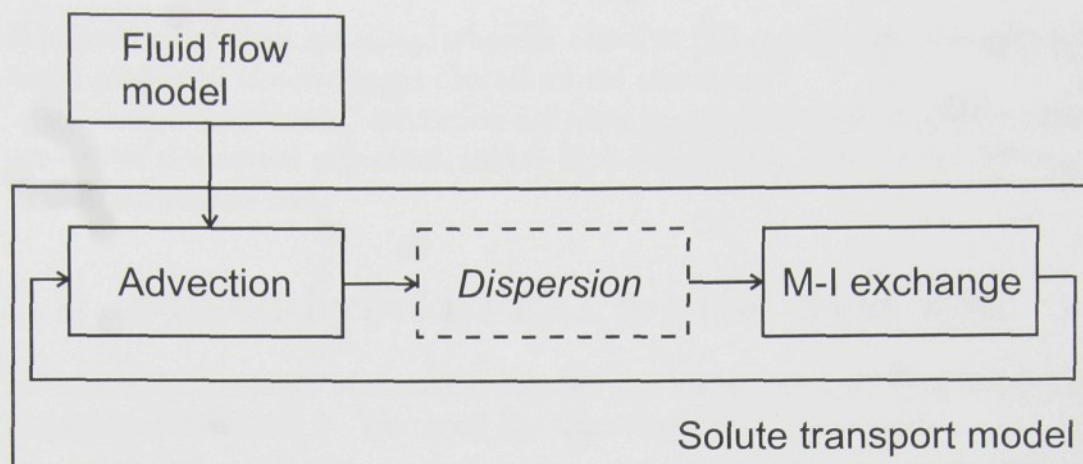
Figure 3.1: The scheme of the overall model structure: communication of the flow and transport model and operator splitting in the transport model.

librium adsorption is solved and in [Rem03] the non-equilibrium non-linear case. Due to the necessary special care for the non-linearity, the methods are limited to specific small-scale problems.

Proposed model structure

The structure of the model (communication of the numerical methods for each process) is schematically expressed by Fig. 3.1. The results of the fluid flow model (velocities or fluxes) are the input values for calculation of the advection. The solute transport model is composed of three parts, sequentially running in a time-loop according to the principle of the operator splitting.

As specified below, there is a joint discretisation mesh for all the parts, in the flow model representing the finite elements, in the transport model representing the finite volumes. The discrete values of fluxes resulting from the MH-FEM are directly used as the input value in the scheme (3.81), which is convenient when operating with large unstructured meshes.

The operator splitting (section 3.3) is formulated for the general problem of advection, dispersion and mobile–immobile exchange. For practical realisation, we considered simpler model, containing only the advection and the exchange and particular methods of solution are discussed for these two processes (sections 3.5 and 3.6). In this way, we demonstrate a function of

this kind of process splitting, whereas a use of full model with dispersion is also possible in the proposed overall model structure.

The models of "pure" advection are often a sufficient approximation of the advection-dispersion processes, taking into account the substantial difference in computational cost.

3.2   Mixed-hybrid FEM for the fluid flow

We solve the problem of steady saturated porous media fluid flow defined in the previous chapter 2. We recall the **classical form** (2.1)–(2.5)

$$\boldsymbol{u} = -\boldsymbol{A}^{-1}\nabla\phi, \tag{3.1}$$

$$\nabla \cdot \boldsymbol{u} = q, \tag{3.2}$$

for the unknowns $\boldsymbol{u}(\boldsymbol{x})$ and $\phi(\boldsymbol{x})$, $\boldsymbol{x} \in \Omega$, with boundary conditions

$$\phi = \phi_D \quad \text{on} \quad \Gamma_D, \tag{3.3}$$

$$\boldsymbol{u} \cdot \boldsymbol{\nu} = -\boldsymbol{A}^{-1}\nabla p \cdot \boldsymbol{\nu} = u_N \quad \text{on} \quad \Gamma_N, \tag{3.4}$$

where $\partial\Omega = \overline{\Gamma}_D \cup \overline{\Gamma}_N$ and $\boldsymbol{\nu}$ is the outward normal of the boundary and the **mixed-hybrid formulation** for the unknowns $(\boldsymbol{u}, \phi, \lambda) \in \boldsymbol{H}(\text{div}, \mathcal{E}_h) \times L^2(\Omega) \times H_D^{\frac{1}{2}}(\Gamma_h)$:

$$\sum_{e\in\mathcal{E}_h}\{(\boldsymbol{A}\boldsymbol{u}^e, \boldsymbol{w}^e)_{0,e} - (\phi^e, \nabla\cdot\boldsymbol{w}^e)_{0,e} + \langle\lambda^e, \boldsymbol{\nu}^e\cdot\boldsymbol{w}^e\rangle_{\partial e\cap\Gamma_h}\} \tag{3.5}$$

$$= \sum_{e\in\mathcal{E}_h}\langle\phi_D^e, \boldsymbol{\nu}^e\cdot\boldsymbol{w}^e\rangle_{\partial e\cap\partial\Omega_D}, \quad \forall\boldsymbol{w} \in \boldsymbol{H}(\text{div}, \mathcal{E}_h),$$

$$-\sum_{e\in\mathcal{E}_h}(\nabla\cdot\boldsymbol{u}^e, \psi^e)_{0,e} = -\sum_{e\in\mathcal{E}_h}(q^e, \psi^e)_{0,e}, \quad \forall\psi \in L_2(\Omega), \tag{3.6}$$

$$\sum_{e\in\mathcal{E}_h}\langle\boldsymbol{\nu}^e\cdot\boldsymbol{u}^e, \mu^e\rangle_{\partial e} = \sum_{e\in\mathcal{E}_h}\langle u_N^e, \mu^e\rangle_{\partial e\cap\partial\Omega_N}, \quad \forall\mu \in H_D^{\frac{1}{2}}(\Gamma_h), \tag{3.7}$$

where the spaces $\boldsymbol{H}(\text{div}, \mathcal{E}_h)$ and $H_D^{\frac{1}{2}}(\Gamma_h)$ were defined by (2.8) and (2.10) respectively.

Now we define the finite-element approximation of the mixed-hybrid formulation with the lowest-order base function. To express the approximation

of the $\boldsymbol{H}(\mathrm{div}, \mathcal{E}_h)$ we need to consider a particular shape of the element. We briefly mention the necessary facts concerning the element shape and mesh structure, a detailed description will be given together with the description of the model implementation (section 4.1).

3.2.1 Discretisation of the domain

We assume in general the domain Ω to be a polyhedron. In this section, we consider that the domain is subdivided into a system of trilateral prismatic subdomains e (coincident with the subdivision, which the continuous mixed-hybrid formulation is based on), each having vertical lateral faces and non-horizontal bases.

For real-world problems, it is necessary to consider more general shapes to appropriately discretise edges of the model boundary and an irregular structure geological layers. In section 4.1 we define degenerate elements for the mentioned prisms, where either one or two couples of points connected by a vertical edge merge (Fig. 4.1).

We will assume that the mesh is strongly regular, i.e. there exists a positive constant ζ independent of the mesh $\mathcal{E}_h$, such that

$$\max_{e \in \mathcal{E}_h} \frac{h_e}{\rho_e} \leq \zeta,\qquad(3.8)$$

where $h_e = \mathrm{diam}\, e$ and ρ_e denote the maximum radius of a ball inside the element e.

We assume the discretisation is compatible with the boundary conditions prescribed, i.e. both Γ_D and Γ_N are unions of some faces of elements $e \in \mathcal{E}_h$ (we recall h the discretisation parameter (2.7)).

3.2.2 Approximation spaces

The velocity function $\boldsymbol{u}(\boldsymbol{x}) \in \boldsymbol{H}(\mathrm{div}, \mathcal{E}_h)$ will be approximated with the vector functions linear on each element $e \in \mathcal{E}_h$.

We first define the approximation functions on a single element. For each element face, we can define a vector function whose flux through that face is equal to one and through the other faces is zero. Thus we have a five-dimensional Raviart-Thomas space for each element

$$\boldsymbol{RT}^0(e) = \{\boldsymbol{w}^e \mid \boldsymbol{w}^e(\boldsymbol{x}) = \sum_{i=1}^{5} \beta_j \boldsymbol{w}_j^e(\boldsymbol{x}),\ \boldsymbol{x} \in e\},\qquad(3.9)$$

where $\beta_j \in \mathbb{R}$ are the coefficients of linear combination and $\boldsymbol{w}_j^e$ are the base function determined by the condition of flux

$$\int_{f_j^e} \boldsymbol{\nu}_j^e \cdot \boldsymbol{w}_i^e dS = \delta_{ij}, \quad i,j = 1, \ldots, 5 \, . \tag{3.10}$$

Here f_j^e denotes the j-th face of the element e and $\boldsymbol{\nu}_j^e$ its outward normal vector (with respect to the element e). The system of functional equations (3.10) generates the unique set of base vector functions $\boldsymbol{w}_i^e$ as proven in [Mar94a].

Considering the prismatic element shape used for the implementation (chapter 4, Fig. 4.1 and Fig. 4.3), we can parametrically express the base functions in the following way:

$$\boldsymbol{w}_1^e = k_1^e \begin{bmatrix} 0 \\ 0 \\ x_3 - \alpha_{13}^e \end{bmatrix}, \ \boldsymbol{w}_2^e = k_2^e \begin{bmatrix} 0 \\ 0 \\ x_3 - \alpha_{23}^e \end{bmatrix},$$

$$\boldsymbol{w}_3^e = k_3^e \begin{bmatrix} x_1 - \alpha_{31}^e \\ x_2 - \alpha_{32}^e \\ \gamma_3^e x_3 - \alpha_{33}^e \end{bmatrix}, \boldsymbol{w}_4^e = k_4^e \begin{bmatrix} x_1 - \alpha_{41}^e \\ x_2 - \alpha_{42}^e \\ \gamma_4^e x_3 - \alpha_{43}^e \end{bmatrix}, \boldsymbol{w}_5^e = k_5^e \begin{bmatrix} x_1 - \alpha_{51}^e \\ x_2 - \alpha_{52}^e \\ \gamma_5^e x_3 - \alpha_{53}^e \end{bmatrix},$$

where the coefficients α_{ij}^e, γ_i^e, and k_i^e have to be determined by the above property of unique flux through the corresponding face (3.10).

Now we can define the approximation space of functions on the whole domain Ω (the system $\mathcal{E}_h$ more precisely) as a combination of the functions on each element. The Raviart-Thomas space (see also [RT77])

$$\boldsymbol{RT}_{-1}^0(\mathcal{E}_h) = \{\boldsymbol{w}_h \in \boldsymbol{L}^2(\Omega) \mid \boldsymbol{w}_h^e \in \boldsymbol{RT}^0(e), \forall e \in \mathcal{E}_h\} \tag{3.11}$$

is a space of vector functions linear on each element, an approximation of $\boldsymbol{H}(\text{div}, \mathcal{E}_h)$. We note that in the case of nonparallel bases, these functions are not continuous across the inter-element boundaries Γ_h and thus not necessarily contained in $\boldsymbol{H}(\text{div}, \Omega)$.

The definition of approximation spaces for the piezometric head $\phi(\boldsymbol{x}) \in L_2(\Omega)$ and for the trace of piezometric head on faces (Lagrange multiplier) $\lambda \in H_D^{\frac{1}{2}}(\Gamma_h)$ will be relatively simpler. Both will be approximated by element-wise or face-wise constant function respectively. We denote $M^0(e \text{ or } f)$ a

space of constant functions either on an element or on a face, i.e. with the base functions of the form

$$\varphi(\boldsymbol{x}) = 1\,, \quad \boldsymbol{x} \in e \text{ or } f\,. \tag{3.12}$$

Then the space of element-wise constant functions for piezometric head is defined by

$$M_{-1}^0(\mathcal{E}_h) = \{\psi_h \in L_2(\Omega) \,|\, \psi_h^e \in M^0(e),\, \forall e \in \mathcal{E}_h\}\,. \tag{3.13}$$

The space of face-wise constant functions for the piezometric head on a face is defined by

$$M_{-1}^0(\Gamma_h) = \{\mu_h : \Gamma_h \to R \,|\, \mu_h^f \in M^0(f),\, \forall f \in \Gamma_h\}\,. \tag{3.14}$$

Finally we express the discrete representation of boundary conditions. For both Dirichlet and Neumann BC we define the approximation by piece-wise constant functions $\phi_{D,h}$ and $u_{N,h}$ from the space $M_{-1}^0(\partial\Omega)$. The functions must satisfy

$$\int_f (\phi_{D,h} - \phi_D)dS = 0 \quad \forall f \in \Gamma_D\,, \tag{3.15}$$

$$\int_f (u_{N,h} - u_N)dS = 0 \quad \forall f \in \Gamma_N\,, \tag{3.16}$$

where ϕ_D and u_N are the boundary conditions of the original problem (3.1)–(3.4).

3.2.3 Discrete formulation

We obtain the discrete MH-FEM formulation of the problem expressing the system of equation (3.5)–(3.7) in the finite-dimensional approximation spaces $\boldsymbol{RT}_{-1}^0(\mathcal{E}_h)$, $M_{-1}^0(\mathcal{E}_h)$ and $M_{-1}^0(\Gamma_h)$ instead of the original $\boldsymbol{H}(\mathrm{div}, \mathcal{E}_h)$, $L_2(\Omega)$ and $H_D^{\frac{1}{2}}(\Gamma_h)$.

The problem is given by the following system of equations for the triplet of unknowns

$$(\boldsymbol{u}_h, \phi_h, \lambda_h) \in \boldsymbol{RT}_{-1}^0(\mathcal{E}_h) \times M_{-1}^0(\mathcal{E}_h) \times M_{-1}^0(\Gamma_h) : \tag{3.17}$$

$$\sum_{e\in\mathcal{E}_h}\{(\boldsymbol{A}\boldsymbol{u}_h,\boldsymbol{w}_h)_{0,e}-(\phi_h,\nabla\cdot\boldsymbol{w}_h)_{0,e}+\langle\lambda_h,\boldsymbol{\nu}^e\cdot\boldsymbol{w}_h\rangle_{\partial e\cap\Gamma_h}\}$$

$$=\sum_{e\in\mathcal{E}_h}\langle\phi_{D,h},\boldsymbol{\nu}^e\cdot\boldsymbol{w}_h\rangle_{\partial e\cup\Gamma_D}\quad\forall\boldsymbol{w}_h\in\boldsymbol{RT}^0_{-1}(\mathcal{E}_h)\,,\qquad(3.18)$$

$$-\sum_{e\in\mathcal{E}_h}(\nabla\cdot\boldsymbol{u}_h,\psi_h)_{0,e}=-(q_h,\psi_h)_{0,\Omega}\quad\forall\psi_h\in M^0_{-1}(\mathcal{E}_h)\,,\qquad(3.19)$$

$$\sum_{e\in\mathcal{E}_h}\langle\boldsymbol{\nu}^e\cdot\boldsymbol{u}_h,\mu_h\rangle_{\partial e}=\langle u_{N,h},\mu_h\rangle_{\Gamma_N}\quad\forall\mu_h\in M^0_{-1}(\Gamma_h)\,,\qquad(3.20)$$

where the boundary conditions are incorporated by functions $\phi_{D,h}$ and $u_{N,h}$ and by the choice of Γ_h.

Expressing the integrals (scalar products) in the system (3.18)–(3.20) for the base functions, we obtain an equivalent system of linear algebraic equation with a specific structure. First, we introduce some necessary additional notations:

We define a numbering of the elements $e_j\in\mathcal{E}_h$, $j=1,\dots,J$ covering the domain Ω, i.e. $\bigcup_{j=1}^{J}\overline{e}_j=\overline{\Omega}$. Since we have five base functions $\boldsymbol{w}^e_i$ for each element e, the space $\boldsymbol{RT}^0_{-1}(\mathcal{E}_h)$ is $(5J)$-dimensional and we denote $I=5J$ and a numbering of the base functions $\boldsymbol{u}_i$, $i=1,\dots,I$. Finally we numerize the inter-element and boundary faces: we consider Γ_h a system of faces f_k, $k=1,\dots,K$.

We express the approximation functions $\boldsymbol{u}_h$, ϕ_h, and λ_h as a span of the base functions in the form

$$\boldsymbol{u}_h(\boldsymbol{x})=\sum_{i\in I}U_i\boldsymbol{w}_i(\boldsymbol{x}),\qquad\phi_h(\boldsymbol{x})=\sum_{j\in J}\Phi_j\psi_j(\boldsymbol{x}),\ \boldsymbol{x}\in\Omega,\qquad(3.21)$$

$$\lambda_h(\boldsymbol{x})=\sum_{k\in K}\Lambda_k\mu_k(\boldsymbol{x}),\ \boldsymbol{x}\in\Gamma_h\,,\qquad(3.22)$$

where we introduced the coefficients U_i, Φ_j, and Λ_k, which will be the unknown of the algebraic system and their physical meaning is clear: U_i is the flux over the correspondent face (i-th), Φ_j is the piezometric head in the center of j-th element and Λ_k is the piezometric head in the center of k-th face in Γ_h.

We denote the algebraic structures

$$U=(U_1,\dots,U_I)^T,\ \Phi=(\Phi_1,\dots,\Phi_J)^T,\ \Lambda=(\Lambda_1,\dots,\Lambda_K)^T\qquad(3.23)$$

and

$$\mathbb{A}_{ij} = (\boldsymbol{A}\boldsymbol{w}_i, \boldsymbol{w}_j)_{0,\Omega} \qquad i = 1, \ldots, I, \; j = 1, \ldots, I\,, \qquad (3.24)$$

$$\mathbb{B}_{ij} = -(\nabla \cdot \boldsymbol{w}_i, 1)_{0,e_j} \qquad i = 1, \ldots, I, \; j = 1, \ldots, J\,, \qquad (3.25)$$

$$\mathbb{C}_{ik} = \langle \boldsymbol{\nu}_k \cdot \boldsymbol{w}_i, 1 \rangle_{f_k} \qquad i = 1, \ldots, I, \; k = 1, \ldots, K\,. \qquad (3.26)$$

Concerning (3.26), we must specify the orientation of the outward normal $\boldsymbol{\nu}_k$. We naturally define it to be outward with respect to the element corresponding to the support of the base function $\boldsymbol{w}_i$. We easily see that $\mathbb{B}_{ij}$ and $\mathbb{C}_{ik}$ express the topology of the system, they contain either zeros or ones depending on the correspondence of elements, faces and base functions. The matrix $\mathbb{A}_{ij}$ contain the physical information – the resistance of the medium and is block-diagonal with 5×5 blocks corresponding to the elements.

The right-hand side vector is composed of three parts

$$[q_1]_i = -\langle p_{D,h}, \boldsymbol{\nu}_i \cdot \boldsymbol{v}_i \rangle_{\partial\Omega_D} \qquad i = 1, \ldots, I\,, \qquad (3.27)$$

$$[q_2]_j = -(q, 1)_{0,e_j} \qquad j = 1, \ldots, J\,, \qquad (3.28)$$

$$[q_3]_k = \langle u_{N,h}, 1 \rangle_{f_k} \qquad k = 1, \ldots, K\,. \qquad (3.29)$$

where the outward normal $\boldsymbol{\nu}_i$ is understood as in (3.26).

Substituting the base functions into the system (3.18)–(3.20) and using the notation just above, we derive the linear algebraic system

$$\begin{pmatrix} \mathbb{A} & \mathbb{B} & \mathbb{C} \\ \mathbb{B}^T & & \\ \mathbb{C}^T & & \end{pmatrix} \begin{pmatrix} U \\ \Phi \\ \Lambda \end{pmatrix} = \begin{pmatrix} q_1 \\ q_2 \\ q_3 \end{pmatrix}. \qquad (3.30)$$

As a consequence of the symmetry and positive definiteness of the permeability and resistance tensors (2.3), the matrix block $\mathbb{A}$ is also symmetric positive definite (SPD). For $\partial\Omega_D \neq \emptyset$ the matrix $(\mathbb{B}|\mathbb{C}) \in R^{I,J+K}$ defined by (3.25) and (3.26) has full column rank, i.e. $\mathrm{rank}(\mathbb{B}|\mathbb{C}) = J + K$, for proof we refer to [MRT95]. Thus the algebraic system (3.30) has a unique solution.

Overall, the matrix in (3.30) is symmetric and indefinite (and of course sparse, as typical for the discretisations of PDEs). Methods for solving this type of system are discussed e.g. in [MRT00]. The solver used in our computations is based on Schur-complement reduction and conjugate gradient method, tailored for the specific matrix structure (3.30) (author M. Tůma, Institute of Computer Science, Academy of Sciences of the Czech Republic).

Some further information concerning the implementation of the mixed-hybrid flow model and the user interface are given in chapter 4.

3.3   Operator splitting for the system of transport equations

We first define the operator-splitting (OS) time discretisation for the general problem of advection-dispersion-exchange (ADX) transport (2.15)–(2.16). In the next subsection, we formulate a simplified problem, whose numerical solution is described and realised – as stated in the introduction, we solve the problem of advection and exchange as a first approximation and test of suitability of the OS method for non-equilibrium exchange.

3.3.1   Definition of OS for the general ADX problem

The system of equations governing the transport (2.15)–(2.16) can be written in a transparent operator form. When we define the couple of unknown concentrations

$$c = \begin{pmatrix} c_m \\ c_i \end{pmatrix},$$
(3.31)

we can write

$$\frac{\partial c}{\partial t} = \mathcal{A}(c) + \mathcal{D}(c) + \mathcal{X}(c),$$
(3.32)

where the operators of advection $\mathcal{A}$, dispersion $\mathcal{D}$ and exchange $\mathcal{X}$ are defined as follows

$$\mathcal{A}(c) = \begin{pmatrix} -\nabla \cdot (c_m v) + c^* q^+ + c_m q^- \\ 0 \end{pmatrix},$$
(3.33)

$$\mathcal{D}(c) = \begin{pmatrix} -\nabla \cdot (D \nabla c_m) \\ 0 \end{pmatrix},$$
(3.34)

$$\mathcal{X}(c) = \begin{pmatrix} \dfrac{1}{n_m} \alpha \left(c_i - c_m \right) \\ -\dfrac{1}{n_i} \alpha \left(c_i - c_m \right) \end{pmatrix},$$
(3.35)

and the initial and boundary conditions stay in the unchanged form.

To split the processes mentioned to separate equations (see [KL98, CM80, KLN+01]), we consider a time discretisation with constant steps Δt (without loss of generality):

$$t_n = n \cdot \Delta t \quad n \in \mathbb{N}.$$
(3.36)

The solution of the equation (3.32) in an interval $[t_n; t_{n+1}]$ can be replaced by a successive solution of the following initial value problems:

1. $\dfrac{\partial}{\partial t} c_A = \mathcal{A} c_A \qquad c_A(t_n, \boldsymbol{x}) = \boldsymbol{c}(t_n, \boldsymbol{x})\,,$ (3.37)

$c_A(t_{n+1}, \boldsymbol{x}) \overset{\mathrm{df}}{=} \mathcal{A}_{\Delta t}\, c_A(t_n, \boldsymbol{x})\,,$

2. $\dfrac{\partial}{\partial t} c_D = \mathcal{D} c_D \qquad c_D(t_n, \boldsymbol{x}) = c_A(t_{n+1}, \boldsymbol{x})\,,$ (3.38)

$c_D(t_{n+1}, \boldsymbol{x}) \overset{\mathrm{df}}{=} \mathcal{D}_{\Delta t}\, c_D(t_n, \boldsymbol{x})\,,$

3. $\dfrac{\partial}{\partial t} c_X = \mathcal{X} c_X \qquad c_X(t_n, \boldsymbol{x}) = c_D(t_{n+1}, \boldsymbol{x})\,,$ (3.39)

$c_X(t_{n+1}, \boldsymbol{x}) \overset{\mathrm{df}}{=} \mathcal{X}_{\Delta t}\, c_X(t_n, \boldsymbol{x})\,,$

4. $\boldsymbol{c}(t_{n+1}, \boldsymbol{x}) := c_X(t_{n+1}, \boldsymbol{x})\,.$

The solution in an arbitrary time step can be expressed by a symbolic notation of "solution operators" in this way:

$$\boldsymbol{c}(t_n, \boldsymbol{x}) = \left[\mathcal{X}_{\Delta t} \circ \mathcal{D}_{\Delta t} \circ \mathcal{A}_{\Delta t} \right]^n \boldsymbol{c}_0(\boldsymbol{x})\,,$$ (3.40)

where $\boldsymbol{c}_0 = \binom{c_m^0}{c_i^0}$ is the initial condition of the overall transport problem (see (2.22) and (2.23)). We remark not to confuse the notation of the "differential" operators $\mathcal{A}, \mathcal{D}, \mathcal{X}$ and the "solution" (evolution) operators $\mathcal{A}_{\Delta t}, \mathcal{D}_{\Delta t}, \mathcal{X}_{\Delta t}$; using the notation of [KL98], their relation is

$$\mathcal{A}_{\Delta t} = \exp(\Delta t \mathcal{A}) \quad \text{and by analogy for } \mathcal{D} \text{ and } \mathcal{X}$$ (3.41)

and the use of the OS method is in fact a representation the following arrangement (approximation) of the exponential function

$$\exp(\Delta t(\mathcal{A} + \mathcal{D} + \mathcal{X})) \approx \exp(\Delta t \mathcal{A}) \exp(\Delta t \mathcal{D}) \exp(\Delta t \mathcal{X})\,,$$ (3.42)

where the solution of (3.32) without use of OS is on the left-hand side.

This OS time discretisation is general in the sense that an arbitrary methods of solution of the split problems (3.37–3.39) can be used, e.g. both numerical and analytical.

Boundary conditions

An important and non-trivial matter are the boundary conditions for the split problems (3.37–3.39). In general, we cannot simply use the boundary

conditions of the original unsplit problem, because we could lose the well-posedness.

If we consider our advection–dispersion-exchange problem with simplified boundary conditions (as stated in 1.4.2 by (1.44)-(1.44) and recalled (2.20)–(2.21)), we can derive the boundary conditions for the split problems by physical consideration. We deal with a boundary composed of inflow Γ_{in} and outflow (involving the isolated) Γ_{out} with a Dirichlet and Neumann boundary conditions respectively:

$$c_m(\boldsymbol{x}, t) = c_m^{\mathrm{in}}(\boldsymbol{x}, t) \qquad \boldsymbol{x} \in \Gamma_{\mathrm{in}}, \tag{3.43}$$

$$\boldsymbol{D}\nabla c_m(\boldsymbol{x}, t) \cdot \boldsymbol{\nu} = 0 \qquad \boldsymbol{x} \in \Gamma_{\mathrm{out}}, \tag{3.44}$$

where Γ_{in} and Γ_{out} are distinguished by the sign of $\boldsymbol{v} \cdot \boldsymbol{\nu}$ (see above (2.18)–(2.19)). Both the conditions express the fact, that the mass is transferred through the boundary by advection only (which is a natural expectation for advection-dominated problems). In fact, the Dirichlet boundary condition on Γ_{in} implies the validity of the homogeneous Neumann BC (3.44) also on the part Γ_{in} (no dispersion flux against the incoming advection). Thus we can define the following BCs for the split problems:

$$\frac{\partial}{\partial t}\boldsymbol{c}_A = \mathcal{A}\boldsymbol{c}_A \quad \text{with} \quad \begin{cases} c_m(\boldsymbol{x}, t) = c_m^{\mathrm{in}}(\boldsymbol{x}, t) \text{ in } \Gamma_{\mathrm{in}} \\ \text{nothing prescribed in } \Gamma_{\mathrm{out}}, \end{cases} \tag{3.45}$$

$$\frac{\partial}{\partial t}\boldsymbol{c}_D = \mathcal{D}\boldsymbol{c}_D \quad \text{with} \quad \boldsymbol{D}\nabla c_m(\boldsymbol{x}, t) = 0 \text{ in } \Gamma_{\mathrm{in}} \cup \Gamma_{\mathrm{out}}. \tag{3.46}$$

Of course, there are no boundary conditions for the unknown immobile concentration $c_i(\boldsymbol{x}, t)$ and for the split problem of exchange (3.39), $\frac{\partial}{\partial t}\boldsymbol{c}_X = \mathcal{X}\boldsymbol{c}_X$, because the ODEs and initial values problems only are concerned. It physically expresses the fact, that there is no macroscopic space communication in the immobile pore zone (see also section 1.4.2).

3.3.2 Split equations of the numerical model

We rewrite the split equations (3.37–3.39) in the detailed form and define the problems as will be numerically solved in the following two sections 3.5 and 3.6. In contrast to the previous subsection, where the full problem of ADX was considered, we solve the problem of advection and MIE only (without

dispersion) as stated in the preamble of this chapter, i.e.

$$\frac{\partial c_m}{\partial t} + \nabla \cdot (c_m \boldsymbol{v}) = c^* q_s^+ + c_m q_s^- + \frac{1}{n_m} \alpha (c_i - c_m) \tag{3.47}$$

$$\frac{\partial c_i}{\partial t} = -\frac{1}{n_i} \alpha (c_i - c_m), \tag{3.48}$$

with boundary condition

$$c_m(\boldsymbol{x}, t) = c_m^{\text{in}}(\boldsymbol{x}, t) \qquad \boldsymbol{x} \in \Gamma_{\text{in}} \equiv \{ x \in \Gamma \mid \boldsymbol{v} \cdot \boldsymbol{\nu} < 0 \} \tag{3.49}$$

and initial conditions (2.22)-(2.23).

According to the notation of the split problem above, we denote

$$\boldsymbol{c}_A = \begin{pmatrix} c_m^A \\ c_i^A \end{pmatrix} \quad \text{and} \quad \boldsymbol{c}_X = \begin{pmatrix} c_m^X \\ c_i^X \end{pmatrix}. \tag{3.50}$$

In the time step (t_n, t_{n+1}), the two problems below are solved in sequence:

The advection problem   is given by the system of equations

$$\frac{\partial c_m^A}{\partial t} = -\nabla (\boldsymbol{v} \cdot c_m^A) + c^* q_s^+ + c_m^A q_s^- \tag{3.51}$$

$$\frac{\partial c_i^A}{\partial t} = 0 \tag{3.52}$$

with boundary condition

$$c_m^A(\boldsymbol{x}, t) = c_m^{\text{in}}(\boldsymbol{x}, t) \qquad \boldsymbol{x} \in \Gamma_{\text{in}}, \ t \in (t_n, t_{n+1}) \tag{3.53}$$

and initial conditions ($\forall \boldsymbol{x} \in \Omega$)

$$c_m^A(\boldsymbol{x}, t_n) = \begin{cases} c_m^0(\boldsymbol{x}) & \text{for } n = 0 \\ c_m(\boldsymbol{x}, t_n) & \text{for } n \geq 1, \end{cases} \tag{3.54}$$

$$c_i^A(\boldsymbol{x}, t_n) = \begin{cases} c_i^0(\boldsymbol{x}) & \text{for } n = 0 \\ c_i(\boldsymbol{x}, t_n) & \text{for } n \geq 1, \end{cases} \tag{3.55}$$

where we distinguished between the initial condition of the problem solved ($n = 0$) and result of the previous step of the OS time discretisation ($n \geq 1$). We denote the results of the advection problem solution

$$c_m^A(\boldsymbol{x}, t_{n+1}) \quad \text{and} \quad c_i^A(\boldsymbol{x}, t_{n+1}), \tag{3.56}$$

where trivially holds $c_i^A(\boldsymbol{x}, t_{n+1}) = c_i^A(\boldsymbol{x}, t_n)$ in the immobile zone.

The exchange problem   is given by the system of equations

$$\frac{\mathrm{d}c_m^X}{\mathrm{d}t} \;\; = \;\; \frac{1}{n_m}\alpha(c_i^X - c_m^X)\,, \tag{3.57}$$

$$\frac{\mathrm{d}c_i^X}{\mathrm{d}t} \;\; = \;\; -\frac{1}{n_i}\alpha(c_i^X - c_m^X)\,, \tag{3.58}$$

where we use ordinary derivatives instead of partial of the original equation system. The initial conditions are

$$c_m^X(\boldsymbol{x}, t_n) \;\; = \;\; c_m^A(\boldsymbol{x}, t_{n+1})\,, \tag{3.59}$$

$$c_i^X(\boldsymbol{x}, t_n) \;\; = \;\; c_i^A(\boldsymbol{x}, t_{n+1})\,, \tag{3.60}$$

where $\boldsymbol{x} \in \Omega$.

The final solution of the time step concerned is given by

$$c_m(\boldsymbol{x}, t_{n+1}) \;\; := \;\; c_m^X(\boldsymbol{x}, t_{n+1}) \tag{3.61}$$

$$c_i(\boldsymbol{x}, t_{n+1}) \;\; := \;\; c_i^X(\boldsymbol{x}, t_{n+1}) \tag{3.62}$$

for $\boldsymbol{x} \in \Omega$ and the time point named.

3.4   Finite-volume space discretisation

We define the finite volume discretisation for the transport problem (3.47)-(3.48) (advection and MIE). Both the split problems above will be solved using joint space discretisation and joint discrete values (no interpolation).

We will use the standard cell-centred finite volume method (FVM), where the unknown quantity is represented by values in centres of cells (see [Hir91, EGH00] for details). The volumes (cells) are geometrically identical with the finite elements used in the flow model, thus we can directly use the values of fluid flux through cell sides (discrete results provided by the MH-FEM flow model, section 3.2) in the upwind scheme of advective transport (section 3.5).

The space discretisation is thus primarily tailored for the solution of the split advection problem (in fact, also the time discretisation to comply the stability condition, see section 3.5.2), while for the split problem of mobile–immobile exchange has a secondary importance. Since the scheme for MIE (below) is constructed from analytical solution of the problem, there are no

special requirements on the space discretisation. It handles values associated with a space point without regard if these are discrete values or values of a continuous problem in the point.

In this chapter, we describe the method without regard to the topology of space discretisation, for arbitrary polyhedral cell shape. The formulation for a particular mesh shapes and topology is not essentially different and some implementation-specific points are discussed in the chapter 4.

3.4.1   Definition of finite volumes

First we define the system of discrete volumes (cells) covering the problem domain Ω [EGH00]. We denote $\mathcal{K}$ the set of subdomains V_k such that

$$\bigcup_{V_k \in \mathcal{K}} \bar{V}_k = \bar{\Omega} \quad \text{and} \tag{3.63}$$

$$V_j \cap V_k = \emptyset \quad \forall V_j, V_k \in \mathcal{K}, \, j \neq k \,, \tag{3.64}$$

where V_k is understood both as a cell itself (a set) and as a volume of the cell (in cubic meters), depending on the context.

For practical reasons, we pose some common additional requirements on the system $\mathcal{K}$ concerning the boundary conditions (BC) and source/sink function. We assume, that the boundary between different type of BC matches the boundaries between cells V_k. In the case of sources and sinks, each particular cell V_k contains either source or sink only.

We consider the cell-centered representation, which means that the unknown concentration is approximated by one value C_m^k assigned with each discretisation cell V_k, i.e. we either regard C_m^k as a mean value of c_m in the volume V_k

$$C_m^k = \frac{1}{V_k} \int\limits_{V_k} c_m \mathrm{d}V \tag{3.65}$$

or we consider the C_m^k as an approximation of c_m by a cell-wise constant function (in the style of "finite elements' " base functions). In the two region transport model, we deal with two discrete values associated with each cell V_k: mobile concentration C_m^k and immobile concentration C_i^k.

To define the numerical scheme clearly and for precise incorporating of the fluxes (results of the MH fluid flow model), we consider the domain Ω to be a polyhedron and the cells $V_k \in \mathcal{K}$ with the following properties (in all the text below):

- each volume V_k is a polyhedron,

- the faces match so that each face is either part of the boundary or is joint for just two cells,

- the compatibility of the discretisation with boundary conditions is automatically fulfilled as the division between Γ_{in} and Γ_{out} is defined by the discrete results of the fluid flow problem.

We consider the mesh as unstructured: we index the cells by the single counter k and we define the index set of neighbour cells N_k for each V_k (the set of cells having joint face with V_k, but N_k contains numbers).

Further we define the notations for discrete values of other quantities in the equations and resume:

C_m^k mobile concentration in the cell V_k

C_i^k immobile concentration in the cell V_k

U_{jk} flux from V_j to V_k through the joint face (volume per area and time)

$$U_{jk} = \int\limits_{\overline{V}_j \cap \overline{V}_k} \boldsymbol{v} \, \mathrm{d}\boldsymbol{S} \quad \text{(outward normal with respect to } V_j)$$

Q_k^- total sink flux in V_k, i.e. $Q_k^- = \int_{V_k} q_s^-$ or $Q_k^- = 0$ if sources exist in V_k

Q_k^+ total source flux in V_k, i.e. $Q_k^+ = \int_{V_k} q_s^+$ or $Q_k^+ = 0$ if sinks exist in V_k

3.4.2 Operator splitting in the space-discrete form

Now we also incorporate the notation for the time discretisation to the discrete values of unknowns. In contrast with the notation of split problems (superscripts A and X), we introduce the common clear notation of "substeps": in a particular time step $(t_n; t_{n+1})$, the point n means the initial value, the point $n + \frac{1}{2}$ means the result of the first split problem (advection) after the time Δt, and the point $n + 1$ means the result of the second split problem (MIE) after the time Δt:

$$C_{m,i}^n \quad \sim \quad c_{m,i}^A(., t_n) \,, \tag{3.66}$$

$$C_{m,i}^{n+\frac{1}{2}} \quad \sim \quad c_{m,i}^A(., t_{n+1}) = c_{m,i}^X(., t_n) \,, \tag{3.67}$$

$$C_{m,i}^{n+1} \quad \sim \quad c_{m,i}^X(., t_{n+1}) \,. \tag{3.68}$$

Compiling the notations of space and time discretisation, we can schematically express the calculation in the following way:

$$\boxed{C_m^{k,n}, \ C_i^{k,n}} \overset{\text{advection}}{\to} \boxed{C_m^{k,n+\frac{1}{2}}, \ C_i^{k,n+\frac{1}{2}}} \overset{\text{exchange}}{\to} \boxed{C_i^{k,n+1}, \ C_i^{k,n+1}}, \quad (3.69)$$

where we recall k the cell index, m and i denote the mobile and immobile zone. We remark that $C_i^{n+\frac{1}{2}} = C_i^n$, due to no advection in the immobile pores).

This full determination of the value is rarely necessary. For readability, we will use only the notation significant in the context, e.g.

$$C_k^n \equiv C_m^{k,n} \tag{3.70}$$

in the advection calculation (in the mobile zone only) and

$$C_m^n \equiv C_m^{k,n}, \ C_i^n \equiv C_i^{k,n} \tag{3.71}$$

in the exchange calculation (when a single particular cell is considered).

3.5 Calculation of advective transport

3.5.1 Numerical scheme

We derive the explicit scheme with upwind flux approximation, which is the basic approach for problems of advection type (1st-order hyperbolic) and complies with the physical nature of the problem [Hir91, ZB95, Kaz97].

First we express the finite volume formulation of the advection equation

$$\frac{\partial c_m}{\partial t} = -\nabla(\boldsymbol{v} \cdot c_m) + c^* q_s^+ + c_m q_s^- . \tag{3.72}$$

Integrating over arbitrary discrete volume V_k and using standard treatment by the Gauss' theorem, we obtain[1]

$$\frac{\partial}{\partial t} \int_{V_k} c_m \mathrm{d}V = -\int_{\partial V_k} c_m \boldsymbol{v} \cdot \mathrm{d}\boldsymbol{S} + \int_{V_k} (c^* q_s^+ + c q_s^-) \mathrm{d}V , \tag{3.73}$$

---

[1]In fact, the physical derivation of the equation start for the integral form (3.73) (on elementary volume) and we obtain the equation (3.72) by a reverse procedure.

where all the terms now have to be approximated by discrete values in mesh points.

The space integrals are immediately represented by the cell-centred values of concentrations and source/sink intensities (according to the simplified notation (3.70))

$$
\int_{V_k} c_m \mathrm{d}V = V_k C_k \,, \qquad \int_{V_k} c_m q_s^- \mathrm{d}V \approx V_k C_k Q_k^- \,, \qquad \int_{V_k} c_m^* q_s^+ \mathrm{d}V \approx V_k \tilde{C}_k Q_k^+ \,,
$$

$$(3.74)$$

where $\tilde{C}_k$ represents the injected concentration (given as an input value together with BCs) into the cell V_k

$$
\tilde{C}_k = \frac{1}{V_k} \int_{V_k} c_m^* \mathrm{d}V \,.
$$

$$(3.75)$$

There are two substantial points which create the features of the numerical scheme: the representation of the time derivative and the representation of the surface integral (flux approximation).

Using the forward difference for the derivative

$$
\frac{\partial C_k}{\partial t} \approx \frac{C_k^{n+1} - C_k^n}{\Delta t}
$$

$$(3.76)$$

the scheme will be explicit.

By the approximation of the surface integral in (3.73) we express the mass flux through the cell boundary, i.e. the actual transport of the solute. We use the upwind (donor-cell) flux approximation: the solute flux between two adjacent cells is calculated using the concentration C_m^k in the cell which the fluid flows from:

$$
\begin{aligned}
\text{flux}[j - k] &\approx C_k U_{kj} & &\text{if } U_{kj} > 0 \text{ (from } V_k \text{ to } V_j) \,, & (3.77)\\
\text{flux}[j - k] &\approx C_j U_{kj} & &\text{if } U_{kj} < 0 \text{ (from } V_j \text{ to } V_k) \,. & (3.78)
\end{aligned}
$$

For convenience, we denote the distinction of the flux direction by the signs $+$ and $-$:

$$
U_{jk}^+ = \left\langle \begin{array}{ll} U_{jk} & \text{for } U_{jk} > 0 \\ 0 & \text{for } U_{jk} <= 0 \end{array} \right. \qquad \text{and as well for } U_{jk}^- \qquad (3.79)
$$

(in accordance with the common notation for positive and negative part of function).

Thus the surface integral (total flux) can be expressed as a sum of fluxes through faces with neighbouring cells as follows

$$\int_{\partial V_k} c_m \boldsymbol{v} \cdot \mathrm{d}\boldsymbol{S} = \sum_{j \in N_k} (U_{kj}^+ C_k^n + U_{kj}^- C_j^n) \,. \tag{3.80}$$

Substituting into the equation (3.73) and expressing the unknown $C_k^{n+\frac{1}{2}}$, we obtain the scheme

$$C_k^{n+\frac{1}{2}} = C_k^n + \frac{\Delta t}{V_k} \cdot [-\sum_{j \in N_k} (U_{kj}^+ C_k^n + U_{kj}^- C_j^n) + C_k^n Q_k^- + \tilde{C}_k^n Q_k^+] \,. \tag{3.81}$$

Since the values U_{kj} are calculated by the mixed-hybrid FEM approximation, the relation $U_{kj} = -U_{jk}$ automatically holds, implying the overall mass balance in the domain Ω.

3.5.2   Stability

The explicit upwind scheme for advection equation is not in general stable and requires to fulfill a certain additional condition. The condition expresses a natural physical consideration, that during one step, the total fluid flux into a cell must not exceed the volume of cell, because it would correspond to a situation, when the fluid cross more than one cell in one time step. In case of solute transport, it would mean that the concentration in the cell would have to influence farther cells than the only neighbouring as the scheme do. By contrast, the scheme would cause an unnatural change of concentration in the neighbour cell in the direction of flow ("overflow" of the cell).

In 1D, the above described principle is expressed by a well-known condition, often called CFL condition(Courant–Friedrichs–Levy), between mesh size, time step, and fluid velocity

$$\mathrm{Cr} = \frac{v \Delta t}{\Delta x} \leq 1 \,, \tag{3.82}$$

where the expression on the left-hand side is called Courant number (Cr). For a numerical method, this is usually a restrictive condition on the time step, while the velocity and mesh are given.

For our 3D model, we must state a more general form of the CFL condition, using the idea in the opening paragraph. Without regard on a possible dependence of the conditions, we express the "non-overflow" condition for both outflow and inflow at each cell

$$\Delta t \sum_{j \in N_k} U_{kj}^{+} \leq V_k \qquad \text{and} \qquad \Delta t \sum_{j \in N_k} (-U_{kj}^{-}) \leq V_k \qquad \forall k \in \mathcal{K} . \qquad (3.83)$$

As was said in the previous paragraph, the condition (3.83) is a restriction on the time step Δt which must not exceed certain value.

For 1D case and uniform mesh, we can easily find such a limit from the inequality (3.82). The practical compliance of the more complicated relations (3.83) is performed successive halving of a user-given time step and repeated checking all the cells until the condition holds is the whole mesh. We can obtain a immediate rough information about the necessary time step using the relation (3.82) for 1D and substituting an estimation of maximum velocity in the mesh and the minimum volume of a cell in the mesh. Such an estimation is adequate and reasonably exact, if the places with maximum velocity and smallest cell dimension coincide.

In practical problems, the meshes are often constructed appropriately to the expected distribution of flow – they are finer in the neighbourhood of drawing and injecting wells, where maximum flow variations are expected. This implies that the large velocities are in place of small cells and the CFL condition is more restrictive because of quite few smallest cells while in the most of the domain $\text{Cr} \ll 1$.

The question of relation of mesh geometry, velocity field and distribution of Cr is further discussed in connection with the numerical dispersion, which is mainly influenced by them. See also the example of real-world problem (section 6.2.1, Tab. 6.1).

3.5.3 Estimates of numerical dispersion

As said above, the use of the explicit upwind scheme (no matter whether FDM or FVM is concerned) for the advection equation brings so called *numerical dispersion* into the method and results (see also e.g. [Hir91, Kaz97]). The term numerical dispersion denotes the fact that the numerical discretisation causes that the results of advection resemble a solutions of advection-dispersion problem.

The "amount" of dispersion caused by the numerical method depends on both the numerical method and physical parameters of the solved advection equation: mesh cells dimensions, time step and fluid velocity field. The existence of the numerical dispersion is clearly seen if the difference replacements of the space derivatives are expressed with a term of one more order in the Taylor expansion: the term with second order derivative standing for the error of the 1-st order approximation of derivatives represents the dispersion.

In special cases, we can express the numerical dispersion by the equivalent coefficient D in the ADE. The most simple case is 1D problem with constant fluid velocity (without sources and sinks, in homogeneous material), solved on a uniform mesh. The dispersion coefficient can be derived using the Taylor polynomial representation and we obtain the formula (see [Odm97, ZB95] for details)

$$D_{\text{num}} = \frac{1}{2} v \Delta x (1 - \text{Cr}), \qquad (3.84)$$

where Cr is the Courant number mentioned above by (3.82).

Without exact proof or derivation, we express a natural generalisation of (3.84) for general velocity field and nonuniform mesh: We replace the definition of Cr for 1D by a fraction of left-hand and right-hand sides of the inequalities (3.83)

$$\text{Cr} = \frac{\Delta t \sum\limits_{j \in N_k} U_{kj}^+}{V_k}. \qquad (3.85)$$

For use of the relation (3.84) we also need to define the mesh step Δx in a suitable way. We can use any characteristic dimension of a cell instead of Δx, e.g. the diameter or the distance of cell-centres (if the mesh is approximately uniform and we can associate the distance with both the neighbouring cells).

Thus the coefficient D_{num} is inhomogeneous, i.e. dependent on a chosen cell. Since we started from a one-dimensional relation, we do not have any information about the anisotropy of the numerical dispersion, which is in general very complicated. Based on the experiments in the section 5.2 we can briefly characterize the influence as the relation D_{num} mostly controls the longitudinal numerical dispersion, while the transversal is given by the geometry of mesh and velocity field.

Justness of this idea as an estimation of the dispersion in general case will be confirmed by the numerical experiments in the chapter 5, where the results of a few problems with nonuniform mesh and velocity field are compared with analytical solution of ADE.

We can give clearer approximate relations for numerical dispersion taking into account possible special properties of mesh and velocity field.

- For mesh and velocity exactly uniform and suitably oriented, the Courant number is the same in all the cells and for given mesh and velocity, we can control the value of dispersion by a choice of time step (i.e. setting Cr) within the limits $D_{num} = 0$ for maximum possible time step and $D_{num} \to \frac{1}{2} v \Delta x \equiv D_{num}^{max}$ for Δt very small.

- For mesh adjusted to the velocity field (see previous section), the Courant number is higher than $\frac{1}{2}$ in very few cells while in the most of the mesh Cr $\ll 1$. This implies that $D_{num} \approx D_{num}^{max}$ without regard on the choice of Δt.

Relation of physical and numerical dispersion

Thanks to numerical dispersion, the results of the advection model appear more "realistic" in the context of coarse approximation of the advection-dispersion process by pure advection, but the practical use of this fact is complicated. The numerical dispersion depends on the space and time discretisation and we cannot expect that it will exactly match the physical dispersion, including its anisotropy.

Problems are also met in the context of advection-dispersion models, when the physical dispersion coefficients are proportionally reduced according to the numerical dispersion [ZB95]. Another complication relates to solution of inverse problems: if the direct problem is solved by a method with numerical dispersion, it is impossible to identify the real coefficients of physical dispersion.

On the other hand, in many applications, the exact representation of the dispersion is not required. The estimates of numerical dispersion can be used as an a-posteriori check of accuracy of the model: for given mesh and time step, we can compare the numerical dispersion with expected physical and decide whether the results are satisfactory or not.

As a special case in 1D (and also other problems with suitable symmetry), it is possible to match the physical and numerical dispersion, using the formula (3.84). Since the dispersion coefficient (only longitudinal in 1D) is calculated by the product $\alpha_L v$, where α_L is dispersivity, we observe, that the rest of the terms in (3.84) stand for the dispersivity. Considering the special

case $Cr \ll 1$, when the numerical dispersion is $D_{\text{num}} = \frac{1}{2}v\Delta x$, we can identify

$$\alpha_L^{\text{num}} \approx \frac{\Delta x}{2}. \tag{3.86}$$

We apply this consideration conveniently in comparisons of numerical results with analytical solutions (section 5.2. It is also interesting to remark, concerning the underground problems, that the values of dispersivity and mesh sizes have appropriate order of magnitude: $10^0 - 10^2$ meters [ZB95].

3.6 Mobile–immobile exchange

For expression of the mobile-immobile exchange, we derived a semi-analytical method. The operator splitting in the system (2.15)-(2.16) leads to a solution of two coupled ODE in a given space point (or discretisation volume) in each time step of splitting. We recall the system (3.57)-(3.58)

$$\frac{dc_m}{dt} = \frac{1}{n_m}\alpha(c_i - c_m), \tag{3.87}$$

$$\frac{dc_i}{dt} = -\frac{1}{n_i}\alpha(c_i - c_m), \tag{3.88}$$

which can be easily analytically solved and thus it can give a numerical scheme for time step of arbitrary size.

3.6.1 Solution of the split problem

Summing the equations (3.87) and (3.88), we obtain the property of mass balance

$$n_m c_m + n_i c_i = \text{const} = \bar{c}\,(n_m + n_i), \tag{3.89}$$

where we denoted the weighted average value of concentration $((n_m + n_i)V_{\text{REV}}\bar{c}$ is the total solute mass in REV). Substituting for c_i from (3.89) into (3.87), we obtain a single ODE for the unknown $c_m(t)$

$$n_m \cdot \frac{dc_m}{dt} = \alpha \cdot \left(\frac{\bar{c}(n_m + n_i) - n_m c_m}{n_i} - c_m\right), \tag{3.90}$$

rearranged to

$$\frac{dc_m}{dt} = -\alpha \cdot \frac{n_m + n_i}{n_m n_i} \cdot c_m + \alpha \cdot \frac{\bar{c}\,(n_m + n_i)}{n_m n_i}. \tag{3.91}$$

By separation of variables, we figure out the general solution of the equation

$$c_m(t) = \frac{k}{-\alpha\frac{n_m+n_i}{n_m n_i}}e^{-\alpha\frac{n_m+n_i}{n_m n_i}\cdot t} + \frac{\frac{\bar{c}(n_m+n_i)}{n_m n_i}}{\frac{n_m+n_i}{n_m n_i}} = \tag{3.92}$$

$$= -\frac{k}{\alpha}\frac{n_m n_i}{n_m + n_i}e^{-\alpha\frac{n_m+n_i}{n_m n_i}\cdot t} + \bar{c}, \tag{3.93}$$

where k is an integration constant, to be determined from the initial conditions

$$c_m(0) = c_m^{(0)} \qquad \text{and} \qquad c_i(0) = c_i^{(0)}, \tag{3.94}$$

where we denoted $c_m^{(0)}$ a $c_i^{(0)}$ the given initial concentration values (either initial values of the problem or results of previous OS time steps).

The average concentration is constant and equal to its initial value. Thus for $t = 0$, it must hold

$$-\frac{k}{\alpha}\frac{n_m n_i}{n_m + n_i} = c_m^{(0)} - \bar{c}, \tag{3.95}$$

whereby the integration constant k is determined.

Thus, the exact solution of (3.87)-(3.88) with initial conditions $c_m^{(0)}$ and $c_i^{(0)}$ for arbitrary time $t \geq 0$ is

$$c_m(t) = (c_m^{(0)} - \bar{c}^{(0)})e^{-\alpha\frac{n_m+n_i}{n_m n_i}t} + \bar{c}^{(0)} \tag{3.96}$$

and by analogy for $c_i(t)$

$$c_i(t) = (c_i^{(0)} - \bar{c}^{(0)})e^{-\alpha\frac{n_m+n_i}{n_m n_i}t} + \bar{c}^{(0)}. \tag{3.97}$$

In terms of the initial value problem, the average concentration is expressed as

$$\bar{c}^{(0)} = \frac{n_m c_m^{(0)} + n_i c_i^{(0)}}{n_m + n_i}. \tag{3.98}$$

Finally we define some convenient notations for coefficients. We denote

$$\tilde{\alpha} = \alpha\frac{n_m + n_i}{n_m n_i} \tag{3.99}$$

the modified exchange coefficient and

$$T_{1/2} = \frac{\ln 2}{\tilde{\alpha}} \tag{3.100}$$

the *characteristic time of exchange*, which gives clear information about the rate of exchange: the time when the half of total possible mass is transferred. This is the value used as input value in the model user interface (section 4.1).

3.6.2 FVM numerical scheme of MI exchange

The solution (3.96)-(3.97) can be directly written in terms of discrete values of concentrations in the finite volumes (see the definition (3.65) and the notations (3.69) and (3.71)).

As the problem of mobile-immobile exchange was the second one in the operator splitting, we solve the problem with initial values $C_m^{n+\frac{1}{2}}$ and $C_i^{n+\frac{1}{2}}$ and we express the final values $C_{i,m}^{n+1}$ after the time step Δt, for each discretisation volume k (not explicitly written in the formula, for readability).

The discretisation scheme for both mobile (m) and immobile (i) concentrations is

$$C_{m,i}^{n+1} = (C_{m,i}^{n+\frac{1}{2}} - \overline{C}^{n+\frac{1}{2}}) \, e^{-\tilde{\alpha}\Delta t} + \overline{C}^{n+\frac{1}{2}}, \tag{3.101}$$

where

$$\overline{C}^{n+\frac{1}{2}} = \frac{n_m C_m^{n+\frac{1}{2}} + n_i C_i^{n+\frac{1}{2}}}{n_m + n_i}, \tag{3.102}$$

and

$$C_{m,i}^{n+1} \equiv C_{m,i}^{X}(\Delta t), \qquad C_{m,i}^{X}(0) \equiv C_{i,m}^{n+\frac{1}{2}} \equiv C_{m,i}^{A}(\Delta t) \tag{3.103}$$

are used in the sense of the split problem (3.57)-(3.58).

The expression (3.101) can be used for a time step Δt of any size, thus, comparing with the advection term alone, there is no more requirement on the time step of the model (operator splitting).

The type of function corresponds with our natural expectation, that the concentration varies from its initial value towards the average concentration (given by mass conservation (3.89)), which expresses the limit state of in the discrete volume between in the infinite time (equilibrium).

The rate of the exchange depends on the diffusion coefficient, on the characteristic microscopic dimensions of porous media (both included in the coefficient α, see (1.27) and section 1.3.3 for details), and on the relation between the size of the mobile and immobile volumes (n_m and n_i).

In terms of characteristic time $T_{1/2}$, which is the preferred input value in the model user interface (as expressed in days, having a good physical interpretation of intensity of exchange in relation to other processes), the numerical scheme is

$$C_{m,i}^{n+1} = (C_{m,i}^{n+\frac{1}{2}} - \overline{C}^{n+\frac{1}{2}}) \, \exp(\ln 2 \, \frac{\Delta t}{T_{1/2}}) + \overline{C}^{n+\frac{1}{2}}. \tag{3.104}$$

Chapter 4

Model Implementation

The aim of this chapter is a brief description of the implementation of the numerical method derived in the last chapter on a particular mesh topology and the overview of user interface and model parameters used in the practical problems.

The structure of the model corresponds to the models used in DIAMO Stráž pod Ralskem, see e.g. [MF92, Fry02]. Some of the program code modules were used for construction of the model presented here. The matching with the former programs is important for use of the preprocessing and postprocessing software for applicational problems in DIAMO, where the model for dual-porosity media had been currently desired (year 2001).

By reason of limited space in this thesis, we reduce the description of the model interface and implementation-specific algorithms and we mostly refer to the technical reports of the author [Hok01a, Hok01b] and cooperating team [Š+01].

4.1   Mesh topology and data structures

The mesh topology is chosen to link the demands on reasonable handling of complicated geological structure of the underground and the moderate computational complexity. A good compromise for implementation of 3D mesh is so called $2\frac{1}{2}$D topology, meaning that the mesh composed of 2D layers with joint discretisation topology [MF92]. The mesh is thus unstructured in horizontal direction (arbitrary triangulation, see below) and structured in the vertical direction (linear set of elements associated with certain 2D triangle,
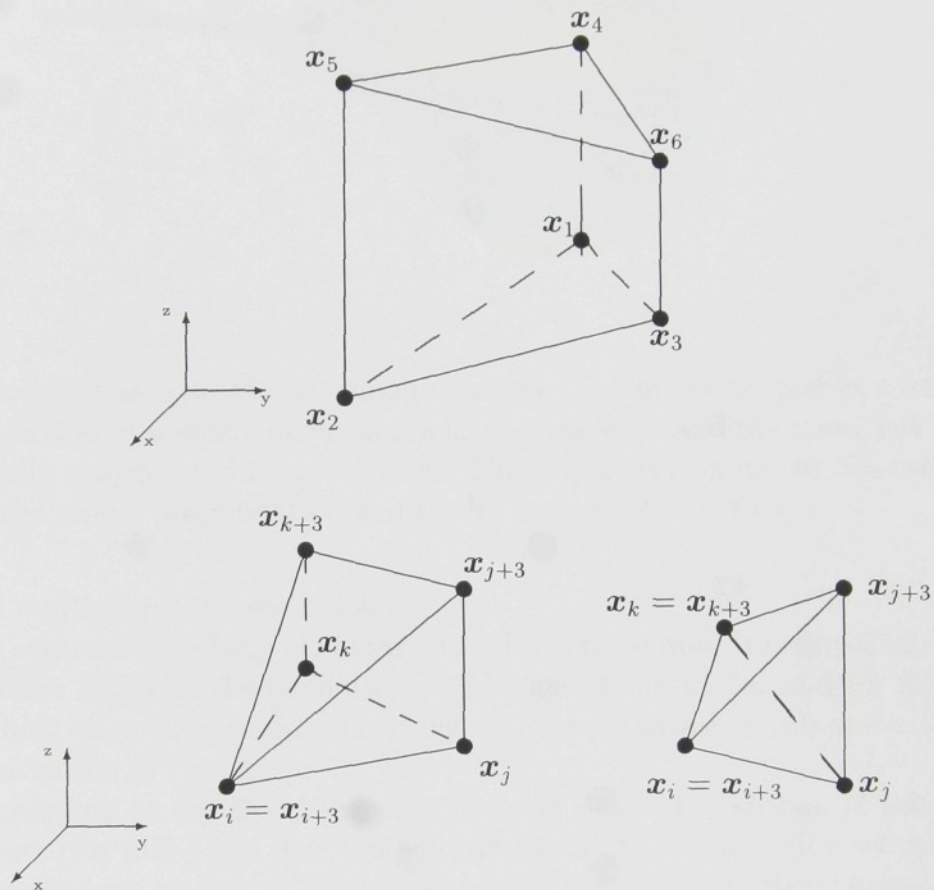
Figure 4.1: Element (FEM) and cell (FVM) shapes used in the model. The bottom two are degenerate variants of the above trilateral prisms.
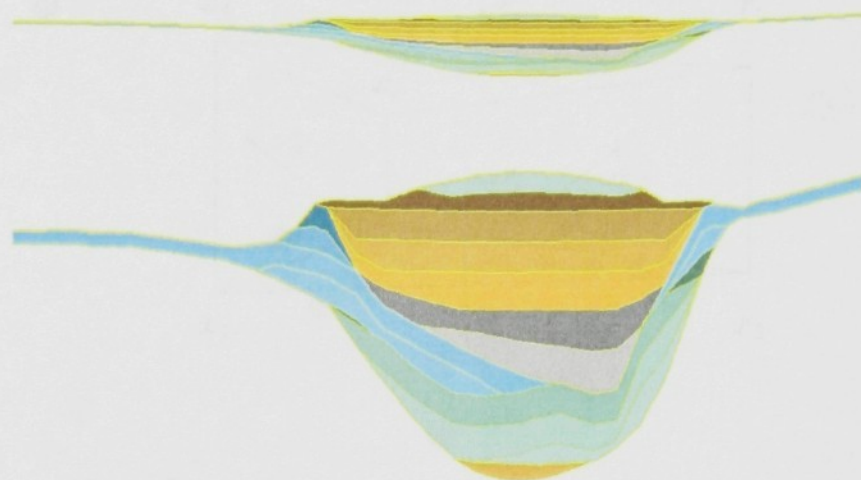
Figure 4.2: Example of "incomplete" layers. The upper picture is a vertical cross-section in uniform horizontal and vertical scale and the lower is 5 times vertically exaggerated for clear view. The colors correspond to the layers in both the model discretisation and in the geological structure.

called *multi-element* – see below).

In contrast with fully 3D unstructured discretisation, it is important simplification for both the computational kernel of the model and for users of the whole software system, concerning e.g. the preparation of input data and interpretation of results.

According to the described structure, we define the shapes of the finite elements (for MH-FEM flow model) and the finite volumes (for cell-centred FVM transport model) as follows: The basic shape is a trilateral prism, with vertical lateral sides and generally non-horizontal bases (see Fig. 4.1 at the top). For correct representation of the model boundaries and borders of geological layers, we define the degenerated pyramidal shapes, see Fig. 4.1 at the bottom. An example of situation for use of the degenerate prisms is in Fig. 4.2, with many cases when certain geologic layers exist only in a part of the area.

We denote the vertices of the prisms and pyramids (degenerated from the basic prismatic shape) as $x_1, x_2, x_3, x_4, x_5, x_6$ (see also Fig. 4.1 and Fig. 4.3)
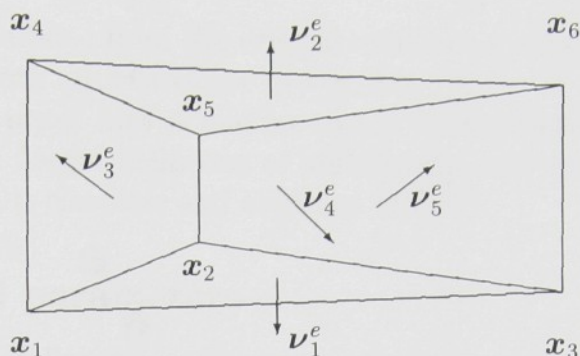
Figure 4.3: Normals to the element/cell sides. We note that the vertex labeling matches Fig. 4.1 and the numbering of the sides is the following: 1 bottom, 2 top, 3–5 lateral, starting from $\boldsymbol{x}_1\boldsymbol{x}_2\boldsymbol{x}_4\boldsymbol{x}_5$ counterclockwise from the top view.

in this way:

$$\boldsymbol{x}_1 = (x_1, y_1, z_1), \quad \boldsymbol{x}_2 = (x_2, y_2, z_2), \quad \boldsymbol{x}_3 = (x_3, y_3, z_3),$$
$$\boldsymbol{x}_4 = (x_1, y_1, z_4), \quad \boldsymbol{x}_5 = (x_2, y_2, z_5), \quad \boldsymbol{x}_6 = (x_3, y_3, z_6),$$

where we note $x_i = x_{i+3}$ and $y_i = y_{i+3}$ (vertical sides). Considering the degenerate elements, using the notation for general position i, j, k, the respective elements are determined by $\boldsymbol{x}_i = \boldsymbol{x}_{i+3}$ either for a single $i \in \{1, 2, 3\}$ or for $i, j \in \{1, 2, 3\}$ $i \neq j$.

4.1.1 Definition of the mesh

As stated above, the elements and nodes are "grouped" (by the vertical projection) to operate with 2D topology. The set of nodes associated with certain projection in a plane is called *multi-node* and the set of elements associated with certain projection in a plane is called *multi-element*.

The mesh is defined as 2D topology of multi-nodes and multi-elements (triangularization) and the definition of each multi-node (simply determined by the x and y coordinates) is supplemented with information about the vertical structure: number of nodes and the respective set of z coordinates.

The elements are determined by the triangular topology and by the global

numbering of layers, arising from the vertical numbering of nodes in a multi-node. The internal data structures are in Fig. 4.4.

The structure of input files is similar to the internal structure of data storage. There is one file for definition of multi-nodes and nodes (STU) and one for definition multi-elements and elements (STE).

4.1.2 Material parameters

In general sense, the following parameters have to be entered, considering the general inhomogeneity of the material:

- permeability (only the diagonal components k_x, k_y, k_z are implemented) of the medium in each element

- mobile n_m and immobile n_i porosity in each element

- characteristic time of exchange in each element and for each chemical component of the transported solution

- parameters of the Van Genuchten curve α_{vg}, m_{vg} of the material in each element[1]

As the amount of data is very excessive, it is convenient to group some of the coefficient, mainly those which cannot be accurately measured and there is no need for "full inhomogeneity" in the user interface. For example, in the problem domain are zones with approximately same properties, thus the values of coefficients are defined together and then only a reference "material Nr.xx" is given in the list for all elements. The rate of mobile–immobile exchange is input in this way (see the example of problem-definition file below, the code is prepared for other variants besides the linear relation of the transfer term of MIE) and as well the Van Genuchten parameters in the model of saturated-unsaturated zone.

The possible different mobile-immobile transfer coefficient for different chemical species is input by additional multiplicative factor for each chemical component (see the report [Hok01a] for details).

This is a part of the global file for options and settings:

---

[1]In fact not the case of the model described in this thesis, but the interface of the input values is joint for other models in DIAMO, also for the flow in saturated-unsaturated zone [Fry02].

```
───────────────────────────── header.h ─────────────────────────────
struct S_muzl                         // multi-node
{
    int     oznac;                    /* label of the multi-node   */
    int     ipuzl;                    /* label of the first node   */
    int     npuzl;                    /* number of nodes           */
    double  x, y;                     /* coordinates               */
    ...
};
...
struct S_uzl
{
    int     imuzl;                    /* label of the multi-node   */
    double  z0;                       /* z coordinate of the node  */
};
```

```
───────────────────────────── header.h ─────────────────────────────
struct S_melm                    // multi-element
{
    int      oznac;         /* label of multi-element       */
    int      ipelm;         /* label of the first elementu  */
    int      npelm;         /* number of elements in the Melm */
    int      muzl[ 3 ];     /* labels of associated multi-nodes*/
    int      odv;           /* number of the first layer    */
    int      dov;           /* number of the last layer     */
    ....
};
...
struct S_elm                     // element
{
    int      imelm;         /* label of multi-element       */
    int      ivrst;         /* number of layer              */
    int      imatr;         /* index of material            */
    float    koef[ MAXELKOEF ]; /* coefficients of the element */
                            /* koef[0,1,2] ...conductivities */
                            /* koef[3,4] mobile,immobile porosity*/
    ...
}
```

Figure 4.4: Data structures for internal storage of the mesh.

```
───────────────── solved-problem.mmf ─────────────────
[DUAL_POROSITY]
Apply_DP=yes
;                    type    function    T_1/2
TTerm_Grp_0=          10        1         100
TTerm_Grp_1=          20        1         80
TTerm_Grp_2=          30        1         130
TTerm_Grp_3=          40        1         400
...


Koef_SO4=1
Koef_NH4=1.2
Koef_NO3=1.2
...
```

The assignment of values to each element is realised in the file type STM, belonging to a group of mesh-definition files (STU and STE for nodes and elements).

```
───────────────── used-mesh.stm ─────────────────
melm# lay# mat#_dp   K_x K_y K_z   n_m  n_i    mat#_fb
  1    0     0        1   1   1    0.1  0.2      1
  1    1     1        1   1   1    0.1  0.2      1
  1    2     2        3   3   3    0.3  0.5      1
```

Each line of the file corresponds to a single element. The first two columns index the element by the number of respective multi-element and number of layer in the multi-element. In the further columns the indices of material groups (for definition of mobile-immobile exchange characteristics and capillarity characteristics, see above) and the values of conductivities and porosities are entered.

4.1.3 Storage for calculated values

The calculated unknowns are associated in each element in the structure joint for the definition of the mesh. The respective values are commented in the example, see also [Š+01, Fry02].

```
───────────────── header.h ─────────────────
struct S_elm                      // element
{
    int         imelm;            /* label of multi-element      */
    ...
```

```
/*-------------------------------------------------------------*/
    double      vyska;                 /* piezometric head in center  */
    double      tlak;                  /* pressure in center of Elm    */
    double      stntlk[ 5 ];           /* pressure in center of side   */
    double      stntok[ 5 ];           /* flux through the side         */
/*-------------------------------------------------------------*/
    double      objem;                 /* volume of Elm                 */
    double      porobjm;               /* mobile pore volume in Elm    */
    double      porobjm_im;            /* immobile pore volume in Elm  */
/*-------------------------------------------------------------*/
    double      *rslo;                 /* concentrations of components  */
    double      *rslo_por;    /* concentrations of components in immo*/
/*-------------------------------------------------------------*/

    ...
};
```

4.2   Numerical structures and algorithms

4.2.1   Model of fluid flow

The overall algorithm of the model is displayed in Fig. 4.5. There are four
main phases: reading the input data (3 blocks), pre-processing of data (2
blocks), the numerical kernel (4 blocks), and the output.

We note that the number of unknowns (and consequently the size of the
algebraic matrix) depends on the topology of the mesh – number of internal
and external elements sides (as the Lagrange multipliers, i.e. pressures at
sides, are joint for two sides of two neighbouring elements). Thus there is
necessary first to analyse the topology, and afterwards to allocate the memory
for the matrix and calculate the values.

The block $\mathbb{A}$ is composed of so called "local matrices" of the dimension
$5{\times}5$ associated with each element (scalar product of linear base functions
from the space $\boldsymbol{RT}^0(e)$, see section 3.2.2). These can be evaluated apart
from the whole algebraic system and the values are stored in the data struc-
ture of elements, which is convenient for repeating of the calculation for
different boundary conditions (the block $\mathbb{A}$ stays unchanged), see e.g.[Fry02]
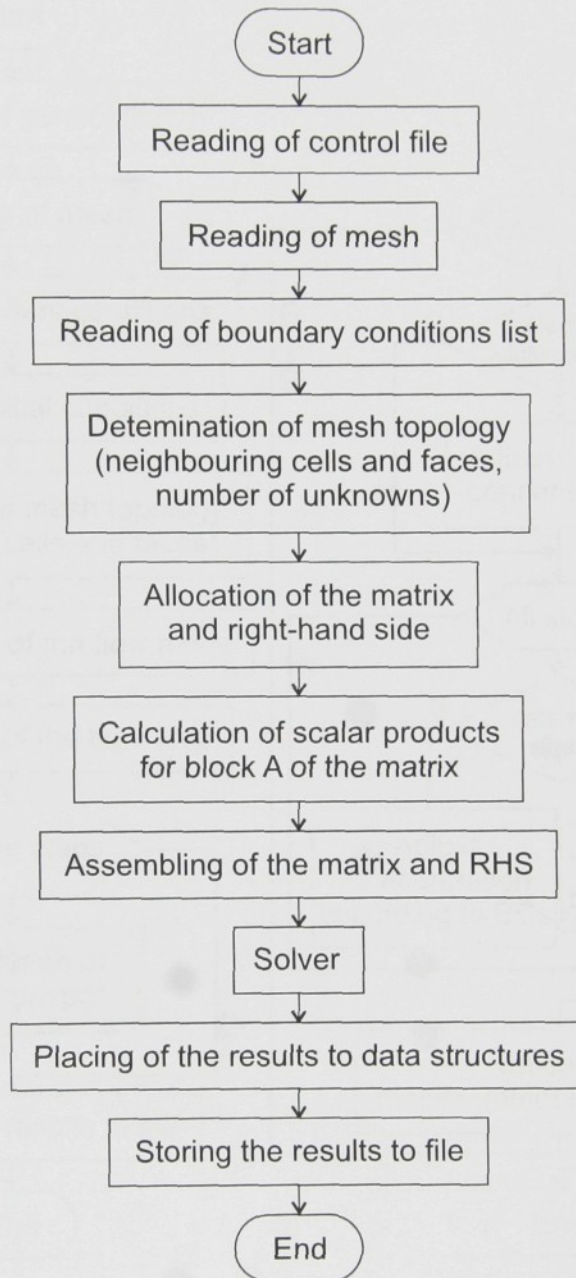for details.

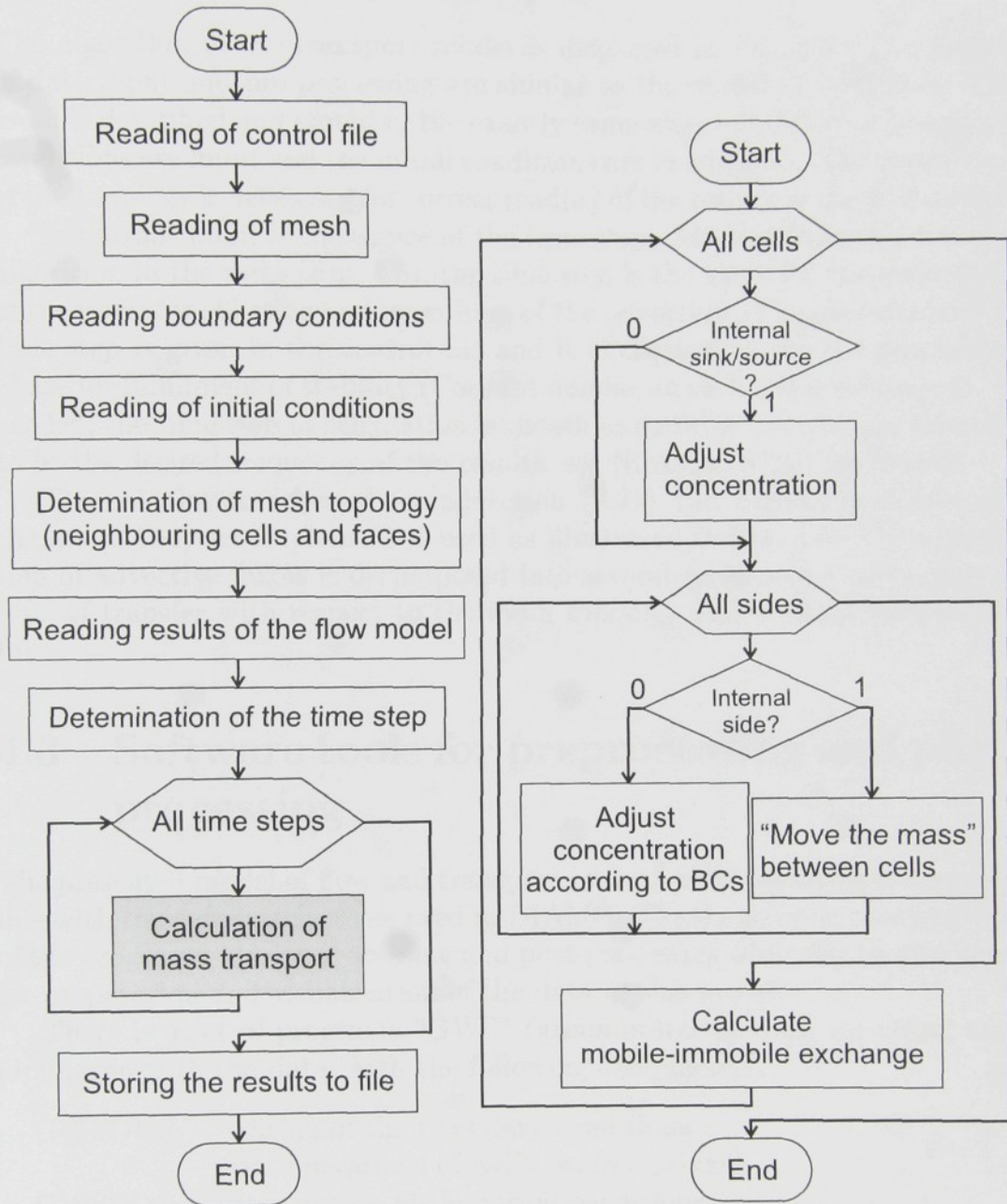Figure 4.5: Scheme of algorithm of the mixed-hybrid flow model.

Figure 4.6: Scheme of algorithm of the transport model. The total algorithm in the left and the detailed block "Calculation of mass transport" in the right.

4.2.2 Model of solute transport

The algorithm of the transport model is displayed in Fig. 4.6. The phases of data input and pre-processing are similar to the model of fluid flow. The mesh is described and stored in the exactly same way, but different boundary conditions are input and the initial conditions are in addition. The processing of the topology is necessary for correct reading of the results of the flow model.

Important point is the choice of the time step. As clear from the detailed algorithm in the right (Fig. 4.6), the time step is the same for the outer loop of the operator splitting and inner loop of the advection. The user-demanded time step is given in the control file and it is checked in the pre-processing phase for fulfillment of stability (Courant number in each cell is evaluated). If needed, the time step of calculation is chosen as suitable fraction (by integer) to fit the desired frequency of the results, see [Hok01a, Š⁺01] for details.

The calculation schemes for advection (3.81) and mobile–immobile exchange (3.104) are implemented used as illustrated in Fig. 4.6. The expression of advective fluxes is decomposed into several serial steps, according to type of transfer with respect to the mesh topology and internal data structures.

4.3 Software tools for preprocessing and post-processing

The presented model of flow and transport in dual-porosity media is compatible with the software systems used in DIAMO. Thanks to open construction of the programs, the preprocessing and post-processing tools can be also used for preparation and visualisation of the data in this model.

There is a set of programs "GWS" (groundwater system) for visual manipulation with the data, with the following components:

GWSOKP	editing of the boundary conditions and operations of wells (sources/sinks)
GWSPOC	preparation of the initial conditions
GWSSIT	preparation of the model mesh and material parameters
GWSVIEW	visualisation of the flow and transport results

For screenshots with the data of the remediation problem solved in the chapter 6 see figures 4.7 and 4.8.
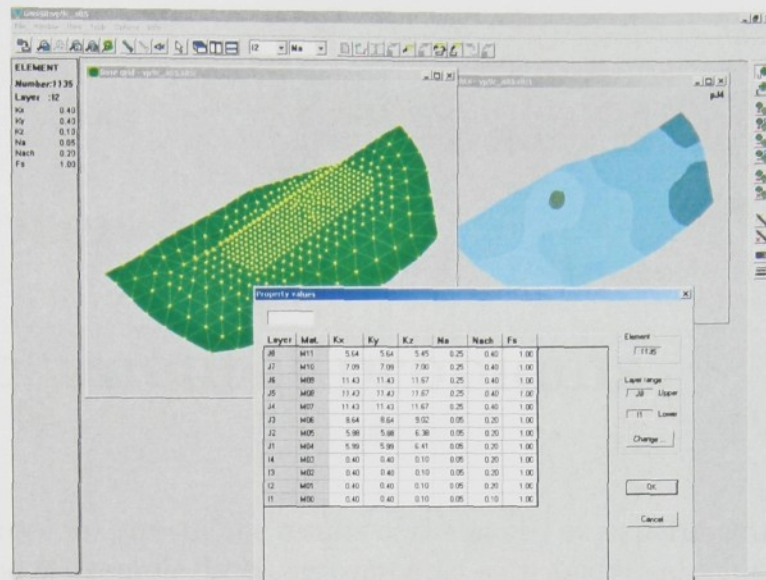
Figure 4.7: Use of the program GWSSIT for preparation of input data (editing of node positions and material parameters).
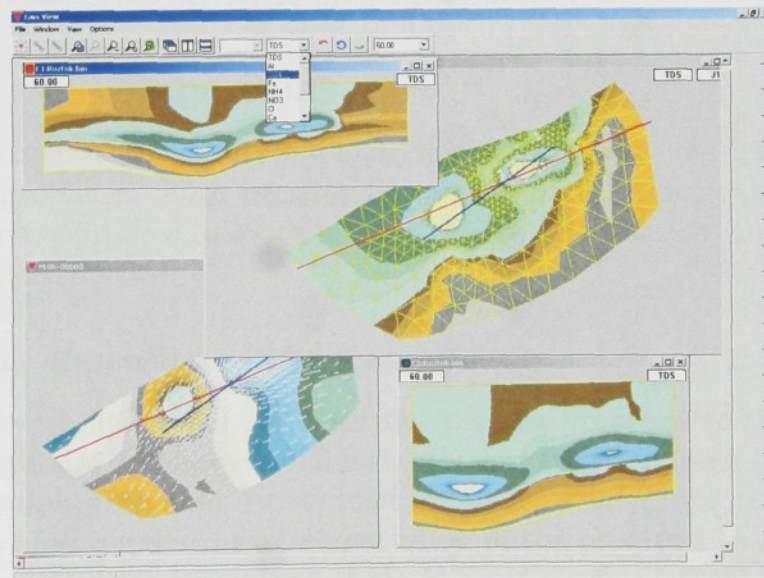

Figure 4.8: Use of the program GWSVIEW for visualisation of result (distribution of pressure and velocity in the left, concentration of selected component in the right and in vertical cross-sections.

Chapter 5

Experimental problems

In this chapter we present the results of the model on experimental problems. The solution of example problems compared with analytical solution confirms a correct function of the model and gives an information about the accuracy of the numerical method. Further, we solve several problems, representing certain typical situation in practice (e.g. the radial flow around a well) to demonstrate the behaviour of the model. The solved problems give also basic information about sensitivity to model parameters.

Concepts of comparisons

For comparisons of the model and analytical solutions, we must use typically 1D or 2D problems: both because the analytical solutions can be derived only for these simpler situations and for clearer visualisation and evaluation of the results.

Remark on dimension of the problems

As we deal with 3D model, we construct the test problems so that they are three-dimensional in the sense of use the 3D discretisation mesh, but they are one- or two-dimensional in the sense of problem's symmetry – the remaining dimensions are insignificant for the solution of the problem. In our opinion, this is a standard technique and there is no inconsistency in denoting the solved problems as 1D or 2D.

When calculating with real physical values, there is a special care for correct dimensions necessary. E.g. in 1D problems, the values are suitably

normalised for a given cross-section area in the numerical 3D problem.

Handling the numerical dispersion in comparisons

As explained in the section 3.5.3, the upwind scheme for advection brings the numerical dispersion, which significantly changes the results compared with the exact solution of the advection.

For our comparisons, we included the numerical dispersion into a considered analytical solution to separate that numerical error (expected) from the possible error of the discretisation of the mobile–immobile exchange and the operator splitting. From the mesh and from the calculated velocity, we first express the coefficient of numerical dispersion and than we consider the analytical solution of the advection-dispersion problem with this value of the dispersion coefficient substituted.

5.1 Reference analytical solutions

We present gathered the analytical solutions used for all the comparisons in this chapter. There are also several aspects of the approximation common for all the problems, concerning e.g. the relation of boundary conditions in the physical representation and in the numerical or analytical solutions:

In general, we consider solutions of problems in infinite and semi-infinite domains, which can be expressed in clear compact forms and are commonly used (often the problems in a bounded domain can be suitably represented in this way). Moreover, in our case the semi-infinite problem exactly matches the function of the numerical method: there is no boundary condition in the advection model at the outflow boundary, the numerical scheme does not reflect anything occurring downstream (which is the feature of advection-dominated problems).

The difference between infinite and semi-infinite problems (with inflow boundary) in our examples is only in exact fulfilling the boundary condition at the inflow. In case of advection-dominated flow, the simpler solution in the infinite domain can be used instead of more complex solution in the semi-infinite domain (which is of our interest for comparison with model results), if we accept only approximate fulfillment of the boundary condition.

We also remark the representation of the Dirac function, which is often used in the simple model problems of dispersion, in the discretised model. In

contrast with the step (Heaviside) function, which is not "damaged" by the discretisation, the Dirac function can be used only with substantial change in its shape and properties. As each discrete value is associated in certain volume in space, the single value in the model represent a "rectangular impulse" instead of a peak in a single point (of course, the value substituted in the model is "1" divided by the associated volume).

Thus the Dirac function is not suitable for comparison and exact evaluation of the dispersion in early stages of calculation (where the influence of initial condition if essential). On the other hand, the Dirac function is useful in 2D uniform problem for its symmetry and clear comparison of the dispersion in different directions.

5.1.1 Analytical solutions of ADE

The solutions of advection-dispersion problem in uniform velocity field (in 1D or 2D) are the simplest possible and are presented in most of the literature dealing with porous media transport, e.g. [ZB95, Ben95]. The case of non-uniform flow (e.g. radial) is much more complicated, see below for details.

1D uniform flow with Dirac initial condition

The problem is given by the equation

$$\frac{\partial c}{\partial t} + v\frac{\partial c}{\partial x} = D\frac{\partial^2 c}{\partial x^2} \tag{5.1}$$

for the unknown $c(x,t)$ in the space domain $\Omega = \mathbb{R} \equiv (-\infty, +\infty)$ and time interval $(0, +\infty)$, the constant velocity v, with the initial condition

$$c(x,0) = \frac{M}{S}\delta(x) \qquad \forall x \in \Omega\,, \tag{5.2}$$

where M [M] represent the total mass in the domain, S [L^2] the cross-sectional area of mobile pore space (for correct normalisation), and $\delta(x)$ is the Dirac δ-function.

The analytical solution is

$$c_D(x,t) = \frac{M}{2S\sqrt{\pi Dt}}\exp\left[-\frac{(x-vt)^2}{4Dt}\right] \qquad x \in \mathbb{R},\ t > 0\,, \tag{5.3}$$

which has the shape of the density of the Gaussian probability distribution.

1D uniform flow with Heaviside step initial condition

We consider the problem both in the infinite and semi-infinite domain. The first case is defined as above (5.1), with the initial condition

$$c(x, 0) = c_0 \quad \text{for} \quad x < 0, \tag{5.4}$$
$$c(x, 0) = 0 \quad \text{for} \quad x > 0 \tag{5.5}$$

(c_0 is the concentration in the "left" part of the domain), and the solution is

$$c_{H1}(x, t) = \frac{c_0}{2}\text{erfc}\left[\frac{x - vt}{2\sqrt{Dt}}\right] \quad x \in \mathbb{R}, \ t > 0, \tag{5.6}$$

where the complementary error function is defined by

$$\text{erfc}(x) = \frac{2}{\sqrt{\pi}} \int_x^\infty e^{-u^2} du = 1 - \frac{2}{\sqrt{\pi}} \int_0^x e^{-u^2} du = 1 - \text{erf}(x) \tag{5.7}$$

(the cumulative Gaussian distribution function).

The problem in semi-infinite domain is defined by the equation (5.1) in the space domain $\mathbb{R} \equiv (0, +\infty)$ with the initial and boundary conditions

$$c(x, 0) = 0 \qquad x > 0 \tag{5.8}$$
$$c(0, t) = c_0 \qquad t > 0 \tag{5.9}$$

(c_0 is the concentration in the water inflowing from the left). The exact solution is

$$c_{H2}(x, t) = \frac{c_0}{2}\text{erfc}\left(\frac{x - vt}{2\sqrt{Dt}}\right) + \frac{c_0}{2}\exp(\frac{vx}{D}) \cdot \text{erfc}\left(\frac{x + vt}{2\sqrt{Dt}}\right) \tag{5.10}$$

For advection-dominated problems, i.e. the large Péclet number $\frac{vL}{D} \gg 1$ (where L represents a characteristic length of the problem, e.g. dimension of the domain for bounded problem), the solutions of both the problems are close to each other, $c_{H2}(x, t) \approx c_{H1}(x, t)$. This allows to use the simpler function c_{H1} for more common semi-infinite problem.

2D uniform flow with Dirac initial

We consider the advection-dispersion problem in the plane $\Omega \equiv \mathbb{R}^2$, $c(x, y, t)$, with uniform velocity field in the x-direction, $\boldsymbol{v} = (v_x, 0) = \text{const}$. Thus

$$\frac{\partial c}{\partial t} + v_x \frac{\partial c}{\partial x} = D_L \frac{\partial^2 c}{\partial x^2} + D_T \frac{\partial^2 c}{\partial y^2}, \qquad (5.11)$$

where D_L and D_T are longitudinal and transversal dispersion coefficients. The Dirac-type initial condition is

$$c(x, y, 0) = \frac{M}{d} \delta(x)\delta(y) \qquad \forall x, y \in \mathbb{R}, \qquad (5.12)$$

where d is the part of thickness of the plane falling on pores ($\frac{d}{n_m}$ is the "real" thickness).

The exact solution is

$$c_{D2}(x, y, t) = \frac{M}{4\pi d \sqrt{D_L D_T} t} \exp\left[-\frac{(x - v_x t)^2}{4 D_L t} - \frac{y^2}{4 D_T t} \right]. \qquad (5.13)$$

The isolines of concentration form ellipses, whose principal radiuses are in the ratio $\frac{\sqrt{D_L}}{\sqrt{D_T}}$. We will apply this relation for identification of anisotropy of numerical dispersion from the graphical results.

Transport in 2D radial flow

This case represent a flow and transport around a drawing/injecting well. The simplest possible problem to solve is injecting of constant concentration to the infinite 2D domain with zero initial condition. Even if the problem seem to be simple and many effort has been done because if its importance, there is no definite result. Some complication is in non-homogeneity of dispersion coefficient caused by non-homogeneity of velocity. Solutions for general power dependence of D on v are considered in [Phi94], there is no result for the case $D = \alpha_L v$ and some other cited solutions are found as erroneous.

For our comparisons (thus not fully significant), we will use a simplified solution presented in [Ben95] (with some probably typing errors, repaired here). Thanks to the symmetry, the solution is expressed in single space variable r meaning the distance from the centre (place of the well). For

simplicity, we omit the second one of the polar coordinates, which are in fact used here. The solution is

$$c_R(r, t) = \frac{c_0}{2} \text{erfc} \frac{\frac{r^2}{2} - At}{\sqrt{\frac{4}{3}\alpha_L r^3}}, \tag{5.14}$$

where α_L is the longitudinal dispersivity[1] and $A = \frac{Q}{2\pi d n_m}$ is the "areal flux" expressing a normalisation of the total injected volume rate Q (in m^3/s).

From A we can easily express the velocity as $v = \frac{A}{r}$. The relation (5.14) exactly fits the front of the concentration, which lies in the distance $r_f(t) = \sqrt{2At}$ (expressed as the mass balance for plain advection).

To define the problem correctly, we should exclude the singular point $r = 0$ (where the velocity is not defined). Typically, the problems is expressed with finite radius of the well, r_w, i.e. $\Omega = \{(x, y) \mid x^2 + y^2 > r_w^2\}$.

5.1.2 Analytical solution of non-equilibrium transport

After auxiliary advection-dispersion problem in the last section, we consider now the coupling of advection, dispersion, and non-equilibrium two-region mass exchange. We will express a solution for one particular problem: uniform flow in 1D semi-infinite domain, with initial condition of Heaviside type (zero initial condition in the domain and constant inflow concentration as the boundary condition).

The analytical solutions of multi-process transport problems are presented in [TLvG93], with our problem as a special case.

For convenience, we transform the model equations to a dimensionless for, following the notation in the above cited article, with minor technical modifications. From (2.15)-(2.15), we obtain

$$\beta \frac{\partial C_m}{\partial T} = -\frac{\partial C_m}{\partial X} + \frac{1}{P} \frac{\partial^2 C_m}{\partial X^2} + \omega(C_i - C_m), \tag{5.15}$$

$$(1 - \beta) \frac{\partial C_i}{\partial T} = -\omega(C_i - C_m), \tag{5.16}$$

---

[1] Thanks to the symmetry, the concentration spread uniformly to all directions and there is no gradient in the direction transversal to the velocity. Thus the transversal dispersion does not occur in this case, which is convenient for comparisons with the numerical model, where also the numerical dispersion in the transversal direction is zero.

defining

$$X = \frac{x}{L} \qquad \text{dimensionless distance}, \qquad (5.17)$$

$$T = \frac{vt}{L} \qquad \text{dimensionless time}, \qquad (5.18)$$

$$P = \frac{vL}{D} \qquad \text{Péclet number}, \qquad (5.19)$$

$$\omega = \frac{\alpha L}{n_m v} \qquad \text{Damkohler number}, \qquad (5.20)$$

$$\beta = \frac{n_m}{n_m + n_i} \qquad \text{weighting factor}, \qquad (5.21)$$

where v is the velocity and D the scalar dispersion coefficient (longitudinal).

We will not introduce a special notation for dimensionless concentration (typically would be $C_{m,i} = c_{m,i}/c_0$ with certain value of characteristic concentration c_0) because the concerned C already represents the discrete numerical values. Moreover, the only difference in the formulae is in presence of the characteristic concentration, which has the clear physical sense of the concentration in the inflowing water.

The characteristic length L represent e.g. the dimension of problem domain, considering the semi-infinite solution as an approximation, neglecting the effect of the outflow boundary (advection-dominated process). Also the use of the Dirichlet condition (prescribed concentration) at the inflow corresponds in fact to the advection-dominated case (the third-type would be physically more correct).

The solution $c_m(X, T)$ for above specified conditions is

$$
\begin{aligned}
c_m(X, T) \;=\;& c_0 \cdot G(X, T) \cdot \exp\!\left(-\frac{\omega T}{\beta}\right) \\
&+ \omega \cdot \int_0^T G(X, \tau) \cdot \exp(-a - b) \cdot \left[\frac{1}{\beta} \mathrm{I}_0(2\sqrt{ab}) \right. \\
&\left. + \sqrt{\frac{\tau}{\beta(1 - \beta)(T - \tau)}} \cdot \mathrm{I}_1(2\sqrt{ab}) \right] d\tau, \qquad (5.22)
\end{aligned}
$$

where I_0 and I_1 are the modified Bessel functions of the order zero and one respectively (see e.g.[Rek95]), $a = \frac{\omega \tau}{\beta}$, $b = \frac{\omega(T - \tau)}{1 - \beta}$.
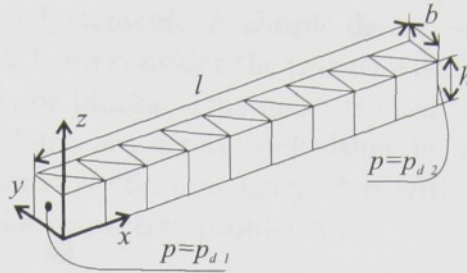
Figure 5.1: The mesh for example calculation of 1D transport.

The function

$$G(X,\tau) = \frac{1}{2}\text{erfc}\left(\frac{\beta X - \tau}{\sqrt{\frac{4\beta\tau}{P}}}\right) + \frac{1}{2}\exp(PX)\cdot\text{erfc}\left(\frac{\beta X + \tau}{\sqrt{\frac{4\beta\tau}{P}}}\right) \qquad (5.23)$$

represents in fact the solution of a plain advection-diffusion problem in the concerned domain and conditions. For advection-dominated problems (i.e. $P \gg 1$), the first term in (5.23) is dominant and the second one can be neglected (the second term provides to fulfil the boundary condition while the first term is a solution of a problem on a "both-side infinite" domain).

The calculation of the analytical solution requires numerical integration. The algebraical operations are relatively sensitive to computational errors (reductions of large values of the exponential functions), which causes some unnatural fluctuation of the displayed curves. It is interesting to remark, that the computational cost of the evaluation of the analytical solution is comparable with the numerical solution by the model analysed.

5.2   Test calculations of advection

In this section, we deal with the model of advection (the MIE is turned-off). Most of the problems serve for identification of numerical dispersion by comparisons with exact solutions of advection-dispersion equation (presented above 5.1.1). The results are important in two ways: give the basic estimation of the numerical dispersion in practical problems and allow to make a better review of the results of the full model.

As stated in the preamble, we consider the 1D and 2D problems solved as three-dimensional, with the remaining dimension "degenerated" to a size

of one discretisation cell/element. A simple discretisation of 1D channel is demonstrated in Fig. 5.1, we consider the prisms with right-triangle bases, by pairs composing cubes or blocks. This mesh is used for all the 1D problems solved. The 2D problems are discretised either by similar way (blocks of two prisms), or by prisms of constant height but with special plane topology (described below at the respective problems).

Problem 1: 1D uniform flow, step input

This is a basic, but most important case as we can exactly fit the numerical dispersion forecasted by the relation (3.84) and the comparison for the non-equilibrium transport will be done for this situation (section 5.3.1).

We consider the domain as a block (see Fig. 5.1, we will refer as the channel) with length $L = 1000$m and cross sectional dimensions 50×50m (in the vertical direction). The following discretisations will be used:

code	length of blocks	Δx: distance of cell centres	number of blocks	number of cells
01	100m	50m	10	20
02	20m	10m	50	100
03	5m	2.5m	200	400

The hydraulic parameters were chosen so that the flow velocity is $v = 1$m/day (for simplicity) and the values were not far from those in practical problems. We consider the pressure head difference 20m ($p_{d1} - p_{d2}$ in Fig. 5.1), hydraulic conductivity 5m/d and porosity $n_m = 0.1$ (but any of them does not explicitly appear in the calculation of advection).

We present the results of two experiments, one demonstrating the influence of Courant number Cr to the numerical dispersion (in the coarsest mesh nr.01) and the second demonstrating the influence of discretisation size. In both we compare the distribution of concentration (a curve for 1D domain) in the fixed final time $t_{\text{fin}} = 500$days with the analytically calculated one.

For the chosen values of Cr (in fact set by a choice of time step Δt) in the channel 01, we derive the following values of the numerical dispersion, according to the relation (3.84) (we note the maximum attainable value of dispersion is 25m^2/d for Cr$\rightarrow 0$):

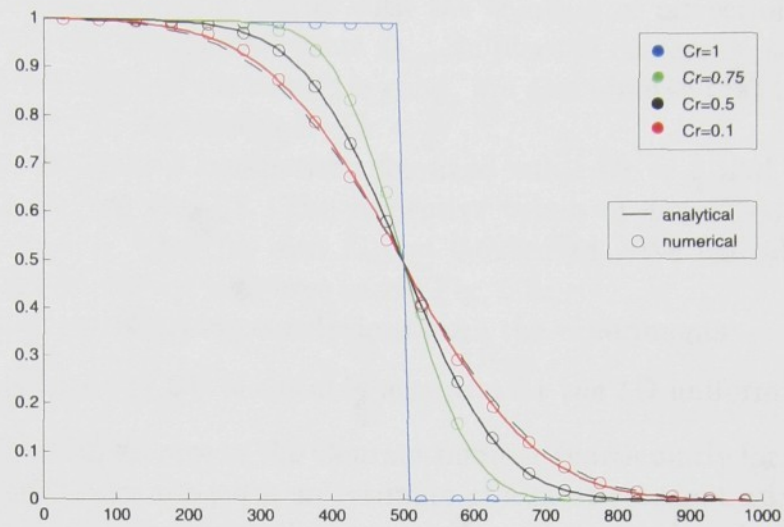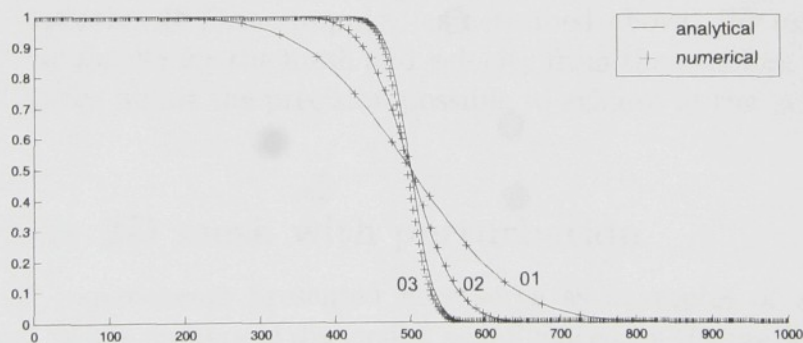| Δt [days]	50	37.5	25	5
Cr	1	0.75	0.5	0.1
D_{num} [m^2/d]	0	6.25	12.5	22.5

Figure 5.2: Relative concentration vs. position [m]. Comparison of the results of the advection calculation with the analytical solution of advection-dispersion problem, where the expected value of numerical dispersion (3.84) is substituted. The dashed line represent the maximum numerical dispersion for Cr→ 0.

Figure 5.3: Relative concentration vs. position [m]. Comparison of the results of the advection calculation with the analytical solution of advection-dispersion problem, where the expected value of numerical dispersion (3.84) is substituted. The codes 01, 02, and 03 denote the meshes used, see the table in the text.

The comparison of model result with the solution of advection-dispersion problem with the appropriate value D_{num} in place of dispersion is in Fig. 5.2. The agreement of both the results is good. We also observe that there is very small difference in the results for $\text{Cr} < \frac{1}{2}$.

Further we make a comparison for fixed value $\text{Cr} = \frac{1}{2}$ and all the discretisations 01, 02, and 03. The respective values of dispersion are $D_{01} = 12.5\text{m}^2/\text{d}$, $D_{02} = 2.5\text{m}^2/\text{d}$, and $D_{03} = 0.625\text{m}^2/\text{d}$. We can also see well matching results for all the three cases, Fig. 5.3.

There are the following conclusions from the experiments:

- The relation (3.84) is suitably accurate for the 1D uniform[2] mesh.

- The small influence of the Courant number (particularly for the smaller values) makes adequate an estimate of almost constant numerical dispersion also in non-uniform mesh (see the consideration in section 3.5.3). In fact, it is known also without the experiment that for the dispersion coefficient, a change of about half an order of magnitude has small effect.

Problem 2: 1D uniform flow, Dirac input

In contrast with the comparable problem with step input, we do not obtain good match of numerical and analytical results, because of impossible discrete representation of Dirac impulse, as described above. We demonstrate in Fig. 5.4 the results for the mesh and velocity from the problem above, obtaining an image about the precision possible to achieve in the 2D problems below.

Problem 3: 2D mesh with perturbation

The two 2D experiments presented here serve as examples of analysis of "anisotropy" of the numerical dispersion as influenced by the mesh geometry. Since it is quite extensive topic, we understand the experiments presented here as a suggestion for separate study (we do not make any conclusion here).

The first experiment is transport by constant velocity in perturbed 2D mesh: the original mesh is composed of right triangles paired to uniform

---

[2]In fact the mesh is not really uniform, the distances cell centres have two alternating vales $\frac{2}{3}\Delta x$ and $\frac{4}{3}\Delta x$ but as observed, these local variation do not influence the result substantially
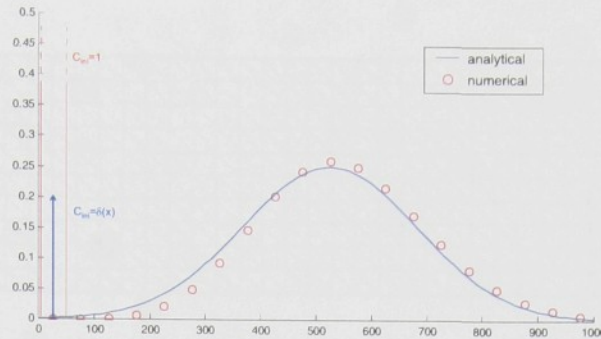
Figure 5.4: Transport calculation with initial Dirac impulse on the mesh "channel 01" (see above). The discrete representation of initial concentration causes the results matching worse than for step function as initial condition.

squares (in plane projection) in x and y direction and both the coordinates are perturbed by random value from Gaussian distribution with chosen variance. The direction of velocity is parallel to the x axis (i.e. parallel with the sides of unperturbed mesh) and the initial condition is chosen as certain non-zero concentration in a single pair of trilateral cells (composing one block) to represent a Dirac impulse.

An example of the perturbed mesh is in Fig. 5.5 with calculated results in Fig. 5.6 (the physical parameters and mesh size correspond to the 1D problem above). In contrast with the unperturbed mesh with the velocity parallel to the direction of square edges (equivalent 1D problem as we can simply "extract" the row of cells), we observe the numerical dispersion in the transversal direction, the higher the higher was the variance of the perturbation.

Problem 4: 2D mesh and general orientation of velocity

We consider the same situation as for the above problem with perturbed mesh – the mesh structure and initial condition. Now the subject of study is relation of the velocity direction to the "characteristic direction" of the mesh (i.e. x axis, y axis and the direction of diagonals of the squares). The influence is quite unclear – the principal directions of the resulting ellipses non-trivially differ from both the mesh directions and velocity directions, e.g. Fig. 5.7. The full analysis would require detailed study, also theoretical.
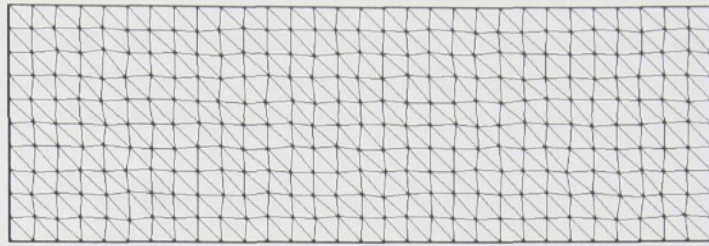
Figure 5.5: Perturbed mesh with variance in node positions 0.5m (with respect to the size of mesh step 10m).
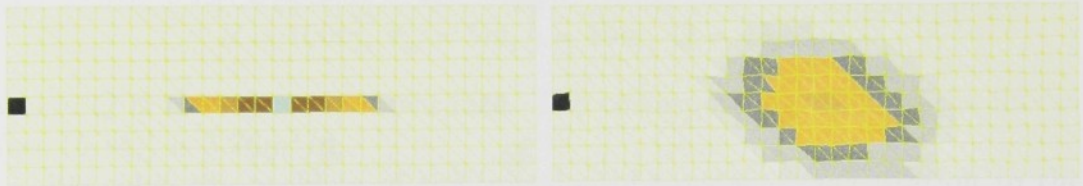

Figure 5.6: Numerical dispersion on the perturbed mesh (Fig. 5.5) as compared with the case of uniform mesh (equivalent to 1D problem). The relation of longitudinal and transversal dispersion depends on the strength of perturbation.
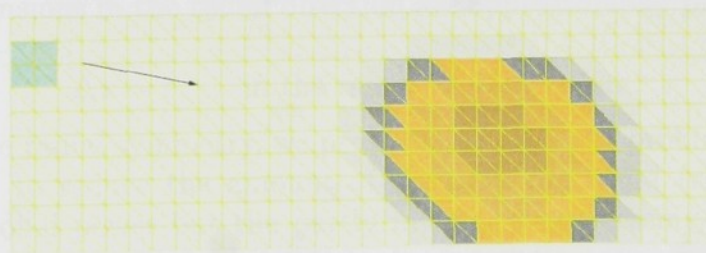

Figure 5.7: Numerical dispersion on the uniform mesh with the flow velocity in the displayed direction and with the initial condition as illustrated.

Problem 5: 2D radial flow, step input

This model problem was chosen to represent a typical situation in the hydro-geological actions – drawing or injecting well. Also it an example of the use of the model on the problem with non-uniform mesh and with non-uniform velocity field.

In this section, we test the advection model, mainly for identification of the numerical dispersion. In the section 5.3.2 a problem with non-equilibrium mobile-immobile exchange is considered.

We consider a circle domain of radius R with the well in the center. For correct physical dimensions and for the use of the 3D model, we consider the thickness h. To avoid problems with singular point in the circle center, we represent the well as a small circle with radius r_w, applying the side flux boundary condition instead of a sink in the equation. We used the values

$$R = 100\text{m}, \ r_w = 5\text{m}, h = 10\text{m}, \ Q = 48\text{m}^3/\text{d},$$

where Q is the injected/drawn rate. The corresponding value of the flux A (see (5.14)) is $3.76\text{m}^2/\text{d}$.

We solve the problem of the injection of constant concentration to the domain with zero initial condition and we observe the distribution of con-tamination in sequential time instants.

Discretisation

The mesh was constructed as non-uniform, finer close to the well and coarser at the outside boundary. The topology with correct dimensional proportions is drawn in Fig. 5.8.

The dimensions in the radial direction are approximately proportional to the position

$$\Delta x \sim r \qquad \text{in the range} \quad 1.75\text{m} - 25\text{m}.$$

Thanks to the radial symmetry, we preferred to solve the problem in a sector of the circle, to reduce the amount of the data processed (not a problem of computational power but the partly manual preprocessing and postpro-cessing). The sector used is the $\frac{\pi}{4}$ angle and the total number of cells is 140.

The numerical dispersion in radial, i.e. longitudinal direction, estimated by (3.84) is expressed by almost constant dispersion coefficient $D_{\text{num}} = 0.5\text{m}^3/\text{day}$, using the assumption $\text{Cr} \approx 0$, which is valid in most of the cells,
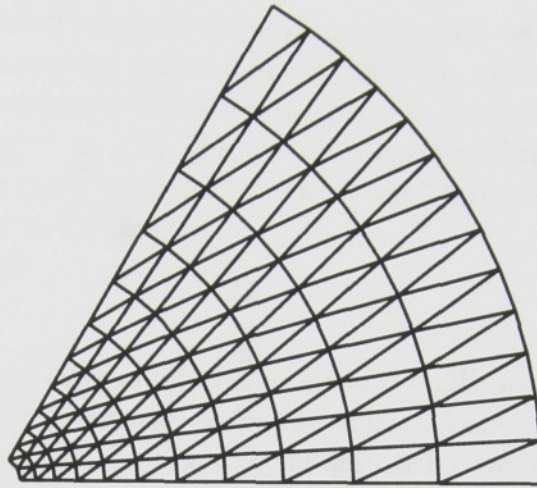
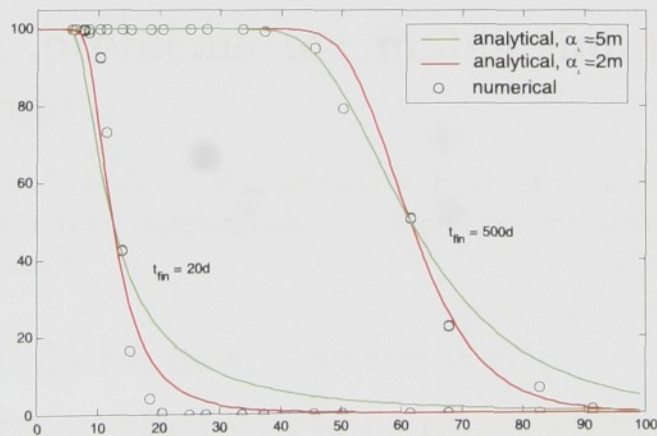Figure 5.8: Topology of the mesh for the model problem of transport in the radial flow regime.

Figure 5.9: Solution of transport problems in 2D radial flow. Concentration vs. position in the radial direction (meters) for the problem of injecting.

except close to the well, and the fact that v is inverse proportional to r (the dependence on v and r cancels).

In terms of hydrodynamical dispersion expressed as the proportional to the velocity, the numerical dispersion corresponds to the non-constant dispersivity in the appropriate advection-dispersion problem. Defining $D_{num} = \alpha_L^{num} v$, we derive $\alpha_L^{num} \approx \frac{1}{2}\Delta x$ (for $Cr \approx 0$, except of the cells close to the well) and the upper limit value 12.5m (the lower limit is zero ($Cr \approx 0$) rather than the value $\frac{1}{2}\Delta x = 0.875$m).

Results

For the comparison of the model with analytical ADE, we use the values $\alpha_L = 2$m and $\alpha_L = 5$m as representative for the non-uniform distribution analysed in the previous paragraph. In Fig. 5.9, the results for two chosen time instants are displayed. We can observe that the numerical results roughly fit to the analytical: in the time 20days, the dispersivity $\alpha_L = 2$m is closer to match (which is reasonable) and in the time 500days, the numerical results partly match both the analytical curves.

We conclude that our estimation is quite rough but it is appropriate to many simplification in calculation of both the results and to geometrical irregularities.

5.3 Test problems for mobile–immobile exchange

The comparison of results in this section is the most important experiment as it confirms correct incorporation of the mobile–immobile exchange into the transport model.

5.3.1 1D uniform flow, step input

We solve the problem defined above for the plain advection: a channel with uniform flow (Fig. 5.1), with zero initial value of both the concentrations c_m and c_i (clean medium) and constant value of concentration at the inflowing water (at the point $x = 0$).

Besides the above mentioned parameters, we introduce the values of mobile and immobile porosities as two choices of values with opposite weighting.

Table 5.1: Values of $T_{1/2}$ chosen for the example calculations and comparison of numerical and analytical solutions. The values of ω are appropriately derived for the use in the analytical solution, see (5.20) and (5.24).

$T_{1/2}$ [days]	$n_m = 0.1$, $n_i = 0.2$	$n_m = 0.2$, $n_i = 0.1$
	ω (dimensionless)	
∞ (turned-off exchange)	0	0
1000	0.462	0.231
100	4.62	2.31
10	46.2	23.1
0 (equilibrium)	∞ (not calculated)	∞

We resume:

length of the domain $\quad L = 1000\text{m}$
velocity $\qquad\qquad\qquad v = 1\text{m/day}$
porosities $\qquad\qquad\quad n_m = 0.1\ n_i = 0.2\ \text{ and }\ n_m = 0.2\ n_i = 0.1$
input concentration $\quad c_0 = 1\text{kg/m}^3$
time of observation $\quad t_{\text{fin}} = 500\text{days}$.

We remark, that for the choice $n_m = 0.2$, the hydraulic conductivity is appropriately changed with respect to the case $n_m = 0.1$, so that the velocity is equal in both the cases.

The calculations are performed for the rates of the mobile–immobile exchange covering the full possible scale, from 0 to ∞, which is important to catch the different transport regimes close or far from the equilibrium. The values are in Tab. 5.1 in terms of the characteristic time of exchange and the dimensionless form of the rate coefficient (Damkohler number) used in the analytical solution

$$\omega = \frac{\alpha L}{n_m v} = \frac{L}{v} \cdot \frac{n_i}{n_m + n_i} \cdot \frac{\ln 2}{T_{1/2}}. \tag{5.24}$$

The channel is discretised as described above and displayed in Fig. 5.1. For this problem, we use 20 blocks, corresponding to 40 trilateral prismatic cells, with the average distance of centres $\Delta x = 25\text{m}$ (i.e. between the medium-coarse (02) and coarsest (01) mesh used in the respective problem

for advection). The time step is chosen $\Delta t = 12.5\mathrm{d}$ to achieve the Courant number $\mathrm{Cr} = \frac{1}{2}$ (and thus a medium numerical dispersion, without excessive time discretisation).

The numerical dispersion, expressed by the formula (3.84) is $D_{\mathrm{num}} = 6.25\mathrm{m}^2/\mathrm{d}$ and this is used as the dispersion coefficient in the ADX problem whose analytical solution we use for comparison. In terms of the dimensionless values for the analytical solution (5.22), we determine

$$P = 160, \qquad \beta = \frac{1}{3} \text{ or } \beta = \frac{2}{3},$$

and the values of ω in Tab. 5.1. The value of Péclet number corresponds to the advection-dominated process and the use of the analytical solution for infinite domain is thus appropriate.

The results and comparisons for both the combinations of porosities are displayed in figures 5.10 and 5.11, by means of the mobile concentration in the channel in the final time of calculation. There is good agreement for all the regimes of non-equilibrium, confirming that the numerical dispersion is the only significant numerical error.

Precisely, for $\omega = 0$ the model calculates with turned-off MIE (i.e. the advection only) and the analytical solution (5.22) reduces to (5.10). Thus we do in fact the same comparison as in Fig. 5.3. Since the values $T_{1/2} = 0$ and ω are impossible to be directly used neither in the numerical model nor in the analytical expression (5.22), the numerical results were obtained with a smallest possible non-zero value not causing a computational error and the analytical solution was expressed as the analytical solution of type (5.6) for the advection-dispersion problem with equilibrium interaction, with retardation factor $R = 1 + \frac{n_i}{n_m}$ which is 3 or $\frac{3}{2}$ respectively. This do not depreciate the comparison, it rather means a "cross-matching".

Further, we demonstrate the time-development of the concentration distribution, but in contrast with Dirac input, it is difficult to display clearly in a static figure. The curves (approximately identical for both analytical and numerical results) for two different time instants are presented in Fig. 5.12. The values of parameters were chosen to demonstrate the meaning of the dimensionless parameter ω together with. Considering the characteristic length L as the final position of the front, the two curves from different physical values correspond to the identical regime (see the caption of the figure for details).

It is also interesting to remark concerning the influence of use of the ADE solutions (5.6) and (5.10) (infinite/semi-infinite): In the case $T_{1/2} = 100$
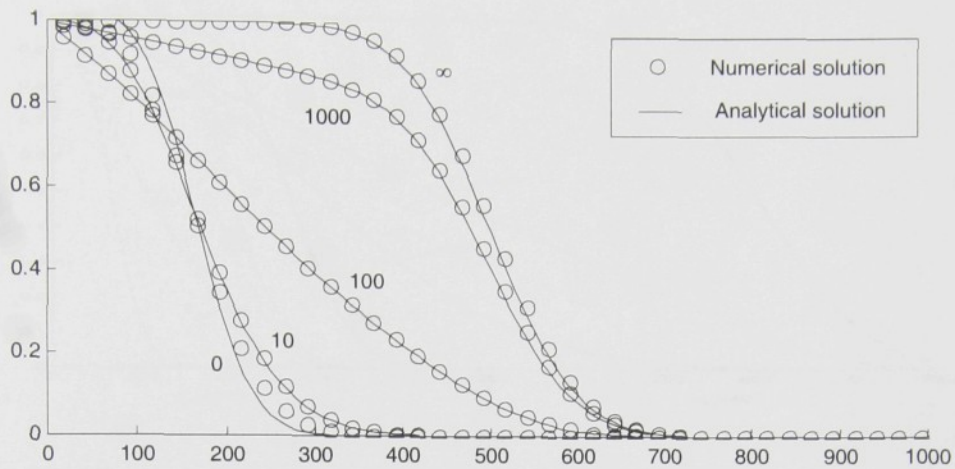
Figure 5.10: Comparison of numerical and analytical solution for the 1D non-equilibrium transport problem, for the porosities $n_m = 0.1$, $n_i = 0.2$. Distribution of the relative concentration in the mobile zone (c_m/c_0) vs. position in meters in the final time of calculation. The labels denote the values of the characteristic time of exchange $T_{1/2}$ used.
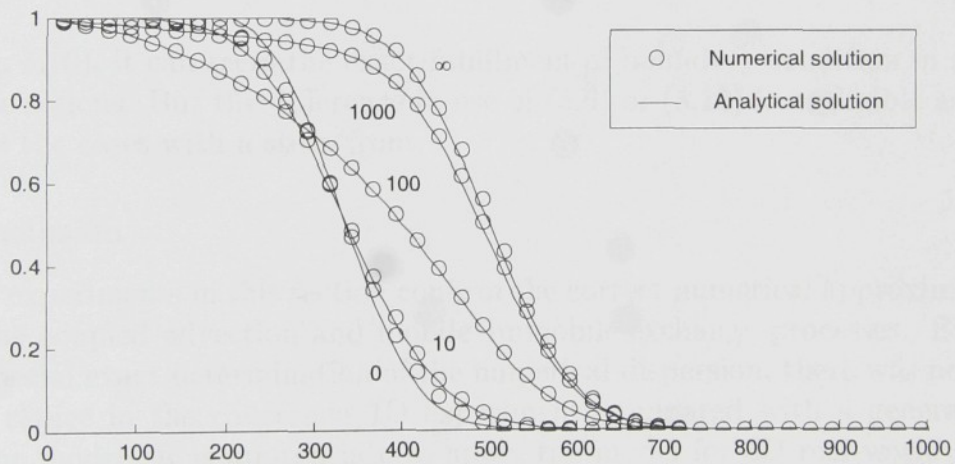

Figure 5.11: Comparison of numerical and analytical solution for the 1D non-equilibrium transport problem, for the porosities $n_m = 0.2$, $n_i = 0.1$. Distribution of the relative concentration in the mobile zone (c_m/c_0) vs. position in meters in the final time of calculation. The labels denote the values of the characteristic time of exchange $T_{1/2}$ used.
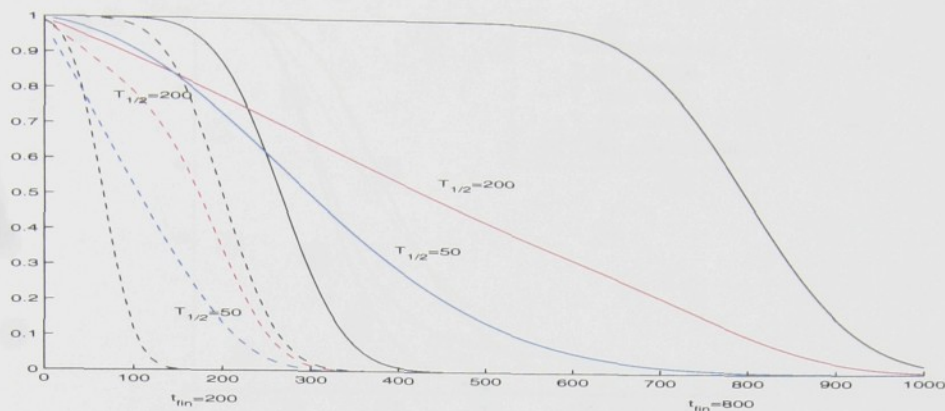
Figure 5.12: Solution of 1D non-equilibrium transport problem, with step input from the "left". Demonstration of time-development (states in 200d dashed and 800d solid lines) and comparison of different situations with same dimensionless Damkohler number ω: $T_{1/2} = 200d$ and $L = 800m$ versus $T_{1/2} = 50d$ and $L = 200m$ (the final position of the "equilibrium front" is used as the characteristic length). The black lines represent the equilibrium exchange and no interaction.

(Fig. 5.10), it can seem the exact fulfillment of boundary condition in $x = 0$ to be serious. But the difference in use of (5.6) or (5.10) is negligible as well as in the cases with a steep front.

Conclusion

The experiments in this section confirm the correct numerical approximation of the coupled advection and mobile–immobile exchange processes. Except of special exact determination of the numerical dispersion, there was no special choice in the concerned 1D experiment, compared with a general use of the model. It is appropriate to apply the model for 3D real-world problems with dominant advection (with respect to the dispersion), as a coarse approximation.

5.3.2 Radial problem with a drawing well

As said above, this model problem represents the transport around a drawing or injecting well. We consider the same problem and mesh geometry as in
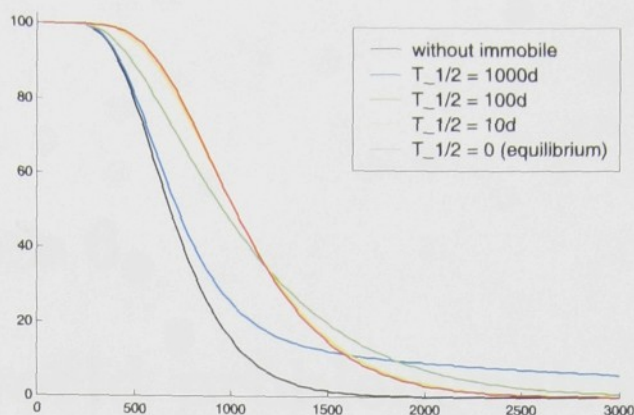
Figure 5.13: Solution of transport problem in 2D radial flow, with non-equilibrium mobile–immobile exchange of various rates. Concentration (percents) vs. time (days), when drawing from the "circle" of constant contamination (with zero concentration outside).

the section 5.2, where we observed the behavior of the advection model on the problem of injection to the domain with zero initial state.

Now we consider the extraction from the domain with non-zero constant concentration at the beginning and assume zero-concentration inflow from the outside. Various regimes of non-equilibrium are considered and compared.

The domain of the problem is a circle with radius $R = 100$m and thickness 10m and the for the numerical calculation we use a $\frac{\pi}{4}$-sector (see Fig. 5.8 for the shape and the non-uniform discretisation). The rate of pumping in the well is $Q = 48$m^3/d (falling on the whole circle).

The numerical dispersion, as estimated and tested above in the problem 5.2 has values of the magnitude comparable with the values of physical dispersion in the longitudinal direction (we recall that thanks to the symmetry, there is no physical and no numerical dispersion in the transversal direction), the dispersivity α_L between 10^0 and 10^1 meters.

In Fig. 5.13, we demonstrate the time-dependences of the drawn concentration for various values of mobile–immobile exchange coefficient $T_{1/2}$. The quicker mobile–immobile exchange takes effect in the earlier part of the time interval, while the slower exchange takes effect in the later time, as expected. A similar behaviour is also observed at the real-world problem solved in the next chapter 6.

Chapter 6

Real-world problem calculation

In this chapter, we present the results of the application of the model described in this thesis for a real-world problem of underground remediation in Stráž pod Ralskem region. The construction of the program code and the preparation of input data is a joint work of the author and the team in DIAMO, s.e. The calculations and processing of results are a work of the author himself.

In the calculations, we touch the solution of inverse problem and the process of calibration, validation and verification. We do not go deeply into the rather complex theory of inverse problems; the presented problem solution is in fact a calibration "ad hoc", manually using the method "trial-and-error" [ZB95] and basic statistical measures. The solution of inverse problems is a recent topic of numerical analysis (e.g. [CKM02]), but the methods can be mostly applied only for special problems. For large problems with strong uncertainty in the coefficients, the basic methods are typically used.

6.1 Description of the problem

6.1.1 Situation

We solved a problem from the Stráž pod Ralskem region in the northern Bohemia (see [Nov01, NSŠ98, MMSŠ00] for further information). The overall situation is demonstrated in Fig. 6.1: there are two important layers, lower is the Cenomanian where the leaching was performed and contains the major contamination, the upper is the Turonian with isolated smaller "clouds" of
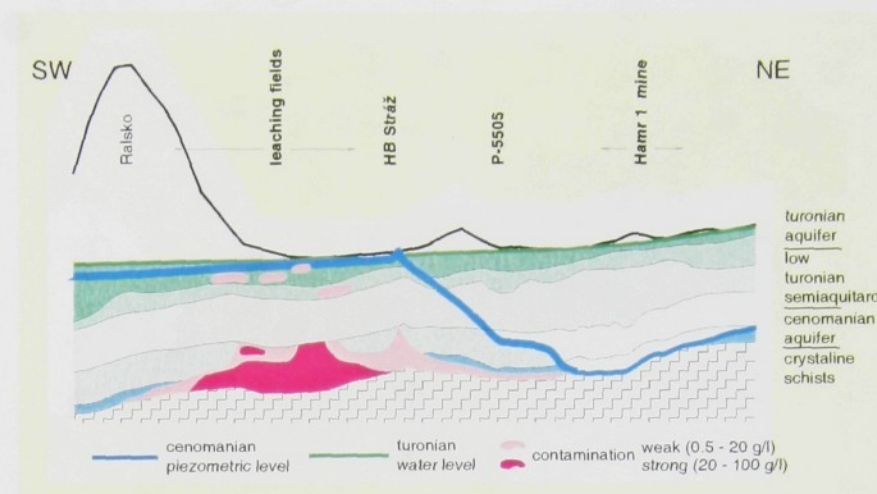
Figure 6.1: Underground situation in the Stráž region in a vertical cross-section. The left part demonstrates the intrusion of contaminants from the Cenomanian to the Turonian aquifer, whose remediation is modelled in this chapter. The right part shows the depressed water level in the deep mine Hamr (not related to the problem solved here).

contamination caused mostly by technical defects of well casings. The problem we deal with here is related to such a single contamination cloud in the Turonian aquifer.

The model was applied to a problem of extraction of the contamination from the underground by pumping wells. It is a typical situation, when dual porosity shows its influence – the cleaning to a level of certain "safe" value of concentration remaining takes markedly more time, because of the pollutants persisting in blind pores with negligible water motion.

In practice, there are two objectives for the operation of extraction wells: to clean the domain in a short time with low expenses and to process the extracted chemicals by further technologies efficiently. Thus the model is expected to forecast the drawn concentrations and the total pollutant mass extracted and remaining, which are subsequently entered to optimization models for choice of extraction scenarios (positions of wells and pumping rates), see e.g.[Čer02].

The problem described here is the remediation of the site "VP-9C" performed on the interval March 2000 – September 2001 (before the dual-
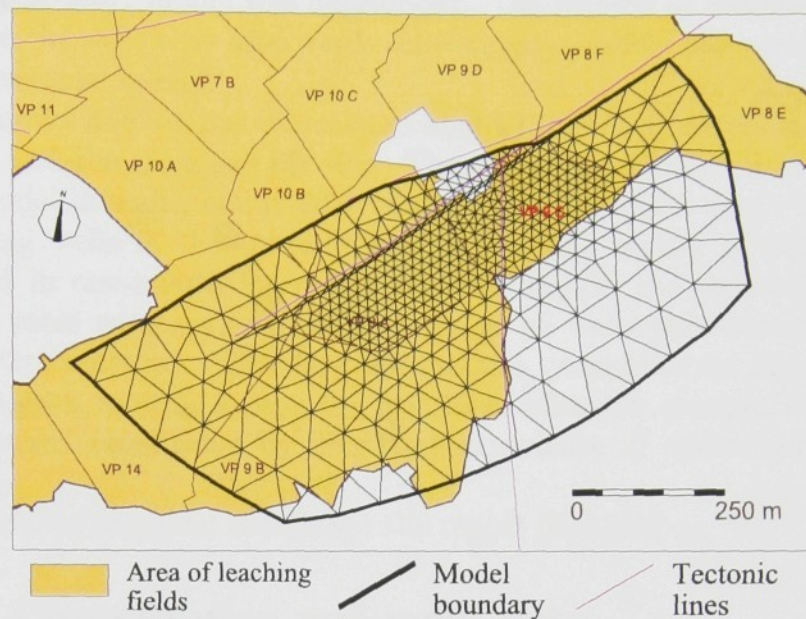
Figure 6.2: Position and structure of the discretisation mesh for the problem of remediation of the site "VP-9C". The mesh also covers the neighbouring area of leaching field "VP-9A", not extracted from (see also Fig. 6.3).
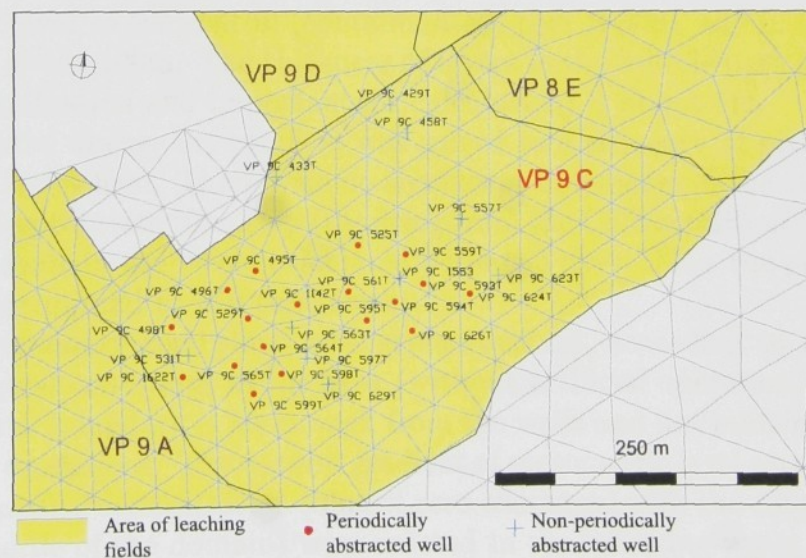

Figure 6.3: Position of extraction wells relative to the discretisation mesh for the problem of remediation of the site "VP-9C".

porosity transport model was developed). The records of measured concentrations in the wells were afterwards conveniently used for test and calibration of the developed model.

The model domain has dimensions about 1200×500 meters in horizontal direction and the thickness 60–90m. The contaminated area is in the centre of the model domain, about 20% of the total horizontal area. There were 20 drawing wells in the contaminated part. The regime of pumping was controlled in one-month intervals. In each month, the generally different pumping rates were set or possibly some or all wells were turned-off (gaps in the graphs below). The flow regime was considered as approximately steady in each month, except the first days after the change, whose effect was neglected (confirmed by long-time experience of concerned people in DIAMO).

For further technical details see the report [Hok01b].

6.1.2   Discretisation and input data

The discretisation mesh in a plan view is shown in Fig. 6.2 and the positions of pumping wells are marked on the detail, Fig. 6.3. The mesh contains 1003 multielements (i.e. elements grouped by a plane projection, see section 4.1), in 12 layers, approximately 12000 elements in total. The average horizontal size of element in the central (contaminated) part is 30m, and in the peripheral part about 100m. The thickness of layers in the middle part (containing the contamination and important for calculation) is about 5m.

As stated above, the problem was solved as a sequence of problems in a steady velocity field. There were no significant differences in the velocity and thus the appropriate time step (resulting from the CFL condition (3.83)) was used the same in the whole calculated period: 3 days. Thus the period of 19 months correspond to 570 time steps.

The boundary conditions were given constant, according to typical hydrogeological conditions in the area (without artificial operation), considering that the boundary is far enough from the wells and not influenced by the pumping operations. The natural gradient of piezometric level was prescribed and the natural concentration (almost zero compared with the contamination in the middle of the domain) were entered in the inflowing-water boundary. In each one-month interval, different values of drawing rates were prescribed (and the new velocity field were re-calculated).

The initial conditions were extrapolated from the set of measurements in the domain (at more places than the drawing wells).

The material parameters were obtained partly by laboratory measurement, partly by calibration during former comparisons with other models. The hydraulic conductivities are known quite well, while the identification of the immobile porosity (or ratio of mobile and immobile porosity) is very difficult. In general, laboratory measurement are impossible for many material properties, because the extraction of a sample from the underground can significantly change the porous structure. Many methods are developed for parameter identification "in situ" [VMVF97, CKM02].

The measured concentration data were sparse in comparison with calculated and also quite irregular. About 1 or 2 measurements fall on each month. Beside these, the more significant values of monthly totals of drawn solute mass were recorded (based of further chemical processing).

6.2 Solution

6.2.1 Numerical process

The problem with 12000 elements is not too large in the current measures. A standard PC (Pentium III, 1GHz) was used for the calculations. For the flow model, the solution of the algebraic system (about 100000 unknowns for the MH-FEM) was the only time-consuming phase, it took approximately 10 seconds for each of the 19 steady flow problems, 3.5 minutes in total. The transport calculation for the whole period took about 1.5 minute.

Check of the numerical dispersion in the mesh

To document the considerations in sections 3.5.3 concerning the numerical dispersion, we present an analyse of the distribution of Courant number in the mesh. According to (3.84), the numerical dispersion is determined by Courant number (no dispersion for $Cr = 1$ and maximum dispersion for $Cr \to 0$), besides cell size and velocity.

Table 6.1 shows that $Cr < 0.1$ for most of the cells and thus the dispersion is not influenced by the Courant number. The reason of this "extreme" distribution is in the velocity field close to the wells: the well is not opened in the full vertical range and causes significant vertical coordinates of velocities,

Table 6.1: Distribution of Courant number for the solved remediation problem (site VP-9C), with a partly non-uniform mesh of approximately 12000 cells. Comparison of a state with all 20 wells and with one operating well (example).

interval of C_r	cell count in 20-wells problem	cell count in 1-well problem
(0.5, 1)	2 (0.02%)	2 (0.02%)
(0.25, 0.5)	32 (0.28%)	1 (0.01%)
(0.1, 0.25)	87 (0.72%)	12 (0.1%)
(0, 0.1)	98.98%	99.87%

which means large cell-side fluxes (together with a fact, that horizontal cell dimensions much larger than vertical).

6.2.2   Comparison measures and criteria

To obtain useful information from the comparison of calculated and measured data, it is not trivial manipulation with quite large amount of data.

One possible problem was already mentioned: the measurements are markedly more distant then the calculated results – the concentrations are known in places of wells and just once a month or as a cumulative one-month drawn mass, while the calculated drawn concentration are resulted in each 3-days time step.

The second substantial problem is large uncertainty of quantities in the space-sense. The initial distribution of the concentration is not reliably accurately determined and together with random inhomogeneities in the porous medium, it can significantly influence a local state around a particular well. In other word, there are no means to fit the results in each well, e.g. by manipulation with in-homogeneous material data.

Thus only a global comparison is possible and a calibration only for homogeneous material parameters is considered. We express the amount of solute mass drawn, summed over one month and all the wells[1] (MTM – monthly

---

[1] In fact, a comparison with certain wells excluded was performed, as the values in these wells differed much more than the other wells, indicating an error in the measurement or in the initial data rather than actually unmatched model and reality, see [Hok01b].

total mass), which value can be simply expressed from both measured and calculated results. The graphs are constructed for this measure as depending on time (19 values in the whole period).

As a single global measure of model–measurement fitting we consider the sum deviations (observed value minus calculated value) of MTM in all months and the sum of square deviations (observed value minus calculated value) of MTM in all months. These are two target functions in the process of calibration. In fact the sum of squares is a "stronger" measure (fitting it automatically implies fitting of sum of deviations), but the sum of deviations is convenient first to find an overall magnitude of the results.

6.2.3 Calibration of parameters

Concerning the solution of the problem by the numerical model and comparisons with measurements it is important to also deal with calibration of the material parameters in the model, which were not accurately determined a-priori: mobile and immobile porosity and the rate of mobile–immobile exchange.

Instead of mobile and immobile porosity, we operate with mobile n_m and total $n_{tot} = n_m + n_i$ porosity. The basic set of values of material parameters for experiments is

Mobile porosity n_m	0,05	0,07	0,1
Total porosity $(n_m + n_i)$	0,2	0,25	0,3
Char. time of exchange $T_{1/2}$ (days)	50	100	200

where the limits were suggested based on the experiences from other modellings in the region (porosity) or on estimation of skilled geologists (the rate of exchange). Moreover, one should notice that the presented interval of values T cover a range for reasonable use of the model for the considered problem: lower T about 10 days already correspond to a state close to equilibrium, while higher T cannot be reliably confirmed by the comparison if we take into account that the time interval of the solved problem is 570 days.

The calibration of these parameters was performed in 3 steps. In each step always the one of the parameters is constant and the other two are varied to achieve a optimum (possible to view in a 2D table or a graph). Two measures were examined in comparison: simple deviations and squares of deviations, the first one tells about the overall magnitude of the results and the second one about the exact fitting of the data.
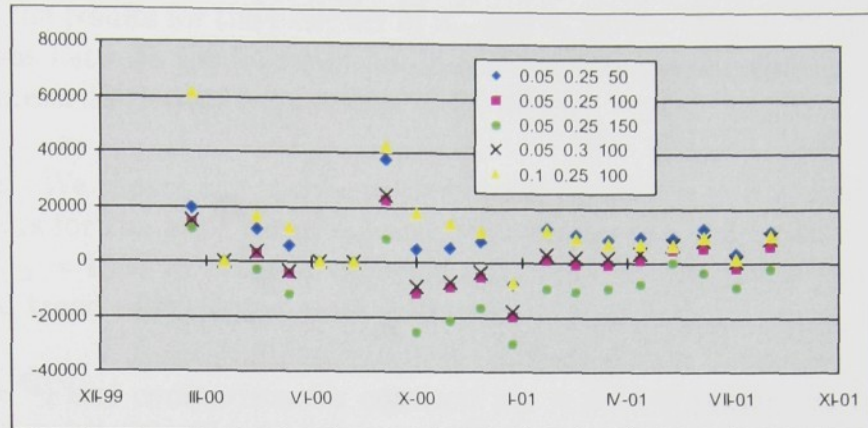
Figure 6.4: Deviations (differences) between measured and calculated values of drawn solute mass in each month (in kilograms). Overview for various sets of material parameters used in the model (in the order: mobile porosity n_m, total porosity $n_{\text{tot}} = n_m + n_i$, and characteristic time of mobile–immobile exchange $T_{1/2}$).
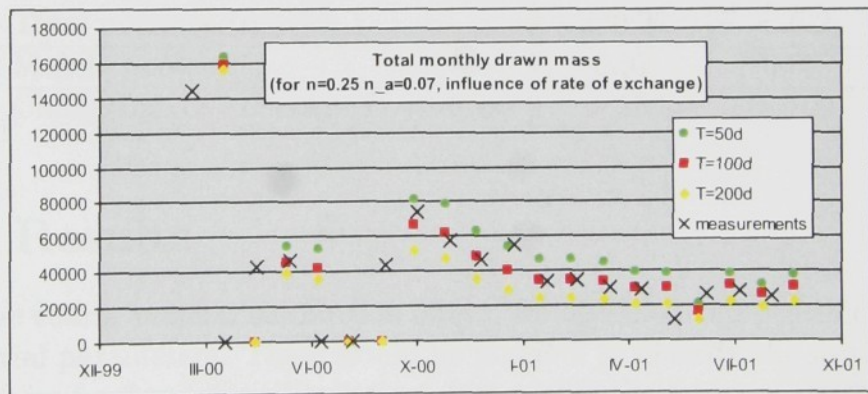

Figure 6.5: Drawn solute mass in each month (in kilograms) – absolute values in contrast with Fig. 6.4. Comparison of measured values and calculated with model for various choices of characteristic time of mobile–immobile exchange $T_{1/2}$ for calibration.

Step 1: We choose the middle value of characteristic time $T_{1/2} = 100$d and observe the results for the basic set of n_m and n_i values: Tab. 6.2. In Fig. 6.4, deviations between model result and measurements are shown, for wider set of parameter for better comparison.

Step 2: We choose the middle value of total porosity $n = 0.25$ and observe the results for the basic set of n_m and $T_{1/2}$ values: Tab. 6.3 (with additional value $T_{1/2} = 150$d in place of expected optimum. In Fig. 6.5, a comparison of global trend of extracted mass is drawn.

Step 3: Final comparison for constant $n_m = 0.07$ is performed and only the expected "critical" values or intervals are examined (not a full table like steps 1 and 2), with additional interpolation. The important results are

	deviations	square deviations
$n_m = 0.07$, $n_{tot} = 0.2$, $T_{1/2} = 120$d	-11025	$172.21 \cdot 10^9$
$n_m = 0.07$, $n_{tot} = 0.27$, $T_{1/2} = 150$d	6036.0	$181.62 \cdot 10^9$

There are two possible choices of parameters, their deviations during the whole solved interval are compared in Fig. 6.6. The values can be identified already from the tables 6.2 and 6.3:

Total porosity $(n_m + n_i)$	< 0.27	< 0.2
Mobile porosity	0.07	0.07
Char. time of exchange $T_{1/2}$ (days)	> 150	> 100

6.3 Results

From the coarse manual calibration above, we obtained two possible choices of material parameters. There would be possible to identify the values more precisely by further interval splitting. But within the limits of practical use of the model, the obtained values are accurate enough.

Moreover, the process of generating further comparisons is quite complicated: a preparation of additional calculation for new material parameter requires manipulation with several input data files and on the other hand, performing the process automatically would require to construct additional software tool.

sums of deviations $T_{1/2} = 100$			
	$n = 0.2$	$n = 0.25$	$n = 0.3$
$n_a = 0.05$	-46801.82182	-11316.5	14182.79
$n_a = 0.07$	13124.92516	62898.18	
$n_a = 0.1$	68134.14891	135718.3	186443.8

sums of square deviations (divided 10^9) $T_{1/2} = 100$			
	$n = 0.2$	$n = 0.25$	$n = 0.3$
$n_a = 0.05$	515.1201495	361.6122	389.7547
$n_a = 0.07$	144.8591036	401.2554	
$n_a = 0.1$	677.9773423	1653.804	2877.647

Table 6.2: Results of comparison during the calibration (step 1) – differences of field measurements and model with various material parameters summed to a single objective function.

sums of deviations $n = 0.25$				
	$T_{1/2} = 50$	$T_{1/2} = 100$	$T_{1/2} = 150$	$T_{1/2} = 200$
$n_a = 0.05$	114692.7	-11316.5	-84329.1	-131226
$n_a = 0.07$		62898.18	-5179.88	-51015.9
$n_a = 0.1$	213388.8	135718.3	80037.27	40402.78

sums of square deviations (divided 10^9) $n = 0.25$				
	$T_{1/2} = 50$	$T_{1/2} = 100$	$T_{1/2} = 150$	$T_{1/2} = 200$
$n_a = 0.05$	1121.471	361.6122	1091.956	2002.77
$n_a = 0.07$		401.2554	186.1499	468.192
$n_a = 0.1$	4157.623	1653.804	670.3575	315.4905

Table 6.3: Results of comparison during the calibration (step 2) – differences of field measurements and model with various material parameters summed to a single objective function..
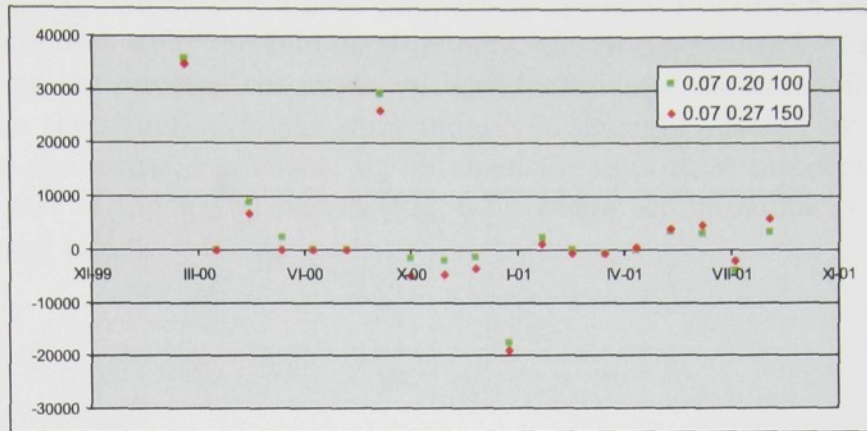
Figure 6.6: Deviations (differences) between measured and calculated values of drawn solute mass in each month (in kilograms). Comparison of two possible choices of mobile porosity n_m, total porosity $n_{tot} = n_m + n_i$, and characteristic time of exchange $T_{1/2}$ as resulted from the calibration.
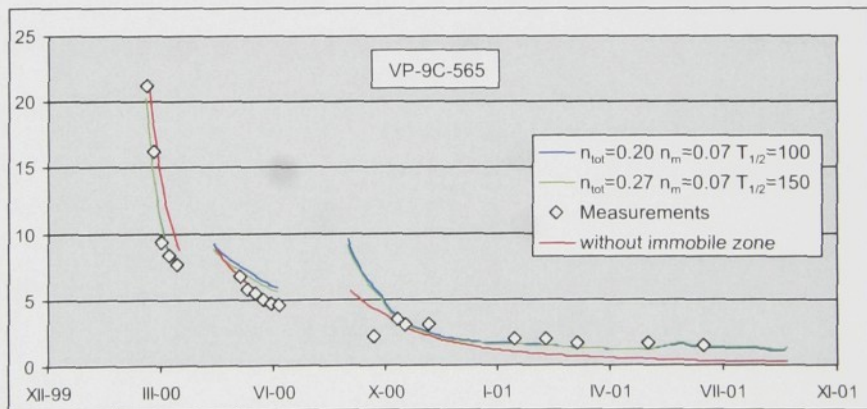

Figure 6.7: Concentration (kg/m^3) in the single well "VP9C-565". Comparison of measured values, results of the model for two possible calibrated sets, and results of the advective model (without immobile pores).

For both the results above, the fit of global trend of the time-dependence curve is good. We present a final comparison in Fig. 6.7 of drawn concentration in a chosen well: the field measurement, the model results for calibrated values and the result of the model without inclusion of the immobile zone.

While the situation in the early months is strongly affected by possible errors in the initial conditions, we obtained the important matching in the second part of the solved period (Fig. 6.7), where the immobile pores play substantial role.

Conclusion

The results presented in the thesis contribute to modelling of underground contamination problems, which is important for efficient management of the underground natural resources. The effect of dual porosity (blind pore zone with immobile water) appears in many porous media; according to the described transport mechanism, it belongs to intensively studied topics of interaction between flowing chemical substances and the solid matrix of porous media.

We derived numerical methods for the composed problem of fluid flow and particular mechanisms of the mass transport. Based on the presented test problems and computed solution of real-world application problem, the chosen approach seems to be efficient, in spite of many limitations given by typical contradiction between quality of reality representation and numerical accuracy on one side and complexity and requirements on input data and computational power on the other side.

Careful application tests of the model on real problems and comparison with measurements represent important "feedback" for the construction and application of numerical methods. Moreover, the obtained agreement between model results and field observations confirmed the expected dual-porosity properties; it provides extended possibilities of modelling and forecasting for the remediation operation in the region of Stráž pod Ralskem.

There are many directions for further work related to the presented model. The method of operator splitting for the transport equations gives the overall framework of solution of various transport mechanisms by various methods and allows further improvements in advection and dispersion as well as a connection with models of other physical and chemical processes. Also, the detailed study of numerical properties of the applied particular implementation can be useful in order to find its limitations for practical use of the model, as mentioned in the text.

Bibliography

[ABBM98] I. Aavatsmark, T. Barkve, O. Boe, and T. Mannseth, *Discretization on unstructured grids for inhomogeneous, anisotropic media. I. derivation of the methods*, SIAM J. Sci. Comput. **19** (1998), no. 5, 1700–1716.

[Ben95] V. Beneš, *Hydrodynamika transportních a transformačních procesů polutantů v podzemních vodách*, Academia Praha, 1995.

[BER93] M. Bai, D. Elsworth, and J.C. Roegiers, *Multiporosity multipermeability approach to the simulation of naturally fractured reservoirs*, Water Resour. Res. **29** (1993), no. 6, 1621–1633.

[BF91] F. Brezzi and M. Fortin, *Mixed and hybrid finite element methods*, Springer, New York, 1991.

[BKT01] M. Benzi, R. Kouhia, and M. Tůma, *Stabilized and block approximate inverse preconditioners for problems in solid and structural mechanics*, Computer Methods in Applied Mechanics and Engineering **190** (2001), 6533–6554.

[BR97] M. Bai and J. C. Roegiers, *Triple-porosity analysis of solute transport*, J. of Contaminant Hydrology **28** (1997), no. 3, 247–266.

[Bru91] M. L. Brusseau, *Application of a multiprocess nonequilibrium sorption model to solute transport in a stratified porous medium*, Water Resour. Res. **27** (1991), no. 4, 589–595.

[BV90] J. Bear and V. Verruijt, *Modeling groundwater flow and pollution*, D. Reidel, Dordrecht, Holland, 1990.

[Čer02]   H. Čermáková, *Optimizing the remediation of the subsurface environment in the Stráž deposit*, Uranium in the Aquatic Environment (B. Merkel et al., ed.), Springer Verlag Berlin Heidelberg, 2002, pp. 793–802.

[CFH99]   O.A. Cirpka, E.O. Frind, and R. Helmig, *Streamline-oriented grid generation for transport modelling in two-dimensional domains including wells*, Adv. Water Resour. **22** (1999), no. 7, 697–710.

[CGMZ76]   I. Christie, D. F. Griffiths, A. R. Mitchell, and O. C. Zienkiewicz, *Finite element methods for second order differential equations with significant first derivatives*, Int. J. Numer. Methods Eng. **10** (1976), 1389–1396.

[Cia78]   P.G. Ciarlet, *The finite element method for elliptic problems*, North-Holland, Amsterdam, 1978.

[CK77]   D.R. Cameron and A. Klute, *Convective-dispersive solute transport with a combined equilibrium and kinetic adsorption model*, Water Resour. Res. **13** (1977), no. 1, 183–188.

[CKM02]   D. Constales, J. Kačur, and B. Malengier, *Parameter identification by means of dual-well tests*, Accepted in Advances in Water Resources, 2002.

[CM80]   M. Crandall and A. Majda, *The method of fractional steps for conservation-laws*, Numerische Mathematik **34** (1980), no. 3, 285–314.

[CR91]   G. Chavent and J. E. Roberts, *A unified physical presentation of mixed, mixed-hybrid finite-elements and standard finite-difference approximations for the determination of velocities in waterflow problems*, Adv. Water Resour. **14** (1991), no. 6, 329–348.

[CS64]   K. H. Coats and B. D. Smith, *Dead-end pore volume and dispersion in porous media*, Soc. Pet. Eng. J. **4** (1964), 73–84.

[Dou99]   C. Doughty, *Investigation of conceptual and numerical approaches for evaluating moisture, gas, chemical, and heat transport in fractured unsaturated rock*, J. of Contaminant Hydrology **38** (1999), no. 1–3, 69–106.

[DR82]   J. Douglas and T.F. Russell, *Numerical-methods for convection-dominted diffusion-problems based on combining the method of characteristics with finite-element or finite-difference procedures*, SIAM J. Numer. Anal. **19** (1982), no. 5, 871–885.

[EGH00]   R. Eymard, T. Gallouët, and R. Herbin, *Finite volume methods*, Handbook of Numerical Analysis, vol. VII, North-Holland, 2000.

[Fro02]   P. Frolkovič, *Flux-based method of characteristics for contaminant transport in flowing groundwater*, Computing and Visualization in Science **5** (2002), no. 2, 73–83.

[Fry02]   D. Frydrych, *Model transportu chemických látek v neustáleném režimu proudění (Model of transport of chemicals in the unsteady flow regime)*, Ph.D. thesis, Technical University of Liberec, Liberec, Czech Republic, 2002.

[GPG96]   C. Gallo, C. Paniconi, and G. Gambolati, *Comparison of solution approaches for the two-domain model of nonequilibrium transport in porous media*, Adv. Water Resour. **19** (1996), 241–253.

[GvG93]   H.H. Gerke and M.T. van Genuchten, *A dual-porosity model for simulating the preferential movement of water and solutes in structured porous-media*, Water Resour. Res. **29** (1993), no. 2, 305–319.

[Hir91]   C. Hirsch, *Numerical computation of internal and external flows, Volume 1 – Fundamentals of numerical discretization*, John Wiley & Sons Ltd., 1991.

[Hok01a]   M. Hokr, *Implementace modelu transportu s vlivem dvojí porozity*, Tech. Report TUL-KMO-TZ/PM–01/001/C1–CZ, Technical University of Liberec, 2001.

[Hok01b]   _____, *Kalibrace modelu transportu se zahrnutím dvojí porozity pro vyluhovací pole 9C*, Tech. Report TUL-KMO-TZ/PM–01/002/C1–CZ, Technical University of Liberec, 2001.

[HS00]   M. Hokr and O. Severýn, *Verification of MH-model in various underground flow problems*, Proceedings of ALGORITMY 2000

(Bratislava, Slovakia) (K. Mikula et al., ed.), Slovak University of Technology, 2000, pp. 94–99.

[Irm54]   S. Irmay, *On the hydraulic conductivity of unsaturated soils*, Trans. Amer. Geophys. Union **35** (1954), 463–468.

[Kaz97]   Ivo Kazda, *Podzemní hydraulika v ekologických a inženýrských aplikacích*, Academia, Praha, 1997.

[KF02]   J. Kačur and P. Frolkovič, *Semi-analytical solutions for contaminant transport with nonlinear sorption in 1D*, IWR/SFB preprint, University of Heidelberg, 2002.

[KH90]   E. F. Kaasschieter and A. J. M. Huijben, *Mixed-hybrid finite elements and streamline computation for the potential flow problem*, TNO Institute of Applied Geoscience, Delft, 1990.

[KL98]   L.A. Khan and P.L.F. Liu, *Numerical analyses of operator-splitting algorithms for the two-dimensional advection-diffusion equation*, Comput. Method Appl. Math. **152** (1998), no. 3–4, 337–359.

[KLN+01]   K. H. Karlsen, K.-A. Lie, J. R. Natvig, H. F. Nordhaug, and H. K. Dahle, *Operator splitting methods for systems of convection-diffusion equations: Nonlinear error mechanisms and correction strategies*, Journal of Computational Physics **173** (2001), no. 2, 636–663.

[KO00]   P. Knabner and F. Otto, *Solute transport in porous media with equilibrium and nonequilibrium multiple-site adsorption: uniqueness of weak solutions*, Nonlinear Analysis **42** (2000), no. 3, 381–403.

[KvK01]   J. Kačur and R. van Keer, *Solution of contaminant transport with adsorption in porous media by the method of characteristics*, ESAIM – Math. Model Num. **35** (2001), no. 5, 981–1006.

[Mar94a]   J. Maryška, *Existence, uniqueness and approximation of the hybrid mixed formulation of the porous media flow problem*, Tech. Report 635, UIVT AV ČR, 1994.

[Mar94b]   _____, *Matematické modely proudění podzemních vod a transportu chemických látek*, Ph.D. thesis, FJFI, ČVUT, Praha, 1994.

[MF92]   J. Maryška and D. Frydrych, *Užití prizmatických prvků při řešení variačních úloh v oblastech s vrstevnatou strukturou*, Tech. Report VZ 67/92, DIAMO Stráž pod Ralskem, 1992.

[MM00]   J. Maryška and J. Mužák, *Mathematical model of unsteady unsaturated porous media fluid flow*, Proceedings of the 3rd European Conference Numerical Mathemetics and Advanced Applications (ENUMATH99), World Scientific Publ., 2000, pp. 665–672.

[MMS96]   J. Maryška, J. Mužák, and M. Stýblo, *Solution of convection-diffusion equation based on mixed-hybrid finite element method*, Proceedings of the Prague Mathematical Conference (Prague), 1996.

[MMSŠ00]   J. Maryška, J. Mužák, O. Severýn, and J. Šembera, *Mathematical modelling of the inter-collector transfer of water contaminants*, Proceedings of ALGORITMY 2000 (Bratislava, Slovakia) (K. Mikula et al., ed.), Slovak University of Technology, 2000, pp. 120–129.

[Mor96]   K. W. Morton, *Numerical solution of convection-diffusion problems*, Chapman & Hall, London, 1996.

[MRT95]   J. Maryška, M. Rozložník, and M. Tůma, *Mixed-hybrid finite-element approximation of the potential fluid-flow problem*, J. Comput. Appl. Math. **63** (1995), 383–392.

[MRT00]   _____, *Schur complement systems in the mixed-hybrid finite element approximation of the potential fluid flow problem*, SIAM J. Sci. Comput. **22** (2000), 704–723.

[NIS00]   C. J. Neville, M. Ibaraki, and E. A. Sudicky, *Solute transport with multiprocess nonequilibrium: a semi-analytical solution approach*, J. of Contaminant Hydrology **44** (2000), 141–159.

[Nov01]   J. Novák, *Groundwater remediation in the Stráž leaching operation*, Mine Water and the Environment **20** (2001), 158–169.

[NSŠ98]   J. Novák, R. Smetana, and J. Šlosar, *Remediation of a sandstone aquifer following chemical mining of uranium in the Stráž deposit, Czech Republic*, Proceedings of the 9th International Symposium on Water-Rock Interaction (G.B. Arehart and J.R. Hulston, eds.), A. A. Balkema, 1998, pp. 989–992.

[Odm97]   M. T. Odman, *A quantitative analysis of numerical diffusion introduced by advection algorithms in air quality models*, Atmospheric Environment **31** (1997), no. 13, 1933–1940.

[OL77]   J.T. Oden and J.K. Lee, *Dual-mixed hybrid finite element method for second-order elliptic problems*, Mathematical Aspects of Finite Element Methods, Lecture Notes in Mathematics, Volume 606 (Berlin) (I. Galliani and E. Magenes, eds.), Springer-Verlag, 1977, pp. 275–291.

[Phi94]   J.R. Philip, *Some exact-solutions of convection-diffusion and diffusion equations*, Water Resour. Res. **30** (1994), no. 12, 3545–3551.

[PL01]   T.H. Pulliam and H. Lomax, *Fundamentals of computational fluid dynamics*, Springer, 2001.

[PV86]   J. C. Parker and A. J. Valocchi, *Constraints on the validity of equilibrium and first-order kinetic transport models in structured soils*, Water Resour. Res. **22** (1986), no. 3, 399–407.

[Rek95]   K. Rektorys, *Přehled užité matematiky*, Prometheus, Praha, 1995.

[Rek99]   _____, *Variační metody v inženýrských problémech a v problémech matematické fyziky*, Academia, Praha, 1999.

[Rem03]   M. Remešíková, *Solution of convection-diffusion problems with nonequilibrium adsorption*, in preparation, 2003.

[RT77]   P.A. Raviart and J.M. Thomas, *A mixed finite element method for 2-nd order elliptic problems*, Mathematical Aspects of Finite Element Methods, Lecture Notes in Mathematics, Volume 606 (Berlin) (I. Galliani and E. Magenes, eds.), Springer-Verlag, 1977, pp. 292–315.

[Š+01]   J. Šembera et al., *Realizace programových modulů pro sanační modely DIAMO*, Tech. report, DIAMO, s.p., Stráž pod Ralskem, Czech Rep., 2001.

[Sev02]   O. Severýn, *Model proudění a transportu látek v puklinovém prostředí (Model of flow and solute transport in fractured environment)*, Ph.D. thesis, Technical University of Liberec, Liberec, Czech Republic, 2002.

[TLvG93] N. Toride, F.J. Leij, and M.T. van Genuchten, *A comprehensive set of analytical solutions for nonequilibrium solute transport with first-order decay and zero-order production*, Water Resour. Res. **29** (1993), 2167–2182.

[vG80]   M. T. van Genuchten, *A closed-form equation for predicting the hydraulic conductivity of unsaturated soils*, Soil Sci. Soc. Am. J. **44** (1980), no. 5, 892–898.

[vGW76]   M.T. van Genuchten and P.J. Wierenga, *Mass transfer studies in sorbing porous media: analytical solutions*, Soil Sci. Soc. Am. J. **40** (1976), 473–480.

[vK96]   J.J.A. van Kooten, *A method to solve the advection-dispersion equation with a kinetic adsorption isotherm*, Adv. Water Resour. **19** (1996), no. 4, 193–206.

[VMVF97] J. Vanderborght, D. Mallants, M. Vanclooster, and J. Feyen, *Parameter uncertainty in the mobile-immobile solute transport model*, J. of Hydrology **190** (1997), no. 1–2, 75–101.

[XB95]   L.L. Xu and M.L. Brusseau, *A combined laplace transform and streamline upwind approach for nonideal transport of solutes in porous-media*, Water Resour. Res. **31** (1995), no. 10, 2483–2489.

[ZB95]   C. Zheng and G. D. Bennett, *Applied contaminant transport modeling*, Van Nostrand Reinhold, New York, 1995.